Analysis of p97-mediated Ku80 extraction in DNA double-strand break repair in cells

Inaugural-Dissertation

zur

Erlangung des Doktorgrades

Dr. rer. nat.

der Fakultät für

Biologie

an der

Universität Duisburg-Essen

vorgelegt von

Markus Andreas Wolf

aus Essen

September 2018

Die der vorliegenden Arbeit zugrunde liegenden Experimente wurden am Institut für Molekularbiologie I der Universität Duisburg-Essen durchgeführt.

1. Gutachter: Prof. Dr. Hemmo Meyer

2. Gutachter: Prof. Dr. Stefan Westermann

Vorsitzender des Prüfungsausschusses: Prof. Dr. George Iliakis

Tag der mündlichen Prüfung: 01.02.2019

DOI: 10.17185/duepublico/70001
URN: urn:nbn:de:hbz:464-20210602-074820-1

Summary

DNA double strand breaks (DSBs) are the most deleterious kind of DNA damage and threaten genomic integrity. Therefore, DSBs need to be repaired to avoid chromosomal aberrations, cell death, and malignant transformation. Sophisticated repair mechanisms have evolved and at least three competing pathways, non-homologous end-joining (NHEJ), homologous recombination repair (HRR), and alternative end-joining can repair DSBs. To ensure successful DSB repair, the complex multistep repair pathways are tightly controlled and the ubiquitin-proteasome system (UPS) has a fundamental role in this regulation. The AAA+-ATPase p97 is a critical factor of the UPS and facilitates extraction and unfolding of ubiquitinated substrate proteins. A set of bifunctional adaptor proteins, which can bind to ubiquitin and to p97, act as cofactors and form a variety of active p97 complexes.

Previous studies have identified that p97 localizes to DSBs and is involved in DSB repair by NHEJ and HRR, which are impaired upon loss of p97. However, the underlying mechanisms and the substrates were unknown. Therefore, we aimed at clarifying the role of p97 and its cofactor proteins in DSB repair. In the present study, p97 was established as factor for Ku80 extraction, which was a promising candidate from a mass spectrometry approach performed in our lab. Ku80 is part of the ring-shaped heterodimer Ku that is essential for NHEJ. Ku rings slide onto open DNA ends and fully encircle the double helix. This special structure and mode of DNA binding prevents dissociation from chromatin and Ku becomes sterically trapped after religation of the DSBs. Hence, extraction of trapped Ku from chromatin requires substantial unfolding by an active mechanism.

In this study, cell-based assays provided strong evidence that p97 extracts Ku80 from chromatin and that this is the major role of p97 in NHEJ. Sophisticated immunofluorescence techniques were established and enabled the visualization and kinetic analysis of DSB-bound Ku80. Additionally, the functionality of p97 cofactors was impaired by RNAi-mediated depletion and CRISPR/Cas9-mediated knockout. The experiments revealed that the p97 cofactors Ufd1-Npl4 and FAF1 participate in p97-mediated Ku80 extraction. For this function, FAF1 was hypostatic to Ufd1 and might contribute to a backup pathway that compensates loss of Ufd1. Moreover, loss of p97 abolished Ku80 extraction and the results indicated that this cannot be compensated. Further, K48-linked polyubiquitin persisted upon loss of p97, but was significantly reduced by Ku80 depletion. This suggests that Ku80 constitutes a major substrate of K48-Ub at DSBs and that p97 targets K48-Ub-modified Ku80 for extraction.

Ku is trapped at the end of NHEJ repair and was described to block end resection, which is an early step in HRR. To analyze whether p97 extracts Ku80 also from open DNA ends to promote HRR, DNA damage was induced with the topoisomerase I (Top1) inhibitor camptothecin (CPT). The transient Top1 cleavage complexes (Top1ccs) are stabilized by

CPT and encountering replisomes convert them into single-ended (se) DSBs, which are specifically repaired by HRR. Ku bound to seDSBs and a p97-independent pathway that required MRE11 and CtIP released Ku80 from these lesions. Interestingly, loss of p97 activity reduced the CPT-induced γH2AX level but not the DNA synthesis that was measured simultaneously by incorporation of a nucleotide analogue. Impaired seDSB induction during unperturbed replication suggested that p97-dependent processing sets free CPT-induced seDSBs. Measurement of DNA-bound Top1 and Top1ccs showed that the removal from chromatin was independent of p97, which suggests replisome factors as candidate p97 substrates for future studies.

Zusammenfassung

DNS-Doppelstrangbrüche (DSB) sind die gefährlichste Art der DNS-Schäden und ihre Reparatur ist von zentraler Bedeutung, da die DSB sonst zu Chromosomenabberationen, Zelltod oder maligner Transformation führen können. In den Zellen haben sich spezialisierte Reparaturprozesse entwickelt und DSB können mittels nichthomologer Endverknüpfung (NHEJ), homologer Rekombination (HRR) oder alternativer Endverknüpfung repariert werden. Diese Prozesse sind komplex und müssen genau kontrolliert werden um eine präzise Reparatur zu gewährleisten. Das Ubiquitin-Proteasom-System (UPS) hat eine zentrale Funktion in der Regulation der DSB-Reparatur. Die essentielle AAA+-ATPase p97 ist ein wichtiger Bestandteil des UPS und extrahiert und entfaltet ubiquitinierte Proteine. p97 ist maßgeblich an einer Vielzahl zellulärer Prozesse und interagiert dafür mit bifunktionellen Adapterproteinen, welche an die ATPase und an Ubiquitin binden können. Die Adapter vermitteln die spezifischen Substratbindungen und wirken als Kofaktoren in verschiedenen funktionellen p97-Komplexen.

Vorangegangene Studien haben gezeigt, dass p97 zu Chromatin mit DSB rekrutiert wird und an der DSB-Reparatur über NHEJ und HRR beteiligt ist, da beide Prozesse ohne p97 beeinträchtigt sind. Allerdings waren die zugrundeliegenden Mechanismen und die p97-Substrate unbekannt. Daher war es unser Ziel, die Funktion von p97 und seinen Kofaktoren in der DSB-Reparatur aufzuklären. In der vorliegenden Arbeit wurde beschrieben, dass p97 während der DSB-Reparatur Ku80 extrahiert, welches ein aussichtsreicher Kandidat aus einer massenspektrometrischen Messung unserer Gruppe war. Ku80 ist Bestandteil des ringförmigen Heterodimers Ku, welcher essentiell für die DSB-Reparatur über NHEJ ist. Die beiden Ku-Proteinringe schieben sich auf offene DSB-Enden und umschließen die DNS-Doppelhelix vollständig. Aufgrund der besonderen Struktur und Art der DNA-Bindung wird eine Dissoziation vom Chromatin verhindert und führt dazu, dass Ku nach der DSB-Reparatur sterisch gefangen ist. Folglich erfordert die Ku-Extraktion vom Chromatin ein erhebliches Maß an Proteinentfaltung durch einen aktiven Prozess.

In dieser Arbeit haben zelluläre Experimente starke Evidenzen für eine p97-vermittelte Ku80 Extraktion vom Chromatin ergeben und dafür, dass dies die wichtigste Funktion von p97 in NHEJ ist. Komplexe Immunfluoreszenztechniken wurden etabliert und ermöglichten die Visualisierung und kinetische Analyse von DSB-gebundenem Ku80. Zudem wurde die Funktionalität der p97 Kofaktoren mittels RNA-Interferenz und CRISPR/Cas9-Gen-Knockout beeinträchtigt und die Versuche ergaben, dass Ufd1-Npl4 und FAF1 an der Ku80-Extraktion beteiligt sind. In dieser Funktion war FAF1 hypostatisch zum Ufd1 und ist möglicherweise an einem untergeordneten Prozess beteiligt, welcher den Verlust von Ufd1 kompensieren kann. Der Verlust von p97 hingegen verhinderte die Extraktion von Ku80 vollständig und dies konnte nicht kompensiert werden. Des Weiteren persistierte K48-

verküpftes Polyubiquitin nach Hemmung von p97 und dies wurde durch Depletion von Ku80 signifikant reduziert und legt nahe, dass Ku80 ein Hauptsubstrat von K48-verküpftem Ubiquitin an DSB ist und p97 mit K48-Ubiquitin modifiziertes Ku80 extrahiert.

Ku ist am Ende von NHEJ auf dem Chromatin gefangen und wurde zuvor als Blockade für DNS-Endresektion, einem frühen Schritt von HRR, beschrieben. Um zu analysieren ob p97 Ku80 auch von offenen DNS-Enden extrahiert und dadurch HRR fördert, wurden DNS-Schäden mit dem Topoisomerase I Inhibitor Camptothecin (CPT) herbeigeführt. CPT stabilisiert die transienten Topoisomerase I Spaltungskomplexe (Top1cc) die von auftreffenden Replisomen zu einzelendigen DSB (seDSB) umgesetzt werden und folgend nur von HRR repariert werden. Ku80 band an die seDSB und wurde von einem p97-unabhängigen Prozess entfernt, welcher MRE11 und CtIP benötigte. Interessanterweise reduzierte der Verlust der p97-Aktivität die CPT-vermittelte Histon H2AX Phosphorylierung ohne dabei die Replikation zu beeinträchtigen, welche durch den Einbau eines Nukleotidanalogs parallel gemessen wurde. Eine beeinträchtigte seDSB-Induktion bei normaler Replikation deutet darauf hin, dass ein p97-abhängiger Prozess die seDSB freisetzt. Eine Messung der DNS-gebundenen Topoisomerase I und Top1cc zeigte das ihre Entfernung vom Chromatin p97-unabhängig ist. Dies legt die Untersuchung von Replisomproteinen als potentielle p97-Substrate in zukünftigen Studien nahe.

Table of contents

List of figures

List of tables

1 Introduction

1.1 DNA, chromatin, and genomic integrity

Deoxyribonucleic acid (DNA) is one of the most important macromolecules in living organisms, as it encodes the genetic information, which allows cells to express ribonucleic acids (RNAs) and proteins for all cellular functions. In reproduction, DNA enables the inheritance of the genetic information to offspring generations.

DNA is a double-stranded, helical molecule. Each strand has a phosphate-sugar backbone, on which four different nucleobases (adenine [A], cytosine [C], guanine [G], and thymidine [T]) assemble the nucleic acid sequence that encodes the genetic information. Complementary bases form pairs via hydrogen bonds (adenine pairs with thymidine and guanine with cytosine) and thereby form the DNA double strand.

The entire genetic material of an organism is called genome and is divided into several molecules called chromosomes. Chromosomes consist not only of DNA, but organize as chromatin that is composed of DNA, RNA and proteins. The primary class of chromatin proteins are histones that help to pack the DNA more densely. The core histones H2A, H2B, H3, and H4 form the core particle that contains two copies of each histone and the DNA helix is wrapped around in 1.67 turns. Together with the linker histone H1, spiral-shaped fibers with a diameter of 30 nm are formed. Histones function as a platform for regulatory processes, e.g. regulation of transcription. Therefore, histones, especially the N-terminal tails, are substrates of several post-translational modifications, e.g. phosphorylation of serine, threonine, and tyrosine residues; acetylation of lysines; and methylation of arginine and lysine residues.

Many cellular processes affect chromatin. During replication, the DNA is separated into two single strands that serve as template for the synthesis of complementary strands, which results in doubling of the whole genome. The replicated chromosomes are divided equally during mitosis to form two new, genetically identical daughter cells.

To develop tissues or a whole organism, cells need to divide and differentiate. For successful cell division, the propagation of the genomic information to both daughter cells has to be ensured. With the exception of the biogenesis of haploid gametes during meiosis, the full diploid genome is transferred in every cell division. Cells follow a cycle which is divided into replication (S phase), mitosis (M phase), and two gap phases (G_1 and G_2 phase). To ensure genomic integrity, the transitions from G_1 into S phase and from G_2 into M phase are controlled by checkpoints. In addition, there are checkpoints during S and M phase. On the one hand, the physical structure of the chromosomes and the chromatin has to be intact. On the other hand, the encoded genetic information needs to be error-free. Thus, the cells have to ensure genomic integrity to maintain the cellular metabolism, which is a prerequisite for successful mitotic and meiotic cell divisions.

1.2 DNA damage and mutations

DNA is a stable biomolecule, but it has a certain fragility and diverse lesions can be induced by a variety of agents (Figure 1.1; Hoeijmakers, 2001). Sources for DNA damage range from endogenous physiological processes to exogenous toxic agents. Exposure to these agents leads to biochemical changes, e.g. loss of covalent bonds, which causes different alterations depending on the bond that is lost and alterations threaten the chromatin-dependent cellular processes, including replication. Cleavage in the phosphate sugar backbone leads to strand breaks, which threatens the physical integrity of the DNA, may alter the topology and can lead to chromosomal aberrations, such as translocations. If bases are damaged, the DNA sequence and thus the encoded information can be altered, which leads to mutations. Chromosomal aberrations as well as mutations cause cell aging and death, but are also driving carcinogenesis and other pathological changes (Hoeijmakers, 2009). In contrast, mutations and chromosomal aberrations also create genetic variability that drives evolution.

Major classes of DNA damage are base damage, single strand breaks and double strand breaks (DSBs), of which DSBs are the most deleterious ones. Within each class, the lesions can be further separated by the complexity and spatiotemporal distribution of the damage. For this study, DSBs were of special interest and they are described in more detail below.

1.2.1 DSBs occur in different complexities and can be single- or double-ended

Two main types of DSBs can be separated (Figure 1.1 d): Double-ended DSBs (deDSB), which occur upon breaks in both backbones of a DNA double strand, and single-ended DSBs (seDSB) that can arise from replication forks during replication (Cortés-Ledesma & Aguilera, 2006). Therefore, seDSBs are also called replication-borne DSBs and have only one free double-stranded DNA terminus. The other DNA strand still has a continuous backbone, which served as template for replication.

deDSBs exist in different complexity, mostly depending on their origin (reviewed in Schipler & Iliakis, 2013). For example, endonucleases induce DSBs with directly ligatable ends that have a 5'-phosphate and a 3'-OH. DNA damage that is induced by ionizing radiation is often more complex, since base damages, abasic sites and breaks in the backbone can occur in close proximity. These breaks are not directly ligatable and require processing by specialized enzymes, which is integral part of DSB repair pathways (1.5, 1.7, and 1.8).

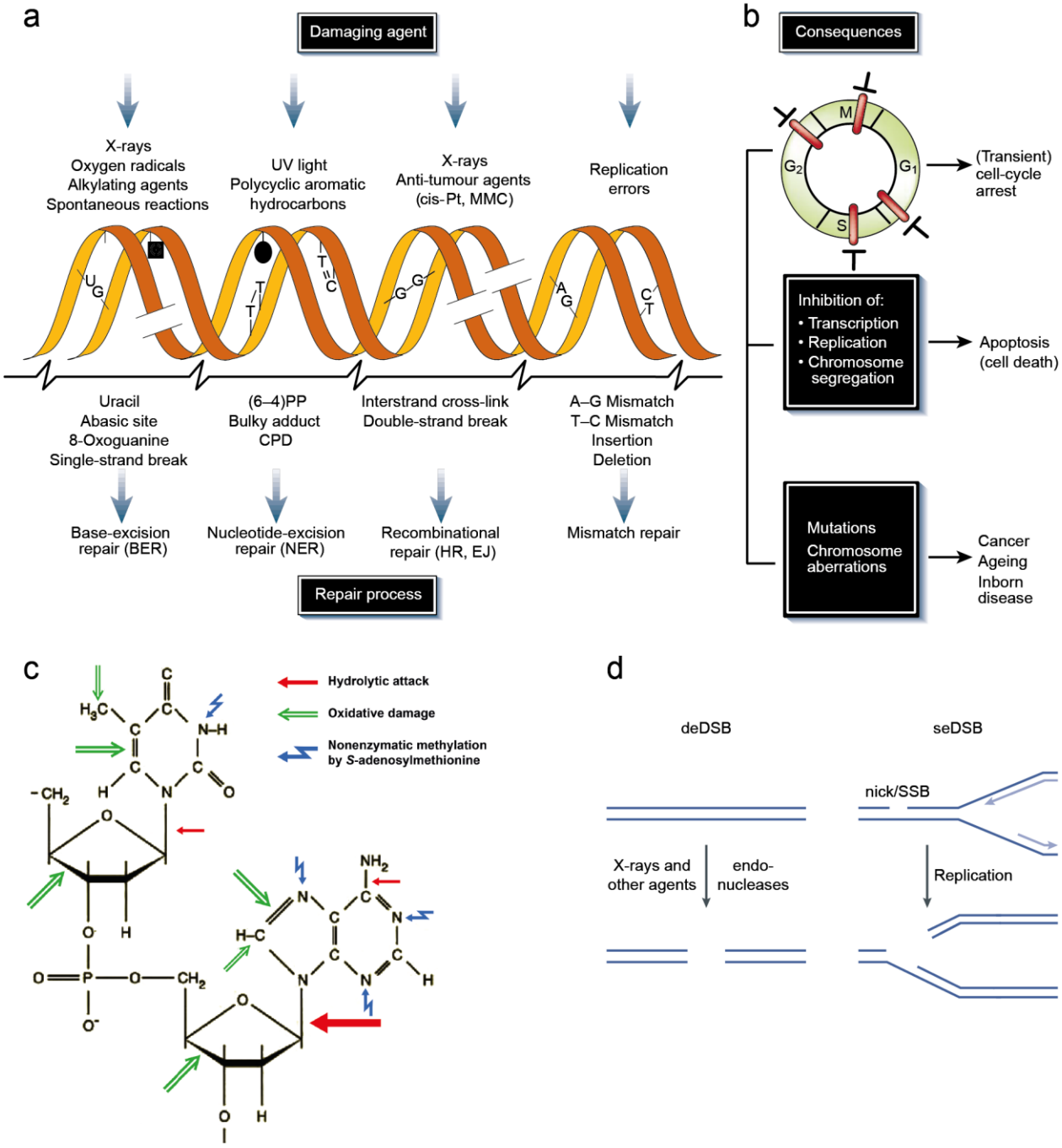

Figure 1.1: Sources, types and consequences of DNA damage

A) A plethora of DNA damaging agents (above DNA) induces various lesions (below DNA) and different repair mechanisms (bottom) have evolved to counteract these lesions.

B) Consequences of DNA damage. The cell cycle checkpoints, G_1, intra S, G_2/M, and in mitosis, are activated as an acute response to DNA damage which inhibits processes of the DNA metabolism (middle). This provides time for DNA repair, but prolonged checkpoint activation results in apoptosis. Low fidelity in DNA repair leads to mutations and chromosomal aberrations that cause ageing and cancer.

C) Target sites of endogenous damage at the example of thymine and adenine. Arrows point to the bonds or atoms that are susceptible to hydrolysis (red), oxidation (green), or methylation (blue).

D) DNA double strand breaks can be double ended (deDSB) or single ended (seDSB). deDSBs are induced by ionizing radiation, chemicals, or enzymatically by endonucleases. seDSBs can arise from nicks or single strand breaks during DNA replication.

A) and B) adopted from (Hoeijmakers, 2001) and C) adopted from (Lindahl, 1993)

1.2.2 Endogenous sources of DNA damage

The main source of endogenous DNA damage is spontaneous hydrolysis, which arises from the fact that DNA is permanently in aqueous conditions. Thus, the chemical bonds are permanently exposed to hydrolytic attacks, which mainly results in abasic sites (esp. A and G) and deamination of bases (esp. A and C) leads to altered, i.e. miscoding, base pairing (Figure 1.1 c; Lindahl, 1993).

Moreover, metabolic processes in the cell generate reactive oxygen and nitrogen species (ROS/NOS). Although cells defend themselves against these byproducts with specialized enzymes (e.g. superoxide dismutase) and scavenging molecules (e.g. glutathione), they still react frequently with and damage DNA and other biomolecules.

Enzymatic processes are another source of damage that occurs during DNA replication and transcription, which involves many enzymatic reactions. Most of these specialized enzymes work with high fidelity. For example, a study in yeast determined the total mutation rate of the replicative polymerases to be $3.3 * 10^{-7}$ (St Charles et al, 2015). In addition to this, the polymerases have high selectivity for the correct base and proofreading mechanisms for wrong insertions. Nevertheless, rare mistakes occur and lead to mismatches that can cause mutations. In translesion synthesis (TLS), a special type of replication that can bypass polymerase-blocking DNA lesions to overcome replication stress, low fidelity polymerases are employed making it an error-prone pathway (Goodman & Tippin, 2000).

The enzyme topoisomerase I (Top1) induces nicks that are usually transient, but can be propagated upon abnormal function into DSBs during replication. Other enzymes such as the RAG-1/2 complex or Spo11are able to induce DSBs directly, which is important during V(D)J recombination (McBlane et al, 1995) or mitosis (Keeney et al, 1997), respectively.

1.2.3 Exogenous sources of DNA damage

Numerous chemicals can cause DNA damage. The source of these substances ranges from inhaling (e.g. cigarette smoke or exhausts) to dietary intake or injection of chemotherapeutic medication (Hoeijmakers, 2009; Mehta & Haber, 2014). Depending on the substance, various types of damage can be induced. Alkylating agents cause base damages and single-strand breaks. Conversely, polycyclic aromatic hydrocarbons create bulky DNA adducts that can be unstable, which causes depurination, or stable, which stalls replication forks. Cisplatin and mitomycin C create intra- and interstrand crosslinks, which interfere with replication and transcription.

Enzymatic DSBs can also be generates from exogenous sources, for example by the CRISPR/Cas9 system. The transfection of CRISPR/Cas9 into cells is used for targeted genome editing processes (Doudna & Charpentier, 2014).

Radiation is another exogenous source of DNA damage and can induce different DNA lesions depending on the type and energy (Kuefner et al, 2015). Types of radiation are for example

electromagnetic waves (e.g. X-rays) or particles (e.g. carbon ion beam). Depending on the energy, two major classes can be discriminated: ionizing and non-ionizing radiation.

Ionizing radiation (e.g. from medical use, nuclear weapons, or accidents in nuclear power plants), induces damage mainly by ionizations of water and the secondary electrons or radicals react with the DNA molecules and cleave covalent bonds. This creates strand breaks and abasic sites, and the more of these events cluster in close proximity, the higher is the likelihood to induce a DSB. The linear energy transfer (LET) describes the energy transferred per distance and thus the density of ionizations. The biological effects caused by ionizing radiation do not only depend on the absorbed dose, but also on the LET, which depends mainly on the type of radiation. Therefore, a weighting factor (W_R) is used to describe the relative biological effectiveness (RBE). For X-rays W_R is defined as 1 and relative to that alpha particles have a value of 20 (Valentin, 2007).

Concerning non-ionizing radiation, exposure to UV light is most threatening for DNA (Richa et al, 2015). UV light catalyzes reactions that primarily affect the nucleobases, which yields cyclobutane pyrimidine dimers (CPC) and 6-4 photoproducts (6-4 PP; both are intrastrand crosslinks).

1.3 The DNA damage response

DNA damage can interrupt cellular processes like transcription or replication and is toxic for the cells. To ensure genomic integrity and cell survival, surveillance mechanisms have evolved and DNA damage is constantly detected and repaired (Ciccia & Elledge, 2010). The concerted signaling mechanisms are termed the DNA damage response (DDR) and regulate cell cycle, repair of the lesions, and may induce senescence or apoptosis. The DDR is active throughout the whole cell cycle and connected to other mechanisms that ensure genomic integrity, e.g. the mitotic spindle assembly checkpoint (Lawrence et al, 2015).

Cells recognize the damage by virtue of proteins binding to DNA lesions, e.g. Ku70/80 to DSBs, which activates DNA damage signaling networks. The signaling promotes repair processes and may result in activation of cell cycle checkpoints.

1.3.1 DNA damage response is mediated by the kinases ATM, ATR, and DNA-PK

Like many other cellular processes, DNA damage is signaled by phosphorylation of proteins. In the DNA damage response of vertebrates, this post-translational modification (PTM) is catalyzed by one of three phosphatidylinositol 3-kinase (PI3K)-related kinases (PIKKs): ataxia-telangiectasia mutated (ATM), ataxia telangiectasia and Rad3-related (ATR), and DNA-dependent protein kinase (DNA-PK; all reviewed in (Blackford & Jackson, 2017). These three structurally related kinases have similar domains and are serine/threonine protein kinases that preferentially phosphorylate their substrates at S/T-Q motifs in vicinity of hydrophobic or acidic

residues. All PIKKs autophosphorylate, which positively regulates their activity (Blackford & Jackson, 2017). Activation of all three kinases requires recruitment to DNA damage sites and they bind to a conserved PIKK interaction motif, but in different proteins (Falck et al, 2005). ATM binds to Nijmegen breakage syndrome protein 1 (Nbs1; also called Nibrin), which is part of the DSB binding MRN complex (Meiotic recombination 11 (MRE11), radiation sensitive 50 (Rad50)-Nbs1 complex) and is considered as master regulator of the DSB response. It orchestrates DNA repair, chromatin remodeling, activation of cell cycle checkpoints, senescence, and apoptosis (Blackford & Jackson, 2017). ATR is recruited to ATR-interacting protein (ATRIP) that is bound to RPA-coated ssDNA and the recruitment is therefore not restricted to DSBs. ATR is activated by variety of genotoxic stresses and is essential for the response to DNA replication stress. DNA-PK is a heterotrimer and the catalytic subunit (DNA-PK_{cs}) is recruited to a binding site in DSB-bound Ku80. DNA-PK is the regulator of the main DSB repair pathway non-homologous end-joining (NHEJ; described in 1.5).

1.3.2 γH2AX

DSBs induce phosphorylation of the histone variant H2AX at serine 139 (Rogakou et al, 1998), which is a well-characterized and widely used marker for DSBs. The modified form is referred to as γH2AX and it is generated by PIKKs rapidly after damage induction (Burma et al, 2001; Stiff et al, 2004). The post-translational modification occurs in a range of several kilobases around the DSB and can be visualized as 'focus' by immunostaining with specific antibodies (Rogakou et al, 1999).

γH2AX orchestrates a variety of DSB repair processes (reviewed in Scully & Xie, 2013), whereof MDC1 recruitment is probably the most important function. MDC1 is directly binding to γH2AX (Stucki et al, 2005), activates the DNA damage checkpoint via Chk2, and recruits the MRN complex (Goldberg et al, 2003; Lou et al, 2003; Stewart et al, 2003).

γH2AX has some limitations as marker for DSBs, since it was reported that γH2AX is induced by ATR in response to replication stress (Ward & Chen, 2001) and that low levels of the marker are not associated with DSBs (Rybak et al, 2016).

1.4 DNA repair

Several distinct repair mechanisms exist in cells and each is specialized on one type of damage. Base excision repair (BER) repairs the majority of endogenous damage including alkylation or oxidative damages of nucleobases (Wallace et al, 2012). Bulky adducts that disturb the helix structure of the DNA, e.g. CPDs and 6-4PPs, are repaired by nucleotide excision repair (NER; (Marteijn et al, 2014). Mismatch repair (MMR) removes non-Watson-Crick base pairs, which result from replication errors that were not removed by the proofreading function of the polymerases (Jiricny, 2013). This decreases the error rate to $0.17 * 10^{-8}$ (St Charles et al, 2015).

Single strand breaks (SSB) are repaired by different mechanism depending on the source of damage. Direct SSBs, e.g. from oxidative damage, are recognized by PARP1 and repaired by end processing of the damaged termini, insertion of missing nucleotide(s) and ligation (Caldecott, 2008). Other SSBs are propagated to seDSBs during replication.

Interstrand crosslinks are detected and repaired by the Fanconi anemia pathway, which includes mechanisms of nucleotide excision repair, translesion synthesis and homologous recombination repair (Ceccaldi et al, 2016).

DNA protein crosslinks (DPCs) are repaired by DPC-specific proteases, including the p97 cofactor DVC1, or by canonical repair pathways including NER and homologous recombination repair (HRR) (Stingele & Jentsch, 2015). Aberrant, i.e. stable, covalent binding of the topoisomerases I and II is reversed by specialized enzymes called tyrosyl-DNA phosphodiesterase 1 and 2 (TDP1 and TDP2; Yang et al, 1996; Cortés-Ledesma et al, 2009).

Three pathways for the repair of DNA double strand breaks are known: NHEJ, HRR, and alternative end-joining (alt-EJ). All facilitate the religation of the break, but the requirements and the outcome are different. The distinct repair pathways for DSBs are described below in more detail (1.5, 1.7, 1.8).

1.5 Non-homologous end-joining

NHEJ is a repair pathway with fast kinetics and works throughout the cell cycle, but it rarely restores the original DNA sequence (reviewed in Pannunzio et al, 2018). Almost every DSB occurring outside of the S and G_2 phase is repaired by NHEJ. During S and G_2, approx. 80 % are repaired by NHEJ, rendering it the dominant DSB repair pathway in mammalian cells. The DNA termini are processed to yield a ligatable configuration regardless of the original DNA sequence, but usually using microhomologies (≤4 bp). End processing includes insertion or deletion of bases that often leads to mutations and frameshifts. The NHEJ pathway is complex and acts on diverse DSBs. However, it can be divided into a few major steps that use discrete enzyme complexes to achieve repair (Figure 1.2):

Sensing of the DSB by Ku binding and recruitment of DNA-PK_{cs}

A ring-shaped heterodimer of Ku70 and Ku80 slides on each end of the dsDNA and recruits the catalytic subunit of the DNA-dependent protein kinase (DNA-PK_{cs}) to form the DNA-PK holoenzyme. DNA-PK_{cs} binds directly to the DNA and to both Ku molecules (Ku is described in more detail in 1.6). The kinase regulates NHEJ processes and its own activity by (auto)phosphorylation (Neal et al, 2014). Furthermore, structural studies indicated that DNA-PK_{cs} dimerizes which bridges the DNA ends and keeps them in close proximity (Sibanda et al, 2017).

End processing

Direct ligation of the DSB is often precluded by incompatible DNA ends that originate from chemical modifications, abasic sites, or mismatching bases. Goal of the end processing is the generation of compatible double-stranded DNA ends that can be ligated. To achieve this, a set of nucleases, polymerases and other enzymes are involved in the process.

The nuclease Artemis is recruited to Ku in complex with DNA-PK_{cs} (Ma et al, 2005). Artemis has 5' exonuclease activity and endonuclease activity that is able to remove 3' and 5' overhangs. The endonuclease is activated by phosphorylation through DNA-PK_{cs}. Other nucleases that are less frequently used are Polynucleotide kinase and aprataxin-like forkhead-associated protein (PALF), flap structure-specific endonuclease 1 (FEN1), DNA replication helicase/nuclease 2 (DNA2), and exonuclease 1 (EXO1). The Werner syndrome helicase (WRN) and the Bloom syndrome helicase (BLM) assist the nucleases by creating cleavable DNA substrates at complex lesions (Pannunzio et al, 2018).

The DNA polymerases mu, lambda, and terminal deoxynucleotidyl transferase (Pol μ, Pol λ, and TdT) participate in NHEJ, but the latter is only expressed in lymphocytes (Ma et al, 2004). These polymerases are able to incorporate nucleotides, TdT also in a template-independent manner, (Nick McElhinny et al, 2005) which explains the possibility of insertions and the overall diversity of NHEJ junctions.

Recently a resection-dependent NHEJ pathway was described, which utilizes enzymes that were known to be involved in HRR and is involved in the repair of heterochromatic DSBs (Biehs et al, 2017). The resection occurs upstream of Artemis processing, is initiated by C-terminal-binding protein 1-interacting protein (CtIP; also called RBBP8), and executed by MRE11 exonuclease, Exonuclease 3'-5' domain-containing protein 2 (EXD2), and EXO1. In contrast to HRR, the resection is short-ranged and followed by canonical NHEJ ligation.

Ligation

After the end processing process has generated a stable ligatable joint, ligation of the DSB is initiated. For this, a multiprotein complex of DNA ligase IV, X-ray cross-complementing group 4 (XRCC4), XRCC4-like factor (XLF; also called Cernunnos), Paralog of XRCC4 and XLF (PAXX), and Ku is formed. Ligase IV catalyzes the covalent rejoining of both DNA backbones after stimulation of the ligase activity by XRCC4. This is supported by Ku staying at the DSB and binding the ligase IV-XRCC4 complex. In addition, XLF, that also directly binds to Ku (Yano et al, 2008), and XRCC4 are able to form helical filaments that protect and align the DNA ends (Mahaney et al, 2013). PAXX forms homodimers and interacts with Ku and thereby probably bridges the break, which prevents dissociation of the DNA termini and stable assembly of the ligation factors (Ochi et al, 2015). Altogether, the accessory proteins create a stable conformation in which the DNA ends are in close proximity, which enables the rejoining by DNA ligase IV.

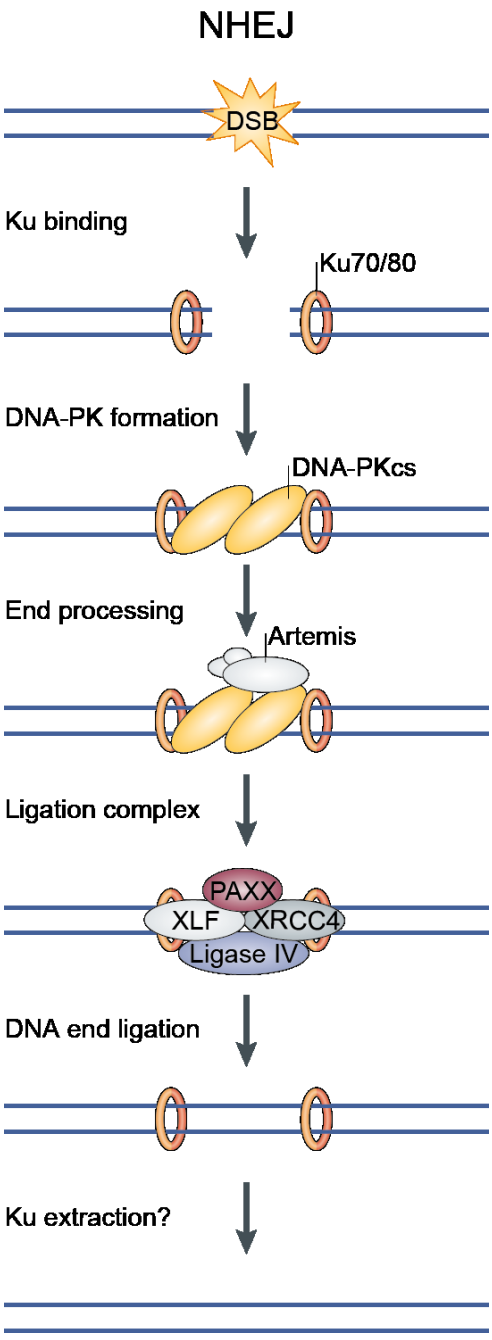

Figure 1.2: Model of non-homologous end-joining
In mammalian cells, NHEJ repairs ~80 % of the DSBs occurring in S and G_2 phase of the cell cycle and nearly all DSBs outside of S/G_2. NHEJ works with fast kinetics, but is error-prone and often results in indels. Various endogenous and exogenous agents induce DSBs.

After damage induction, the Ku heterodimer rapidly binds both sides of the break. Ku is essential for NHEJ and recruits many other NHEJ factors. Therefore, it remains associated to the break beyond ligation. Ku enhances the affinity of DNA-PK_{cs} to DNA ~100-fold, which leads to recruitment of the catalytic subunit and formation of the heterotrimeric DNA-PK holoenzyme. The kinase regulates NHEJ processes by (auto-) phosphorylation.

DNA-PK_{cs} can be recruited in a complex with the Artemis nuclease that accomplishes end processing to yield a ligatable DNA configuration. End processing can also involve other nucleases that often generate microhomologies up to 4 bp to stabilize the break. Besides the cleavage of bases, members of the polymerases X family can add nucleotides in a template-independent manner. Both processes alter the DNA sequence, rendering NHEJ an error-prone repair pathway.

The central components of the ligation complex include Ligase IV and XRCC4, which activates the ligase. XLF and PAXX juxtapose both ends for efficient ligation. Finally, Ligase IV catalyzes formation of the covalent bonds in the DNA backbones and the DSB is repaired.

After covalent rejoining, the repair factors dissociate from chromatin, except for Ku, which is sterically trapped. For full restoration of chromatin at the DSB site, active extraction of Ku is required.

The model was adopted from (Schwertman et al, 2016).

Post-processing

The DSB is repaired upon successful ligation, but for full restoration of the chromatin all proteins of the NHEJ machinery have to disassemble and dissociate from the DNA. Unlike other repair proteins, the Ku heterodimer cannot diffuse away from chromatin, because it is sterically trapped on the dsDNA and requires active extraction.

1.6 Ku

1.6.1 Ku is a DSB sensor and essential for NHEJ

Ku is a heterodimer of Ku70 and Ku80 (also called Ku86) that is stable in solution, abundant in the nucleus, and rapidly binding to free dsDNA termini with high affinity (K_D = 2.4 nM; Blier et al, 1993). Each of the proteins forms a ring with a narrow diameter of 1.15 nm (diameter of B-form DNA is 1.9 nm) that serves as a preformed channel to slide onto the dsDNA end, whereat protein residues enter the major and minor groove to fit onto the DNA helix (Figure 1.3; Walker et al, 2001). Of note, none of the side chain residues of the proteins makes contact to any nucleobases, but the interaction is enhanced by a positively charged surface within the channel binding to the negatively charged DNA backbone. Thus, Ku binding appears to be independent of the DNA sequence. The binding occurs unidirectional with Ku70 located proximal and Ku80 distal to the end (Yoo et al, 1999).

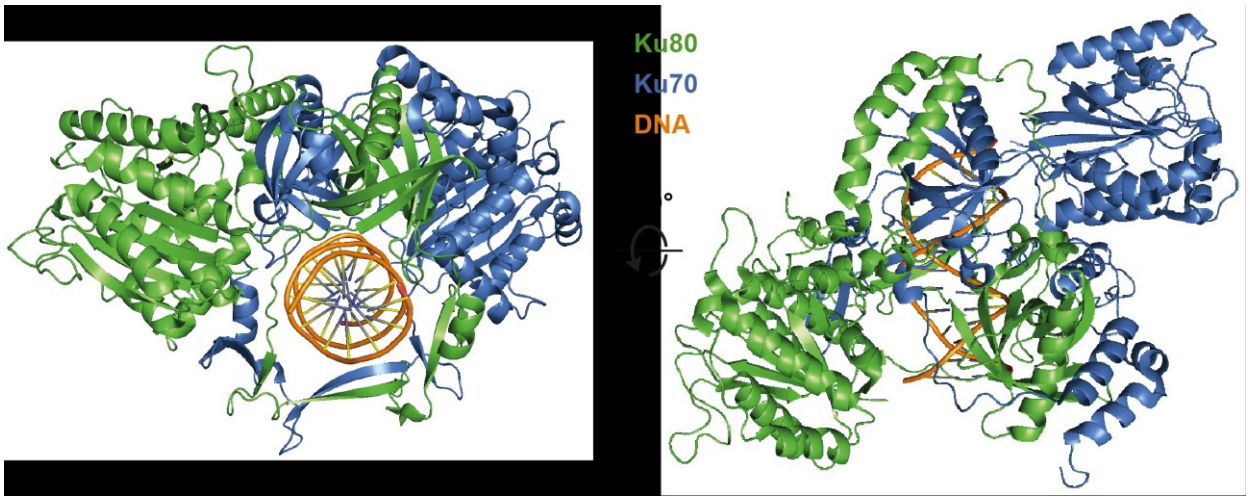

Figure 1.3: Structure of Ku70/80 bound to DNA
Rendering of the Ku heterodimer (full-length Ku70 is shown in blue and Ku80 with C-terminal truncation after Lys565 in green) bound to dsDNA (14-mer, orange). Based on a crystal structure from (Walker et al, 2001) (PDB 1JEJ). Ku80 lacks the 19K domain that is required for DNA-PK_{cs} recruitment, but is dispensable for binding to DSBs. The proteins have a common topology and a large dimer interface that results in a very stable dimerization. Both molecules fully encircle the duplex DNA helix without sequence specificity, but with a preferred orientation with Ku80 on the distal (-) and Ku70 on the proximal (+) site of the break.

The Ku dimer is essential for NHEJ. Ku binding stabilizes the DSB and protects it from degradation by exonucleases. DNA bound Ku70/80 recruits the catalytic subunit DNA-PK_{cs} to form the DNA-PK holoenzyme, a kinase that signals DSB induction and orchestrates NHEJ repair. In addition, Ku recruits many other repair factors and some have a conserved Ku-binding motif (KBM; Grundy et al, 2016).

1.6.2 Ku becomes sterically trapped during DSB repair by NHEJ

Dissociation from chromatin after the ligation step of NHEJ is not possible for the Ku heterodimer, because it encircles the DNA. In contrast to other proteins that encircle dsDNA, Ku has neither oligomers that can detach from each other (e.g. like Proliferating cell nuclear antigen (PCNA)) nor a clasp that can open upon conformational changes (e.g. like Top1). Both Ku subunits have an amino acid sequence forming a bridge that fully encircles DNA and other protein domains are located N- and C-terminally from that bridge region.

After solving the structure of Ku, the question of an unloading mechanism for trapped Ku was raised (Walker et al, 2001). Trapped Ku requires active extraction and protease-dependent or ATP-dependent mechanisms were postulated, but how Ku extraction is facilitated remained a long-standing question in the field.

Ku80 was shown to be modified with ubiquitin (described more detailed in 1.15), which is important for the removal from DNA (Postow et al, 2008). Thus, chromatin-associated degradation (CAD) was discussed as possible mechanism, but polyubiquitinated Ku80 can be extracted without proteasome function.

Phosphorylation of multiple residues in and close to the bridge region of Ku70 were reported to lower the affinity of Ku to DNA (Lee et al, 2016). Weaker binding allowed Ku to be released from open DSBs, but release after religation requires large-scale conformational changes that are not conveyed by phosphorylation.

1.6.3 RNA binding features of Ku

Ku also binds to RNA with an affinity comparable to DNA binding (Yoo & Dynan, 1998). In contrast to DNA binding, a sequence-specific binding to a stem-loop of telomerase RNA was found (Peterson et al, 2001) that contributes to telomerase function and explains massive telomere loss and cell death upon loss of Ku80 (Wang et al, 2009).

The fact that a large fraction of Ku is bound to RNA complicates the visualization of Ku in immunofluorescence. Thus, Britton and colleagues developed a method to visualize Ku specifically at DSBs by using a pre-extraction step with RNase A-mediated removal of RNA, allowing the washout of RNA-bound proteins like Ku (Britton et al, 2013).

1.7 Homologous recombination repair

Homologous recombination repair (HRR) is a DSB repair pathway with slow kinetics that is restricted to late S and G_2 phase of the cell cycle, because it requires a replicated sister chromatid as repair template (reviewed in Wright et al, 2018). In contrast to other DSB repair pathways, HRR restores the original DNA sequence and is therefore not mutagenic, which is also a consequence of template-based repair. Disadvantages of HRR are the slow kinetics and the complex multi-step mechanism (Figure 1.4).

DSB detection and initial steps

Although Ku is thought to inhibit HRR, it is probably detecting also DSBs that will be repaired by this pathway, which can be explained by the rapid binding kinetics that result from the high affinity. The MRN complex is another DSB sensor that is rapidly recruited in a PARP1-dependent manner (Haince et al, 2008). MRN activates the ATM kinase via Nbs1 (Falck et al, 2005) and ATM phosphorylates, among many other substrates, histone H2AX (Matsuoka et al, 2007). MDC1 binds to γH2AX and recruits further MRN complexes to sites of DSBs by direct interaction with Nbs1 and thus enables sustained MRN localization (Lukas et al, 2004).

End resection

DSBs that are repaired by HRR are resected 5' to 3' on one strand, which creates a long 3' ssDNA overhang. The resection is tightly regulated and marks a major step of repair pathway choice (reviewed in Her & Bunting, 2018). The resection is initiated by the MRN complex and CtIP. CtIP is important for activation of the nuclease activity of MRE11 that generates an endonucleolytic nick close to the break, but probably distal of Ku on the free DNA end. Binding of Ku to the DSB ends is thought to block HRR and therefore it has to be removed at an early step in the pathway. Experiments in fission yeast had indicated the requirement of MRE11 nuclease and CtIP activity for release of Ku and the MRN complex from DNA ends in the context of HRR (Langerak et al, 2011). Recent studies on seDSBs repair or *in vitro* end resection revealed that initial resection is carried out towards the break and the flap endonuclease activity of CtIP catalyzes the cleavage of the second DNA backbone. The end resection and flap endonuclease cleavage releases Ku bound to a short piece of dsDNA (Chanut et al, 2016; Myler et al, 2017).

After initialization of end resection by CtIP and MRN, exonucleases (EXO1 or BLM-DNA2) carry out long-range resection, which also requires chromatin remodeling to make the DNA accessible for resection. The ssDNA is quickly bound by replication protein A (RPA). RPA is a heterotrimer of RPA1 (70 kDa), RPA2 (32 kDa), and RPA3 (14 kDa) and protects the resected part from degradation and prevents formation of secondary structures. RPA binding stimulates the exonucleases and thereby enhances end resection. Consequently, long-range resection requires negative regulation to terminate resection at a certain point. p53-binding protein 1 (53BP1) is a negative regulator that limits resection and even promotes repair by NHEJ. The E3 ligase Breast cancer type 1 susceptibility protein (BRCA1; in complex with BRCA1-associated RING (really interesting new gene) domain protein 1 (BARD1)) antagonizes 53BP1 and promotes MRN/CtIP dependent resection. The ubiquitin ligase activity of BRCA1-BARD1 is described in 1.15.

Besides direct antagonistic effects between proteins, many factors of HRR are regulated by numerous post-translational modifications, like phosphorylation or ubiquitination that modulate interactions or regulate enzymatic activity and thereby orchestrate and balance the repair steps.

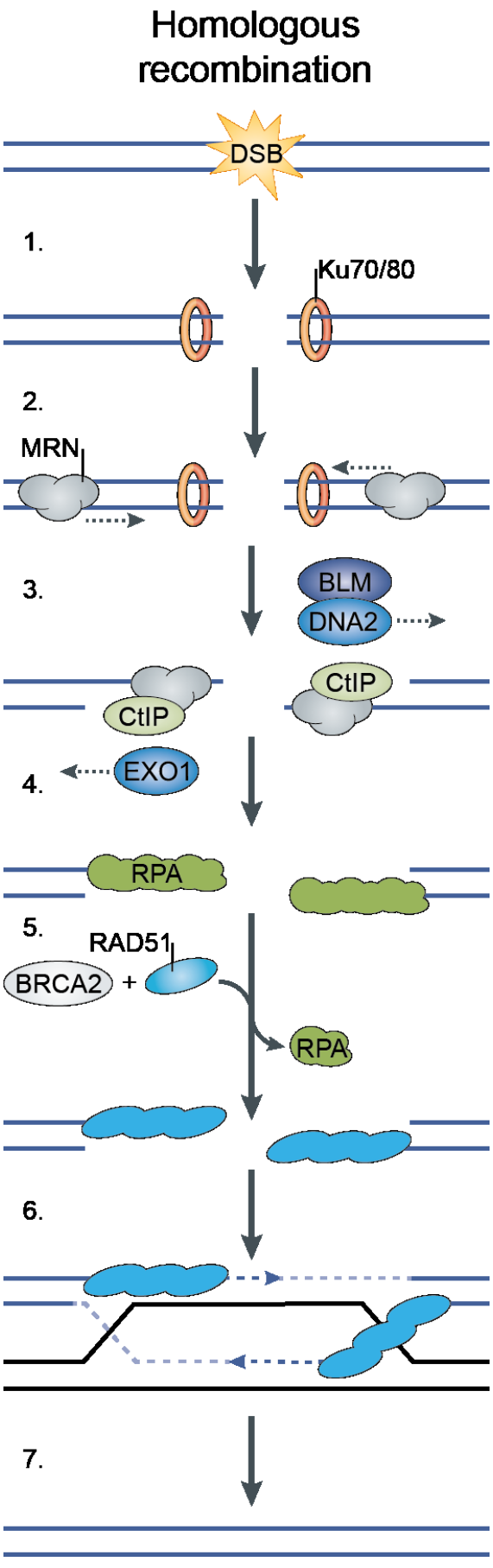

Figure 1.4: Model of homologous recombination repair

Homologous recombination repair (HRR) is a pathway to repair DSBs with the advantage of maintaining the original sequence. It requires a replicated sister chromatid as template and is therefore restricted to late S and G_2 phase of the cell cycle. HRR is a multistep process and the steps until strand invasion are depicted in the model. Steps after repair synthesis for resolution of the HR intermediates are not shown.

1. After DSB induction, Ku is rapidly binding to the open DNA ends. Ku stabilizes the end, protects it from degradation, and initiates DDR signaling via DNA-PK_{cs}. However, Ku is not required for HRR, but even thought to block this pathway.

2. A complex of MRE11, Rad50, and Nbs1 is carries out initial end resection on the distal site of Ku and towards Ku and the DSB. CtIP is binding to MRN and Ku is removed from the break, but the mechanism is not fully understood. Nbs1 activates the DDR kinase ATM.

3. Extensive end resection creates long 3' single-stranded DNA overhangs. This long-ranged resection is mainly achieved by exonuclease 1 (EXO1) and DNA2 helicase/nuclease with the help of Bloom helicase (BLM).

4. Replication protein A (RPA) is a heterotrimeric protein that binds avidly to ssDNA and prevents its degradation or formation of secondary structures. In addition, RPA enhances the processivity of EXO1 and DNA2.

5. BRCA2 assembles Rad51 nucleoprotein filaments that displace the RPA coating. Rad51 is a DNA-dependent ATPase that forms helical filaments, which encase the ssDNA.

6. The nucleoprotein filaments search for the homologous sequence by moving along the repair template. Upon identification of homology, the ssDNA-Rad51 filaments invade into the dsDNA of the sister chromatid and form the displacement loop. DNA synthesis is starting from the 3' end that either is the 3' end of the DSB or generated by cleavage of the invading single strand.

7. During repair synthesis, the second resected end anneals upon extension of the invading strand to a homologous sequence. Several options are possible to proceed with HRR and resolve the structures (D-loops, double Holliday junctions) to yield two intact dsDNA strands. Two major outcomes can be distinguished: a crossover or a noncrossover outcome, whereat somatic cells prefer noncrossover dissolutions to avoid loss of heterozygosity.

The model was adopted from (Schwertman et al, 2016)

RPA2 is phosphorylated by PIKKs at several residues close to the N-terminus. DNA-PK phosphorylates RPA2 at S4 and S8 subsequent to priming phosphorylations at other residues, which can be catalyzed by ATR or CDKs, and is therefore termed hyperphosphorylation (Liu et al, 2012). Hyperphosphorylated RPA leads to cell cycle arrest by activation of the S and G_2/M cell cycle checkpoints via Chk1. Further, signaling to the DNA repair pathways is induced. RPA hyperphosphorylation can also be used as marker for (replication-induced) DNA damage, e.g. after camptothecin treatment.

Nucleoprotein filament formation

BRCA1 recruits Partner and localizer of BRCA2 (PALB2) to the resected DSB, which subsequently localizes Breast cancer type 2 susceptibility protein (BRCA2) to the site of the break. Together with Rad51 paralogs, BRCA2 loads the recombinase Rad51 on the ssDNA, which forms helical filaments around the DNA strand and displaces RPA from the resected DNA.

Homology search, strand invasion and D-loop formation

The main function of Rad51 is the homology search. To initiate the repair synthesis, a homologous donor is required as template. The filaments interact with dsDNA of the sister chromatid (or the homologous chromosome) and search for a complementary sequence. Rad51 paralogs, PALB2 and other factors have a role in bridging the nucleoprotein filaments to the duplex DNA. The mechanism of homology search and how base pairing is arranged in the Rad51-ssDNA-dsDNA complexes is poorly understood. Upon identification of a homologous sequence, the synaptic complex forms and the resected strand invades into the template strand and forms the displacement loop (D-loop). To enable annealing of the 3' end, the Rad54 ATPase removes Rad51.

Repair synthesis and second-end annealing

DNA synthesis emanates from the 3' end, which either is the 3' end of the initial DSB or is generated by cleavage in case of strand invasion of an internal sequence. The 3' end functions like a primer for the DNA polymerase delta (Pol δ) that performs repair synthesis in complex with PCNA, which extends the D-loop. It is unknown how the length of the DNA synthesis is controlled, but it needs to cover the sequence that is homologous to the other resected end of the DSB. Rad52 assists the newly synthetized strand to anneal with the RPA-coated ssDNA of the other resected DSB end in a process called second-end annealing or synthesis dependent strand annealing (SDSA).

Synthesis dependent strand annealing or formation of a double Holliday junction

SDSA is the predominant pathway to resolve HRR in somatic cells and results in a non-crossover outcome, which is important to avoid loss of heterozygosity. However, a crossover event is possible in the nucleolytic resolution of a double Holliday junction, which occurs upon annealing of the second 3' DSB end and synthesis from both ends.

1.8 Alternative end-joining pathways

Besides the two major DSB repair pathways NHEJ and HRR, there are additional ones that are thought to work mainly as backup for abortive repair events from NHEJ and HRR. These are collectively termed alternative end-joining pathways (alt-EJ; reviewed in Sallmyr & Tomkinson, 2018). The subpathways are end-joining (EJ), microhomology-mediated end-joining (MMEJ), and single-strand annealing (SSA). Alt-EJ works throughout the cell cycle, but is upregulated in S and G_2 phase of the cell cycle (Dueva & Iliakis, 2013). The major steps are similar in all alt-EJ pathways:

End resection

Similar to HRR, 5'-3' end resection is the initial step in all of the pathways and is mainly achieved by the MRN complex and CtIP. In contrast to HRR, the resection is limited to a shorter range. In contrast to NHEJ, the ends are bound by PARP1 that competes with Ku for end binding and catalyzes PARylation (Wang et al, 2006). The main difference between alt-EJ pathways is the length of sequence homology used for DSB alignment and accompanying length of end resection. SSA requires long-ranged resection that is dependent on EXO1 and DNA2 and uses complementary sequences of more than 25 bp. MMEJ utilizes sequences of 2-20 bp and requires less end resection. Limited end resection by MRN-CtIP is sufficient for EJ, as it uses little to no homology.

End bridging

The homologous sequences are exposed within the RPA-coated ssDNA and annealed, which bridges the ends and stabilizes the DSB. In EJ and MMEJ, PARP1 and the MRN complex are involved in the end bridging and Rad52 is anneals the ends in SSA. DNA polymerase theta (Pol θ) has emerged as key factor of MMEJ and might be involved in the other alt-EJ pathways as well. It can displace RPA form the ssDNA, search and align microhomologies, which contributes to the end bridging, and inhibit HRR.

Flap cleavage and gap filling

Non-homologous 3' tails are cleaved, thus alt-EJ pathways generate deletions. A complex of excision repair cross-complementing group 1 protein (ERCC1) and Xeroderma pigmentosum group F-complementing protein (XPF) cleaves the flap in SSA and several nucleases were suggested for this function in the other pathways,. Pol θ fills gaps that remain after annealing, but the DNA synthesis is error-prone. It has remained elusive, which polymerases fill gaps in EJ and especially in SSA.

Ligation

After removal of any overhangs and gaps, both strands are ligated and repair is completed. A complex of DNA ligase III and X-ray cross-complementing group 1 (XRCC1) carries out ligation

in the MMEJ pathway and DNA ligase I is ligation the ends in EJ. The ligase involved in SSA has not been identified so far.

1.9 DSB repair pathway choice

Having a set of distinct DSB repair pathways, cells need to decide for one of them to execute the repair of a break. The initial processing steps do not determine commitment to a specific repair pathway and repair might be shifted to another pathway. This fact was subject to intensive research in recent years and the processes of pathway choice (reviewed in Shibata, 2017) are still not fully understood.

The main choice is made between NHEJ and HRR, because alt-EJ pathways function as backup for repair failures. To choose HRR over NHEJ is beneficial for the cell, due to the error-free repair by HRR. A key determinant of pathway choice is the cell cycle phase, because HRR requires a homologous sister chromatid that is only present after replication in S and G_2 phase. Further, a choice is only possible at deDSBs and seDSBs are primarily repaired by HRR. The DSB end structure and its processing has also impact on pathway choice and resection of the DSB end is a major determinant that promotes HRR. Thus, regulation of end resection is an important step in pathway choice and another well-characterized mechanism is the antagonism between 53BP1 and BRCA1, which promote NHEJ or HRR, respectively. The large protein 53BP1 shows no enzymatic activity but it possesses interaction motifs and domains for numerous proteins that are involved is the DSB response and serves as their molecular scaffold (reviewed in Panier & Boulton, 2014). Important binding partners of 53BP1 are RIF1 (Chapman et al, 2013; Escribano-Díaz et al, 2013) and REV7 (Boersma et al, 2015; Xu et al, 2015). RIF1 is recruited to DSBs by direct binding to an ATM-phosphorylated N-terminal domain of 53BP1 and is essential for suppression of 5' end resection in G_1 by excluding BRCA1 from DSB sites. Blocking of end resection promotes NHEJ repair, but in S phase, CtIP in complex with BRCA1 antagonizes 53BP1-RIF1 to enable HRR. REV7 functions downstream of 53BP1 and RIF1 and is, like RIF1, required to counteract end resection and enhance NHEJ, which was found at uncapped telomeres and IR induced DSBs.

53BP1 and BRCA1 act in the vicinity of DSBs and direct completion at the DNA end occurs between the Ku heterodimer and the MRN complex. Ku promotes NHEJ repair and blocks end resection by EXO1 (Sun et al, 2012). The MRN complex initiates end resection and promotes HRR. However, Ku and MRN can also bind to the same DNA end at the same time, as for example seen in single molecule imaging (Myler et al, 2017).

Repair kinetics and spatiotemporal distribution of DSBs and the repair factors contribute to the decision which pathway executes repair. In terms of spatial regulation, the position of the DSB within the nucleus was shown to have an impact on the utilized repair pathway (Lemaître et al, 2014). DSBs that are localized close to the nuclear lamina are more often repaired by alt-EJ

pathways and HRR is suppressed in that environment. Considering temporal regulation, the use of reporter constructs, in which DSBs are induced by the rare cutting endonuclease I-SceI, revealed that the longer a DSB is left unrepaired, the higher is the chance that it is repaired by error prone and mutagenic pathways like alt-EJ or SSA (Bennardo et al, 2009).

The choice between the non-homologous and alternative end-joining is regulated the helicase and exonuclease function of WRN, which is a pro-NHEJ factor (Shamanna et al, 2016). WRN interacts with the Ku heterodimer, which stimulates the activity of WRN (Cooper et al, 2000; Li & Comai, 2001) p97 physically interacts with WRN and the binding is lost upon CPT induced DNA damage (Partridge et al, 2003).

Recently, dedicated pathway regulating proteins were identified that bind to key repair factors and have an inhibitory function. Cell cycle regulator of NHEJ (CYREN) suppresses NHEJ in S and G2 phases by direct binding to the Ku70/80 heterodimer and this inhibition is enhanced at lesions with single stranded overhangs (Arnoult et al, 2017). Ring1-YY1-binding protein (RYBP) is known as a transcriptional regulator and binds to K63-linked ubiquitin chains via an NZF domain (Ali et al, 2018). K63-ubiquitin chains are assembled at DSBs and binding of RYBP inhibits HRR. RYBP itself is ubiquitinated with K48-linked ubiquitin chains by RNF8 and is subsequently extracted by p97, which enables BRCA1 recruitment and HRR.

The ubiquitin system is involved in further processes of repair pathway choice (described in 1.15 and depicted in Figure 1.8), e.g. promotion of HRR through Ku removal by the RNF138 E3 ligase (Ismail et al, 2015).

1.10 Repair of seDSBs induced by the Top1 inhibitor camptothecin

1.10.1 Replication

During S phase of the cell cycle, the genomic DNA is duplicated in the process of DNA replication. This multistep process is tightly regulated, because the complete genetic information needs to be copied exactly once. Spatiotemporal regulation is mainly achieved by cyclin dependent kinases (CDKs). The first step is replication initiation (reviewed in Fragkos et al, 2015). For initiation, origins of replication, i.e. specific DNA sequences spread in the genome, are licensed in G_1, which leads to formation of a multiprotein complex termed pre-replication complex (pre-RC). The pre-replication complex includes a pair of the heterohexameric Mcm2–Mcm7 complex (minichromosome maintenance complex; Mcm). The Mcm complex is the catalytic core of the replicative helicase. In S phase, binding of Cdc45 and the GINS complex (Sld5, Psf1, Psf2, Psf3) activate Mcm and forms the functional DNA helicase (CMG helicase). CDK-mediated processes in S and G_2 prevent re-replication of already duplicated origins by inhibiting the licensing. At the transition from G_1 to S phase, the pre-RC is advanced into the pre-initiation complex, which includes recruitment of the DNA polymerase ε. In S phase, the process of origin firing activates the pairs of Mcm helicases and they separate into two replication forks to unwind the DNA helices.

PCNA, further polymerases, and other factors are recruited and the DNA synthesis is started. The polymerases synthesize the new DNA strand in 5'-3' direction by addition of single nucleotide triphosphates (adenosine, cytidine, guanosine, and thymidine) to the 3'-OH end.

Synthetic thymidine analogues, like 5-ethynyl-2'-desoxyuridine (EdU) or 5-bromo-2'-deoxyuridine (BrdU), can be incorporated instead of desoxythymidinphosphate to label the newly synthesized DNA in cellular assays (Cavanagh et al, 2011).

Replication continues until two converging replication forks meet, which leads to the regulated process of replication termination(see also 1.15 and (Dewar & Walter, 2017).

Perturbed replication can cause DNA damage and replication stress is sensed by the DDR kinase ATR, which signals to the effector kinase Chk1 to activate the intra S checkpoint (Zeman & Cimprich, 2014).

1.10.2 Topoisomerase I and camptothecin

Processes of the DNA metabolism lead to altered DNA topology, e.g. supercoiling ahead of the replicative helicase Mcm2–Mcm7. Thus, the cell has evolved specialized enzymes to resolve altered DNA topologies. Topoisomerases are a class of enzymes that catalyze topological changes in the DNA double helix (reviewed in Pommier et al, 2016). Topoisomerase I (Top1) encircles the DNA (Figure 1.5) with tyrosine 723 of the enzyme binding to a 3'-phosphate of the DNA phosphodiester backbone in a transesterification (3'-phosphotyrosyl linkage). This reaction creates a nick with a 5'-hydroxyl end in one DNA strand and the resulting covalent DNA-protein complex is termed topoisomerase I cleavage complex (Top1cc). Subsequently, DNA supercoils relax by controlled rotation. Afterwards, the Top1cc is resolved and the 3'-phosphate religates with the 5'-hydroxyl end. Top1 binding is therefore transient and it requires no ATP or other cofactors.

Camptothecin (CPT) is a plant alkaloid that acts as a structural inhibitor of Top1 by intercalating at the site of the Top1-generated nick and preventing the resolution step of the Top1 reaction (Staker et al, 2005). This stabilizes the Top1ccs and the single strand breaks. The thereby generated SSBs are propagated into seDSBs upon collision with replisomes or, to lesser extent, transcription complexes (Sakasai & Iwabuchi, 2016). Derivatives of CPT, e.g. topotecan and irinotecan, are used in cancer therapy, because stabilized Top1ccs are propagated to DSBs especially in the fast replicating tumor cells.

Interestingly, CPT treatment and p97 knockdown have synergistic effects on the cell cycle distribution (Magnaghi et al, 2013).

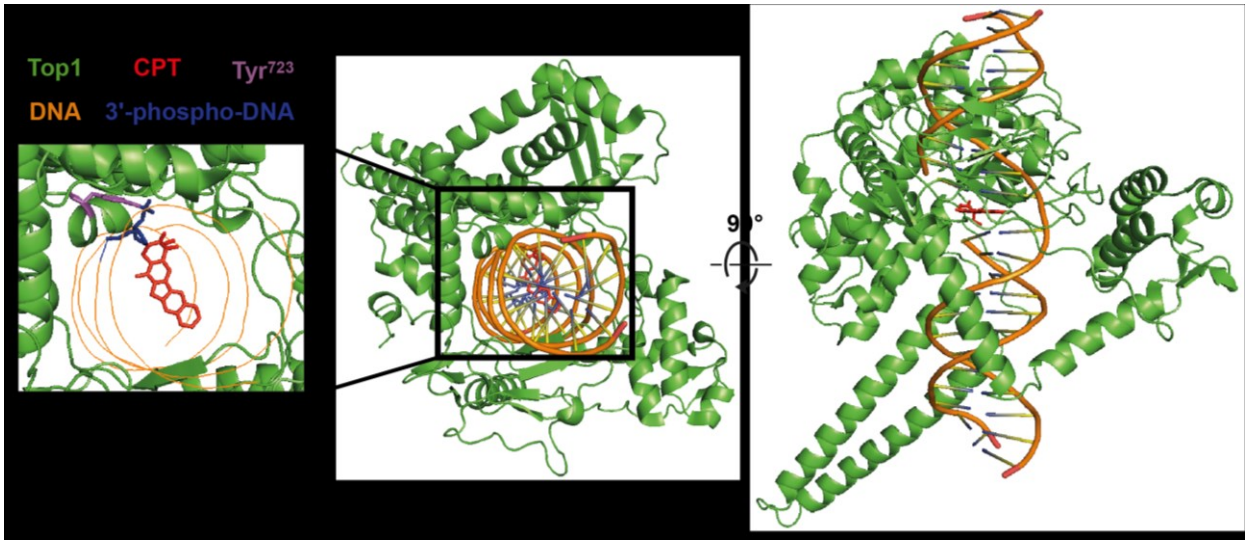

Figure 1.5: Structure of topoisomerase I cleavage complex
The topoisomerase I (Top1; green), shown as N-terminal truncation (Δ1-174), encircles the DNA helix and tyrosine 723 (purple) covalently binds to a 3'-phosphate (blue) of the DNA backbone (orange), which is termed Top1 cleavage complex (Top1cc). This generates a nick in one DNA backbone and allows rotation of the DNA to release supercoils. The rotation is controlled by the surrounding Top1 domains. After relaxation, the 3'-phosphate and the 5'-hydroxyl are religated and Top1 is released from the DNA. Camptothecin (CPT; red) intercalates into the DNA helix and inhibits the religation step of the Top1 reaction, thus stabilizing the Top1cc and the single strand break (best visible in the right panel). Rendering based on PDB 1T8I (Staker et al, 2005).

1.10.3 Repair of camptothecin-induced DNA damage

The stabilized Top1ccs that occur upon camptothecin treatment are substrate of a specialized repair enzyme, Tyrosyl-DNA phosphodiesterase 1 (TDP1), which hydrolyzes the 3'-phosphotyrosyl DNA bond (Yang et al, 1996).

In yeast, removal of CPT-induced Top1ccs can be mediated by a ternary complex of Wss1, Cdc48, and Doa1 (yeast homologues of DVC1/p97/PLAA; (Balakirev et al, 2015) or by the proteasome after ubiquitination of the Top1cc by a Cul3 E3 ligase (Zhang et al, 2004).

Top1ccs block DNA replication and collision of a Top1cc with a replisome can lead to replication run-off at the SSB. DNA unwinding by the replicative Mcm helicase at the nick creates a seDSB (Figure 1.6 b). A replication fork that approaches Top1ccs from the other (non-SSB) side, will be stalled and processed by the structure-specific endonuclease Mus81-Eme1, which generates seDSBs as well (Regairaz et al, 2011). ATM and DNA-PK are activated in response to CPT-induced seDSBs and the breaks are usually repaired by HRR, because no second end is available for repair via the end-joining pathways (Figure 1.6 c; reviewed in Sakasai & Iwabuchi, 2016). The already replicated part of the collapsed fork serves as template for HRR. Further, a process termed break-induced replication (BIR), in which the replication fork might restart from the D-loop, was implied for repair of seDSBs, although this has not been demonstrated for human cells (BIR reviewed in (Anand et al, 2013). Occurrence of two or more seDSBs creates dsDNA ends that can be ligated by end-joining pathways. However, HRR of each seDSB is the preferred

repair pathway and end-joining of two distal seDSBs induces chromosomal aberrations and is cytotoxic (Sakasai & Iwabuchi, 2016).

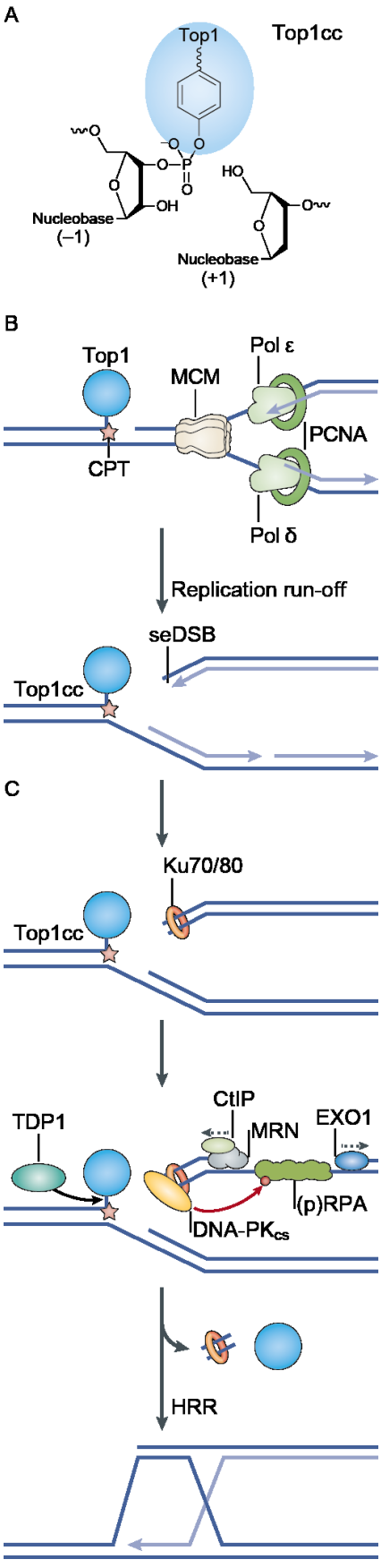

Figure 1.6: Induction and repair of Top1ccs and seDSBs

A) The topoisomerase I enzyme (Top1) binds covalently to a 3'-phospho-DNA end via a tyrosine residue (phosphodiester bond). This creates a single strand break (SSB) and a 5'-hydroxyl end. The crosslinked DNA-protein complex is termed topoisomerase I cleavage complex (Top1cc).

B) CPT-stabilized Top1ccs are replication blocks and the replicative Mcm helicase promotes the SSB into a seDSB. The replication fork runs off and the DNA polymerases (Pol δ and Pol ε) and PCNA dissociate from chromatin.

C) Ku70/80 binds to the DSB and recruits DNA-PK$_{cs}$. HRR that is initiated by the MRN complex (MRE11-Rad50-Nbs1) and CtIP facilitates the repair of seDSBs. MRE11 induced a nick in the dsDNA and resects towards the Ku-bound DNA end. RPA binds to the ssDNA and is phosphorylated (pRPA) by DNA-PK. Exonuclease 1 (EXO1) carries out long-ranged resection. CtIP flap endonuclease activity of CtIP cleaves the DNA backbone of the strand that was not resected by MRE11, which probably removes a short piece of Ku70/80-bound DNA. The Top1cc is targeted by a specialized enzyme called Tyrosyl-DNA phosphodiesterase 1 (TDP1). TDP1 cleaves the covalent bond between DNA and enzyme and Top1 is removed from chromatin. Rad51 is loaded on the resected end and HRR proceeds.

Model is based on (Gaillard et al, 2015; Pommier et al, 2016; Schwertman et al, 2016)

1.11 DNA damage and repair in disease and therapy

1.11.1 Syndromes and disorders of defective DNA repair

DNA repair is very complex and involves several hundreds of proteins. Nevertheless, mutations in a single protein can already lead to severe diseases. Several disorders of cellular DNA repair mechanisms are known and many proteins were in fact discovered and named due to their important role in the pathways. For example, Ataxia Telangiectasia, which is a rare disorder that is characterized by cerebellar neurodegeneration and immunological disorders due to mutations in the ATM kinase (Lavin et al, 2007).

A five base pair deletion in the NBS1 gene causes the rare autosomal disorder Nijmegen breakage syndrome, in which the patients suffer from a range of symptoms including radiosensitivity, immunodeficiency, and increased cancer risk (Digweed & Sperling, 2004). The functions of Nbs1 in response to DSBs can explain these symptoms.

Another example is Fanconi anemia (FA), a rare genetic disorder, in which patients suffer from physical abnormalities, bone marrow failure, and increased cancer risk. Mutations in 21 genes (FANCA-W) have been connected to the development of FA and all of them are involved in the FA pathway that repairs interstrand crosslinks (Mehta & Tolar, 2018).

The E3 ubiquitin ligase RNF168 is critical for a ubiquitination cascade in the response to DSBs and biallelic mutations in RNF168 cause the RIDDLE syndrome (radiosensitivity, immunodeficiency, dysmorphic features, and learning difficulties; Stewart et al, 2009).

Expression of mutant Huntingtin protein (Htt) was found to be associated to DSB induction in neurons and to impair DNA-PK by competitive binding to Ku70, which affects DSB repair (Enokido et al, 2010). Htt mutations are amplifications of a glutamine encoding base triplet (CAG) and cause the neurological disorder Huntington's disease, which belongs to the group of polyglutamine diseases (Caron et al, 2018).

1.11.2 Chemotherapy and targeted therapy of cancer

In the developed countries, cancer is the leading cause of death and the second leading cause in the developing countries (Jemal et al, 2011). Cancer is a neoplastic disease, in which cells are continuously proliferating and have escaped from growth regulating mechanisms (Hanahan & Weinberg, 2011). Chronic proliferation involves high rates of replication and mitosis, which requires genomic integrity. Therefore, tumor cells are particularly susceptible to DNA damage and DNA-damaging chemotherapy is widely used for the treatment of cancers. Systemic chemotherapy is in clinics since decades and has been expanded to targeted therapy, e.g. inhibiting of DDR pathways in the context of certain tumor-specific mutations (reviewed in O'Connor, 2015. Examples for a systemic chemotherapy that induces DNA damage is the administration of cisplatin. It induces intra- and interstrand crosslinks, which interferes with replication and therefore is toxic for fast replicating cells including the carcinogenic cells. Other crosslink-inducing drugs are alkylating agents, e.g. Cyclophosphamide (Emadi et al, 2009).

Side effects in healthy tissues and acquired resistance of the neoplastic tissue are limitations of these chemotherapies. In contrast to systemic therapy, targeted therapy exploits the genetic background of cancers for synthetic lethality. A famous example is the use of PARP inhibitors (e.g. olaparib) in BRCA 1/2-mutated tumors (O'Connor, 2015). Mutations in the BRCA genes lead to deficiency in HRR, which is why the cells rely on PARP for SSB repair as well as alt-EJ and are particularly susceptible to PARP inhibitors. Thus, SSBs persist and are converted into DSB during replication. Since the tumor cells have a high level of replication, they accumulate DSBs that can only be repaired with low-fidelity by NHEJ. In consequence, cells die from increasing genomic instability and DNA damage.

1.11.3 Radiotherapy

The application of ionizing radiation is another long-established therapy for tumors. The mechanism of action is again based on induction of DNA damage. The ionizations create free radicals (mainly hydroxyl radicals from water and ROS from oxygen) that react with the DNA, which generates base damage, single-, and double strand breaks. This is especially true for photon therapy (X-rays). High-LET radiation, e.g. protons, are also able to generate DSBs by direct energy transfer. This is beneficial for treatment of hypoxic tumors, because less ROS can be produced by photons. Further, radioisotopes that enrich in target tissues are used for radiotherapy, such as iodine-131 in thyroid cancer. Some tumors that cannot be resected surgically, e.g. lung cancer, benefit from radiotherapy, but there are limitations by acute and late side effects of healthy surrounding tissue, for example pulmonary fibrosis. In this respect, radiotherapy can be improved by the combination with drugs that increase either radioresistance of healthy tissues (radioprotectors) or the vulnerability of the target (radiosensitizer).

In summary, inducing DNA damage, in particular DSBs, is an important therapeutic method for cancer treatment.

1.12 Proteostasis and the Ubiquitin-Proteasome-System

1.12.1 Proteostasis

Many parameters in organisms are carefully balanced in an equilibrium, e.g. body temperature, concentration of ions, pH and oxygen content of the blood, which is collectively termed homeostasis. Cells also need to maintain a balanced level of many proteins. Thus, proteins have a limited lifespan and stochastically lose their structure or function, which is monitored by cellular protein quality control. To keep cells in a healthy state, dysfunctional proteins need to be degraded and perturbed proteostasis is connected to a variety of pathologies, e.g. neurodegenerative diseases (Hipp et al, 2014). The ubiquitin-proteasome system (UPS) facilitates, among other processes, the degradation of misfolded or damaged proteins. Proteolysis via the UPS is a targeted process and important for the regulation of many cellular processes.

1.12.2 Ubiquitin and ubiquitination

Ubiquitination is a post-translational modification with a variety of functions affecting nearly all cellular processes (reviewed in Swatek & Komander, 2016). Ubiquitin is a small protein (76 amino acids; ~8.5 kDa) that can be covalently conjugated with its C-terminal glycine to the ε-amino group of lysine residues in the target proteins. Formation of the covalent bonds is catalyzed via a three-step enzymatic cascade. First, ubiquitin is bound to the ubiquitin-activating enzyme (E1) via a thioester bond in an ATP-dependent reaction. The ubiquitin molecule is transferred to the ubiquitin-conjugating enzyme (E2) in a transthioesterification and a ubiquitin ligase (E3) is linking the E2 to the substrate, which enables conjugation of ubiquitin to the substrate. In addition, additional conjugation factors that are required for efficient polyubiquitination or modulation of the polyubiquitin chains are named E4 ubiquitin ligases. Ubiquitination is a reversible modification, as deubiquitinating enzymes (DUBs) can cleave ubiquitin from substrates. In humans, two E1 enzymes, around 40 E2 enzymes, more than 600 E3, and around 100 DUBs are known, which points out the participation in a large variety of processes and the importance of the ubiquitin system. Ubiquitin itself has seven lysine residues (K6, K11, K 27, K29, K33, K48, and K63) as well as the N-terminal methionine residue (M1) that can all be used for conjugation, which yields a variety of linkage types. A substrate can be monoubiquitinated or modified with ubiquitin chains that are built by conjugation of several ubiquitin molecules. Depending on the linkage type, the chains are homo- or heterotypic, and the chains can additionally be branched. Further, substrates can be modified at multiple sites. The different forms of protein ubiquitination have been implicated in distinct physiological functions. One of the best-characterized functions is signaling for proteasomal degradation by K11- and K48-linked polyubiquitin chains. Moreover, ubiquitin can be phosphorylated and acetylated, which adds even more complexity to ubiquitin signaling.

Ubiquitination is also important on chromatin and in DNA repair processes, as described below in 1.15.

1.12.3 The proteasome and proteolytic degradation

The 26S proteasome is a large enzyme complex (~2500 kDa) conserved in eukaryotes that is assembled of the barrel-shaped 20S core particle and one or two 19S regulatory particles, which cap the 20S cylinder at the ends (reviewed in Rousseau & Bertolotti, 2018). Proteolysis takes place inside the 20S particle and access to this chamber is controlled to achieve regulated degradation.

With some exceptions, substrates for proteasomal degradation are ubiquitinated and ubiquitin can be recognized directly by three proteasome subunits or shuttling factors that escort the substrate to the proteasome. Deubiquitinases are associated to the proteasome and deubiquitination is connected to substrate degradation.

1.13 The p97-system

1.13.1 The AAA+-ATPase VCP/p97

The human p97, also known as valosin-containing protein (VCP), and its homologs (Cdc48 in yeast and plants, CDC-48 in worms (cell division cycle protein 48); Ter94 in flies (transitional endoplasmic reticulum ATPase)) are highly conserved enzymes. p97 is abundant in the nucleoplasm and the cytoplasm and essential for a range of cellular functions (reviewed in van den Boom & Meyer, 2018). It belongs to the group of AAA+ ATPases (ATPases associated with diverse cellular activities) and uses energy from ATP hydrolysis to generate a mechanical force for structural remodeling, i.e. unfolding, of its substrate proteins. This facilitates extraction from cellular structures like membranes, chromatin, or protein complexes. The substrates of p97 are ubiquitinated proteins and a range of bi-functional adaptors, which can bind to p97 and to ubiquitin, enable substrate recognition. p97 has further cofactors that include ubiquitin ligases and deubiquitinases. Endoplasmic reticulum-associated degradation (ERAD), mitochondria-associated degradation (MAD), chromatin-associated degradation (CAD), protein degradation by the ubiquitin proteasome system (UPS), autophagy, mitophagy, DNA replication, DNA repair, membrane fusion, NF-κB activation, cell cycle regulation, and mitosis are cellular processes for which p97 functions were reported (reviewed in Stach & Freemont, 2017; van den Boom & Meyer, 2018).

p97 has two ATPase domains, named D1 and D2, an N-terminal domain (N), and an unstructured C-terminal part (Figure 1.7). p97 forms stable homohexamers, in which the ATPase domains form two stacked rings with a central channel. The position of the N-domain depends on the bound nucleotide in the D1 domain. In an ADP-bound state, the domain is in a “down” conformation in plane with the D1 domain and the domain is in an “up” conformation in an ATP-bound state (Banerjee et al, 2016). The D1 domain is especially important for the hexamer formation while the D2 domain contributes more to ATP hydrolysis (Song et al, 2003). Nevertheless, the N-domain, flexibility of the ND1 linker and the disordered C-terminal region are required for full ATPase activity (Niwa et al, 2012). ATP hydrolysis and the connected conformational changes probably occur asymmetrically (Tang & Di Xia, 2016). The protomers are in close contact and an interprotomer signaling network is connects ATP binding to opening and closing of the central pore (Hänzelmann & Schindelin, 2016).

p97 itself is regulated by PTMs like phosphorylation and acetylation (Mori-Konya et al, 2009). The modifications can alter cellular localization, association with substrates, and activity of p97 (Madeo et al, 1998; Klein et al, 2005; Li et al, 2008). Specifically in response to DNA damage, p97 is phosphorylated by DNA-PK at serine 784 (Livingstone et al, 2005).

Mutations in p97 cause degenerative disorders that are collectively termed multisystem proteinopathy 1 (Taylor, 2015). Six mutations were found in the first report that linked p97 to the

diseases (Watts, Giles D J et al, 2004) and currently 54 different mutations have been reported (Inoue et al, 2018).

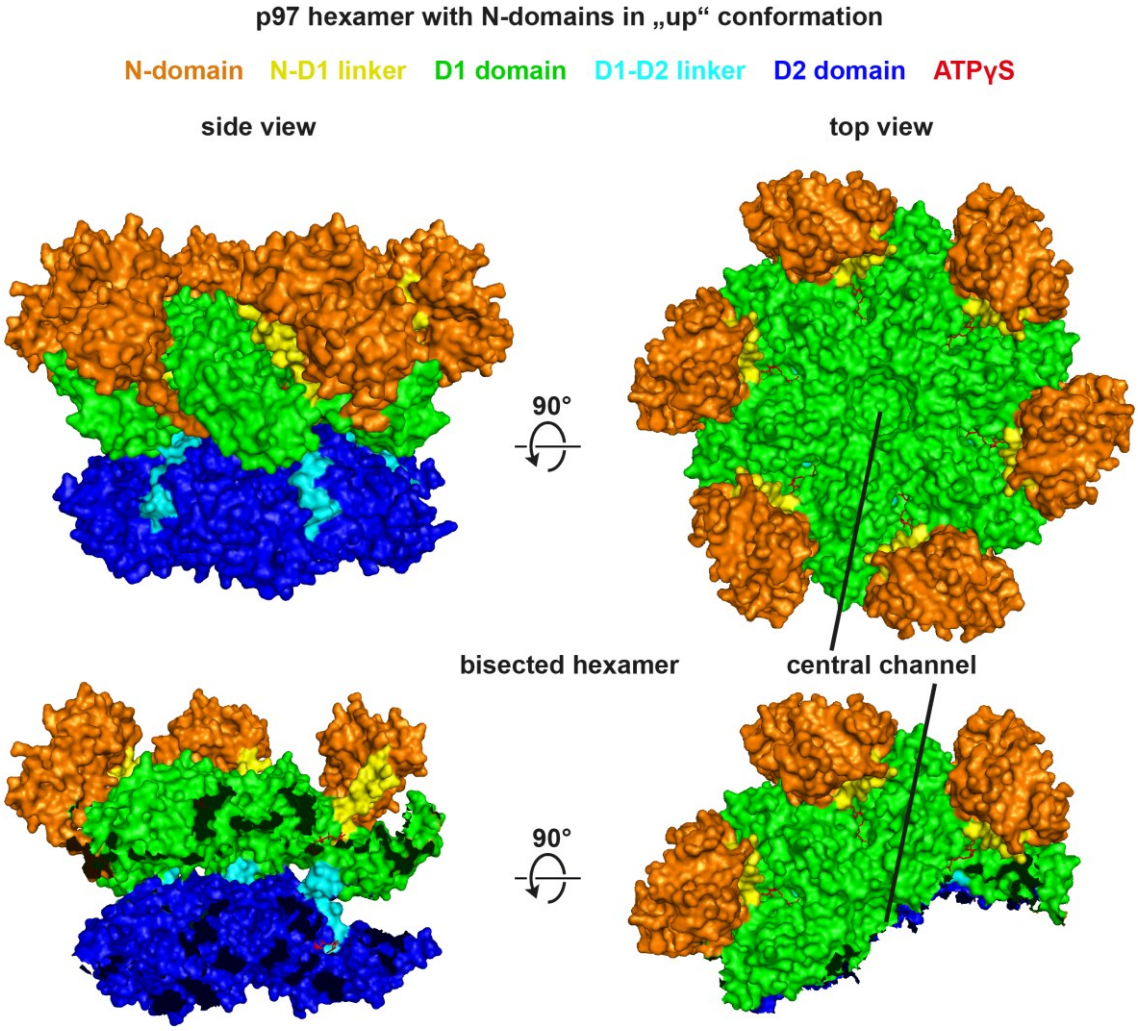

Figure 1.7: Structure of the AAA+ ATPase p97
p97 forms homohexamers, in which the two ATPase domains D1 (green) and D2 (dark blue) that are connected by a short linker (light blue) form stacked rings. The flexible N-domain (orange) arranges coplanar with the D1 ring when ADP is bound in D1 or, as shown here, twisted upwards upon ATP binding (ATPγS is shown in the D1 and D2 domain; red). The N domain is connected to the D1 domain via a flexible linker (yellow) that allows the movement. Each protomer interacts with its neighbors at multiple points (shadows in the bisected view), which coordinates interprotomer signaling that is important for the ATP hydrolysis cycle. The hexamer forms a central channel and substrates of p97 are probably unfolded by threading through this channel. Most cofactors of p97 bind to the N-domain and most disease-associated mutations are located in and around the ND1-linker. Rendering is based on PDB 5FTN (Banerjee et al, 2016).

The mechanism of substrate processing remained elusive for long time. The movements of the N-domain and processing in the central channel, either by partial insertion or by full threading, have been discussed. Recently, major contributions to the understanding of p97 substrate processing were made. Bodnar & Rapoport provided strong evidences for a mechanism, in which the substrates are translocated through the central channel of the hexamer (Bodnar & Rapoport, 2017). This process involves substrate unfolding, (partial) deubiquitination of the branching

ubiquitin chains to make the substrate fit through the pore, and depends on the Ufd1-Npl4 cofactor. Additionally, Blythe et al. described substrate unfolding by a complex of p97 with Ufd1-Npl4 (Blythe et al, 2017).

1.13.2 Cofactors and substrate adaptors

p97 interacts with a set of ~30 cofactors and adaptors that provide spatiotemporal regulation of p97. They form different functional complexes to achieve various functions at different cellular locations. All have p97-interacting domains or motifs and most can also bind to ubiquitin (Meyer & Weihl, 2014). The different p97 complexes have distinct functions and their assembly is highly dynamic (Xue et al, 2016).

Ufd1-Npl4

Ufd1 (ubiquitin fusion degradation 1; Johnson et al, 1995) and Npl4 (nuclear protein localization 4; DeHoratius & Silver, 1996) form a heterodimer that interacts with p97 (Meyer et al, 2000) and mediates the binding to polyubiquitinated proteins (Meyer et al, 2002). One heterodimer of Ufd1-Npl4 binds to one homohexamer of p97 (Pye et al, 2007; Bodnar et al, 2018). Ufd1 and Npl4 can both bind to the N-domains of p97 in different conformations (Bebeacua et al, 2012). Npl4 has an N-terminal UBX-like domain (UBX-L) that mediates binding to p97 and a C-terminal NZF domain (Npl4 zinc finger) that binds to ubiquitin. The N-terminal UT3 domain of Ufd1 can bind mono- and polyubiquitin and a SHP box motif allows binding to p97. However, structural data suggest that general binding is mediated by UBX-L of Npl4, which localizes the heterodimer preferentially on top of the ND1 ring (Bodnar et al, 2018). Ufd1-Npl4 is one of the best-characterized cofactors and was linked to several pathways, e.g. the extraction of substrates from chromatin (described in 1.14) and ERAD (Ye et al, 2003).

FAF1

FAF1 was first described as a proapoptotic factor of Fas-mediated apoptosis (Chu et al, 1995) and to be member of the Fas death-inducing signaling complex (Ryu et al, 2003). The heat-shock protein 70 ATPase inhibits the interaction of FAF1 with Fas by competitive binding and thereby counteracts the proapoptotic function of FAF1 (Gao et al, 2015). Diverse functions of FAF1 have been reported, mainly independent of p97. FAF1 inhibits tumor formation (Lee et al, 2012) and mutations or genomic loss of FAF1 were connected to oncogenesis (Menges et al, 2009; Weber, 2015). The protein has been implied in dopaminergic neurodegeneration, in which FAF1 accumulates and activates PARP1-dependent necrosis (Sul et al, 2013; Yu et al, 2016).

Either a trimer of FAF1 binds to the p97 hexamer (Ewens et al, 2014) or one FAF1 molecule binds to the p97 hexamer in a quaternary complex with Ufd1-Npl4 (Hänzelmann et al, 2011; Lee et al, 2013). Reported functions of p97-FAF1 are ERAD, shown with the model substrate CD3δ and Ufd1-Npl4 as further factors of the complex (Lee et al, 2013). Upon perturbed replication termination, FAF1 has a role in CAD (Franz et al, 2016; described in 1.14).

Other cofactors

The p97 cofactor DVC1 (also known as Spartan or C1orf124; Wss1 in yeast) has functions on chromatin (described in 1.14). Among the p97 cofactors are three DUBs: YOD1, VCIP135, and Ataxin3. Although p97 substrates are ubiquitinated and p97 cofactors recognize ubiquitin, deubiquitination is an important process for p97 activity. Deubiquitination of substrates by p97-associated DUBs has been connected to ERAD (YOD1 and Ataxin3; Liu & Ye, 2012), lysophagy (YOD1; Papadopoulos et al, 2017), the DDR (Nishi et al, 2014; see 1.15) and, as mentioned above, the threading mechanism of p97 unfolding activity requires deubiquitination (YOD1 orthologue Otu1; Bodnar & Rapoport, 2017).

1.13.3 Diverse cellular functions of p97

p97 is involved in a variety of cellular processes. It has a central role in the ubiquitin-proteasome system, in which it binds ubiquitinated substrates and facilitates their proteasomal degradation. One example for p97 function in cellular proteostasis is constant turnover of the hypoxia-inducible factor α (HIF1 α). The p97 cofactor UBXD7 binds to the E3 ubiquitin ligase $CRL2^{VHL}$ that modifies HIF1α and recruits p97. The ATPase targets HIF1α to the proteasome for degradation (Alexandru et al, 2008).

Another cellular pathway to remove damaged proteins and larger cargo is autophagy and p97 is involved in autophagy, which was first identified by accumulation of autophagosomes in muscles of patients with multisystem proteinopathy 1 (Ju et al, 2009). p97 activity is required for selective autophagy of mitochondria (Tanaka et al, 2010) and damaged lysosomes (Papadopoulos et al, 2017).

The potential to extract proteins from membranes involves p97 in ERAD and MAD. In ERAD p97 function drives retrotranslocation of the misfolded proteins from the ER lumen to the cytosol, where they are ubiquitinated and get degraded by the proteasome (Stolz et al, 2011).

p97 participates in cell cycle progression at several steps. It has functions in replication (described in 1.14) and during mitosis. Entry into mitosis is controlled by the G_2/M checkpoint, which ensures that any DNA damage is repaired before mitosis starts. Activation of the checkpoint by ATM/ATR signaling involves proteasomal degradation of CDC25A that is ubiquitinated by $SCF^{\beta TrCP}$ and a complex of p97-Ufd1-Npl4 facilitates the delivery to the proteasome (Riemer et al, 2014). p97 was shown to oppose activity of the mitotic kinase Aurora B in yeast, frogs, and worms. In yeast, p97 facilitates nuclear localization of Glc7/PP1 to antagonize Aurora B (Cheng & Chen, 2010). In *Xenopus* egg extracts and *C. elegans* embryos, p97 extracts Aurora B from chromatin at the end of mitosis, which inactivates the kinase and enables reformation of the nuclear envelope (Ramadan et al, 2007). Further, spindle disassembly at the end of mitosis is also regulated by p97 (Cao et al, 2003).

1.14 Functions of p97 on chromatin and in DNA repair

p97 has been established as factor of DSB repair in previous studies. Meerang et al. introduced p97 as a factor of the DSB response downstream of the E3 ligase RING finger protein 8 (RNF8), but in parallel to RNF168. p97 was specifically recruited to K48-linked ubiquitin chains by Ufd1-Npl4. Segregation of polyubiquitinated substrates was proposed, but they remained unidentified. Recruitment of the important repair factors 53BP1, BRCA1 and Rad51 was shown to depend on functional p97 and established the ATPase as regulator of the ubiquitin-dependent mechanisms of DSB repair (Meerang et al, 2011).

The mechanism of 53BP1 recruitment was described shortly after. A complex of p97 and Ufd1-Npl4 facilitates the ubiquitin-dependent removal of the Polycomb protein L3MBTL1 from the H4K20me2 histone modification. 53BP1 binds to the same histone mark, but with lower affinity, and displacement of L3MBTL1 enables its binding to chromatin. In contrast to the other study, RNF8 and RNF168 were required for the p97-mediated extraction (Acs et al, 2011). However, further substrates in the DSB repair pathways that could explain all observed phenotypes of compromised p97 were unknown.

In budding yeast, Cdc48 together with Ufd1 was found to regulate assembly of Rad51 filaments. Yeast Ufd1 has a SUMO-interacting motif (SIM) and is targeted to SUMOylated Rad52, which is the Rad51 loader in yeast. This function counterbalances Rad51 filament formation and thereby regulates HRR. The same mechanism was hypothesized for mammalian cells. However, mammalian Ufd1 possesses no SIM and BRCA2, instead of Rad52, facilitates nucleoprotein filament formation (Bergink et al, 2013).

Further, p97 was implicated in extraction of proteins from chromatin in other processes. As mentioned above, p97 has functions at the end of mitosis. A complex of p97 and Ufd1-Npl4 extracts the polyubiquitinated Aurora B from chromatin, which inactivates the kinase and enables chromosome decondensation and formation of the nuclear envelope membrane (Ramadan et al, 2007).

Ubiquitinated DNA-PK_{cs} is targeted by p97, which regulates the proteasome-mediated degradation of the kinase. Thus, p97 regulates the amount of a central NHEJ protein and influences the DSB repair capacity. Low p97 expression correlated with reduced survival of mice with xenografted glioblastomas that were treated with radiotherapy. A significant correlation of p97 expression in tumor tissue and patient survival was also found in glioblastoma patients (Jiang et al, 2013).

In yeast, Cdc48 and the cofactor Ubx3 are involved in transcription-coupled chromatin remodeling by controlling H2B monoubiquitination. The monoubiquitination is catalyzed by the E3 ligase Bre1 and Cdc48 controls recruitment of the Bre1 cofactor Lge1 (Bonizec et al, 2014).

During interstrand crosslink repair by the Fanconi anemia pathway, one of the first steps is unloading of the CMG helicase. p97-mediated extraction of K48-ubiquitinated Mcm7 was shown to be the underlying mechanism of helicase unloading and independent of proteasomal degradation (Fullbright et al, 2016).

Exposure to UV irradiation induces turnover of the RNA polymerase II subunit Rpb1 in yeast, especially at sites of stalled transcription. Cdc48 together with its cofactors Ufd1-Npl4, Ubx5 (UBXD7 in human), and Ubx4 (UBXD9 in human) facilitates the segregation and subsequent proteasomal degradation of Rpb1 (Verma et al, 2011).

UV-induced DNA damage is predominantly repaired by global-genome NER. DDB2 and XPC are two factors that function as damage sensors in this pathway and are ubiquitinated by Cul4A in response to UV irradiation. Both factors are segregated from chromatin by p97 in complex with Ufd1-Npl4 and UBXD7. The report further noticed that retention of the repair factors is genotoxic, highlighting the importance of p97-mediated spatiotemporal regulation of DNA repair mechanisms (Puumalainen et al, 2014).

Several studies reported a role of p97 in replication and replication-associated processes. Degradation of the replication licensing factor CDT-1 and the histone methyltransferase SET8 in response to UV-induced DNA damage is facilitated by p97 and Ufd1, subsequent to CDT-1 and SET8 ubiquitination by $CRL4^{CDT2}$ (Raman et al, 2011). In addition, CDT-1 is a substrate of CAD that is mediated by a complex of p97, Ufd1-Npl4, and FAF1. Degradation of CDT-1 leads to dissociation of Cdc-45/GINS from chromatin and contributes to efficient replication fork progression (Franz et al, 2011; Franz et al, 2016).

DVC1 is a DNA-dependent metalloprotease involved in DNA-protein crosslink repair. DVC1 is especially active on ssDNA, binds to the replisome, and cleaves replication-blocking DPCs, which prevents replication fork stalling (Stingele et al, 2016; Vaz et al, 2016). DVC1 also binds to PCNA in post-replication repair (Ghosal et al, 2012). p97, together with Ufd1-Npl4, is recruited to sites of replication stress or DNA damage by DVC1 in an ubiquitin-dependent response. It was suggested that p97-Ufd1-Npl4 extracts the TLS Polymerase eta (Pol η; Davis et al, 2012; Mosbech et al, 2012).

Like in interstrand crosslink repair, p97 extracts the CMG helicase from chromatin in the process of replication termination. Mcm7 is polyubiquitinated with K48-linked chains at the end of DNA replication (Moreno et al, 2014). The ubiquitin ligase SCF^{Dia2} promotes this ubiquitination in yeast and Cdc48-mediated Mcm7 extraction destabilizes the whole CMG helicase, which rapidly leads to its disassembly (Maric et al, 2014). In addition, Mcm7 was found to be ubiquitinated specifically on K29 and the Cdc48 cofactor Ufd1-Npl4 required for disassembly of CMG helicase (Maric et al, 2017). In *Xenopus* and *C. elegans*, the E3 ligase for Mcm7 ubiquitination is $CRL2^{Lrr1}$ (Dewar et al, 2017; Sonneville et al, 2017). An interesting observation was made in *C. elegans*. If CMG persist on chromatin, e.g. upon loss of $CRL2^{Lrr1}$, a mitotic pathway that depends on CDC-48 and

UBXN-3 (the orthologue of FAF1) removes the helicase instead of CDC-48, UFD-1, and NPL-4 (Sonneville et al, 2017).

1.15 Functions of ubiquitin system on chromatin and in DNA repair

Ubiquitination at sites of DSBs orchestrates DSB repair and ubiquitin signaling regulates the cellular DDR (reviewed in Schwertman et al, 2016; Figure 1.8). Many substrates of ubiquitination as well as ubiquitin ligases of the DSB repair pathways are known. A key role of ubiquitination is the regulation of protein-protein or protein-DNA interactions that allows specific recruitment of repair factors and cell cycle-dependent repair pathway choice. The various functions of ubiquitination in DSB repair mainly depend on the chain type. K63-linked polyubiquitin is important for the modulation of protein interactions. K11- and K48-linked ubiquitin chains are signals for extraction from chromatin and for protein degradation.

The RNF8-RNF168 pathway is a well-described and important ubiquitination pathway of the DDR and p97 was shown to be involved in that pathway (Meerang et al, 2011). The ubiquitination of histone H2A(X) by RNF8 is critical for recruitment of important repair factors, e.g. 53BP1 and BRCA1 (Mailand et al, 2007). RNF8 itself is recruited to DSBs by binding to MDC1 that was phosphorylated by the DSB kinase ATM. RNF8 ubiquitinates the linker histone H1, which recruits RNF168 (Thorslund et al, 2015). The E3 ligases RNF8 and subsequently RNF168 cooperate with the E2 enzyme UBC13 to form K63 chains. In addition to K63 chains, RNF168 also forms atypical K27-linked ubiquitin chains on histone H2A, which activates the DDR signaling and is bound by 53BP1 and other repair factors (Gatti et al, 2015).

1.15.1 Ubiquitination of Ku and Nbs1

Postow et al. first described DSB-induced Ku80 ubiquitination in *Xenopus* egg extracts and that it leads to Ku80 removal from DNA (Postow et al, 2008). The first E3 ligase identified to ubiquitinate Ku80 was RNF8 (Feng & Chen, 2012). RNF8 modifies Ku80 with K48-linked polyubiquitin chains, which promotes Ku80 turnover. Further, it ubiquitinates the MRN complex component Nbs1, which promotes HRR (Lu et al, 2012). Several other E3 ligases participate in DSB repair and additional ligases for ubiquitination of Nbs1 and Ku80 have been identified. Nbs1 is modified with K63-linked ubiquitin by the E3 ligase Skp2 and this recruits the kinase ATM (Wu et al, 2012). RNF138, an E3 ligase that is recruited to ssDNA after initial end resection, is ubiquitinating Ku80, which triggers Ku removal from the DNA end and promotes repair via the HRR pathway (Ismail et al, 2015). Interestingly, the study determined cell cycle-depended activity of the E3 ligases. More specifically, RNF138 ubiquitinates Ku80 preferentially in S and G_2 phase of the cell cycle and RNF8 in G_1 phase. For this, RNF138 cooperates with the E2 enzyme UBE2D (Schmidt et al, 2015). In Xenopus, the SCF^{FBXL12} complex ubiquitinates Ku80 upon DNA binding (Postow & Funabiki, 2013). Further, a complex of the E2 enzyme UBE2D3 and the E3 ligase RNF126 ubiquitinates Ku80 to release Ku from DSBs and complete NHEJ (Ishida et al, 2017).

LC-MS/MS analysis identified ubiquitination of 25 lysine residues of Ku80 and mutation of 19 surface-exposed lysine residues to arginine strongly reduced, but did not abolish, Ku80 ubiquitination (Ishida et al, 2017). In contrast to ubiquitin-triggered Ku80 removal, yeast Ku70 is SUMOylated, which increases the association with DNA (Hang et al, 2014).

The E2-E3 complex UBE2D-RNF138 also promotes CtIP ubiquitination (Schmidt et al, 2015). In contrast to removal of ubiquitinated Ku, ubiquitination of CtIP leads to elevated CtIP levels at DSBs. Conversely, CtIP ubiquitination by APC/C^{Cdh1} leads to degradation, which is the mechanism to downregulate CtIP and thus block HRR outside of S and G_2 phase (Lafranchi et al, 2014).

Another important ubiquitin ligase of the DSB repair system is BRCA1, a factor that promotes HRR. The E3 ligase can form K48-linked chains together with the E2 enzyme UBE2K, K63-linked chains in cooperation with UBC13/MMS2, or K6-linked chains with UBCH5 (Ohta et al, 2011). This variability enables BRCA1 to regulate HRR at various steps. The E4 ligase UBE4A adjusts the initial K48- and K63-linked polyubiquitin chains at DSB sites to regulated end resection and to favor HRR over mutagenic alt-EJ (Baranes-Bachar et al, 2018). Localization of BRCA1 to DSBs itself is regulated by ubiquitination in a cell cycle dependent manner, which represents a key mechanism of HRR inhibition in G_1 (Orthwein et al, 2015). The E3 ligase $CRL3^{KEAP1}$ ubiquitinates PALB2, the localizer of BRCA2, which interrupts the interaction of PALB2 and BRCA1 and thereby suppresses HRR.

The single strand binding protein RPA is ubiquitinated by RFWD3 at stalled replication forks (Elia et al, 2015), during interstrand crosslink repair (Feeney et al, 2017), and the RFWD3-mediated removal of RPA and also Rad51 from DSBs is promoting HRR (Inano et al, 2017). Ubiquitination of RPA by the E3 ligase PRP19 leads to recruitment and accumulation of ATRIP, which in turn activates the DDR kinase ATR (Maréchal et al, 2014).

Deubiquitination counteracts the formation of ubiquitin chains and is important to balance the regulatory functions of ubiquitination in DSB repair. A screening approach revealed that many DUBs localize to sites of DSBs and participate in the repair processes (Nishi et al, 2014). The three p97-interacting DUBs VCIP135, YOD1, and Ataxin3 localized to the DNA damage site in laser microirradiation experiments, but loss of the DUBs did not result in repair defects in neutral comet assay. The DUB USP7 that deubiquitinates XPC and thereby prevents its p97-mediated degradation during NER, which was mentioned above (He et al, 2014). The DUB USP4 is a positive regulator of the initial end resection processes in HRR and directly binds to CtIP and via Nbs1 to the MRN complex (Liu et al, 2015; Wijnhoven et al, 2015). The DUB autodeubiquitinates to localize to DSB sites and the recruitment of CtIP to MRN is regulated by USP4. USP11 deubiquitinates PALB2 in G_2 and thereby enables BRCA1 localization and HRR (Orthwein et al, 2015).

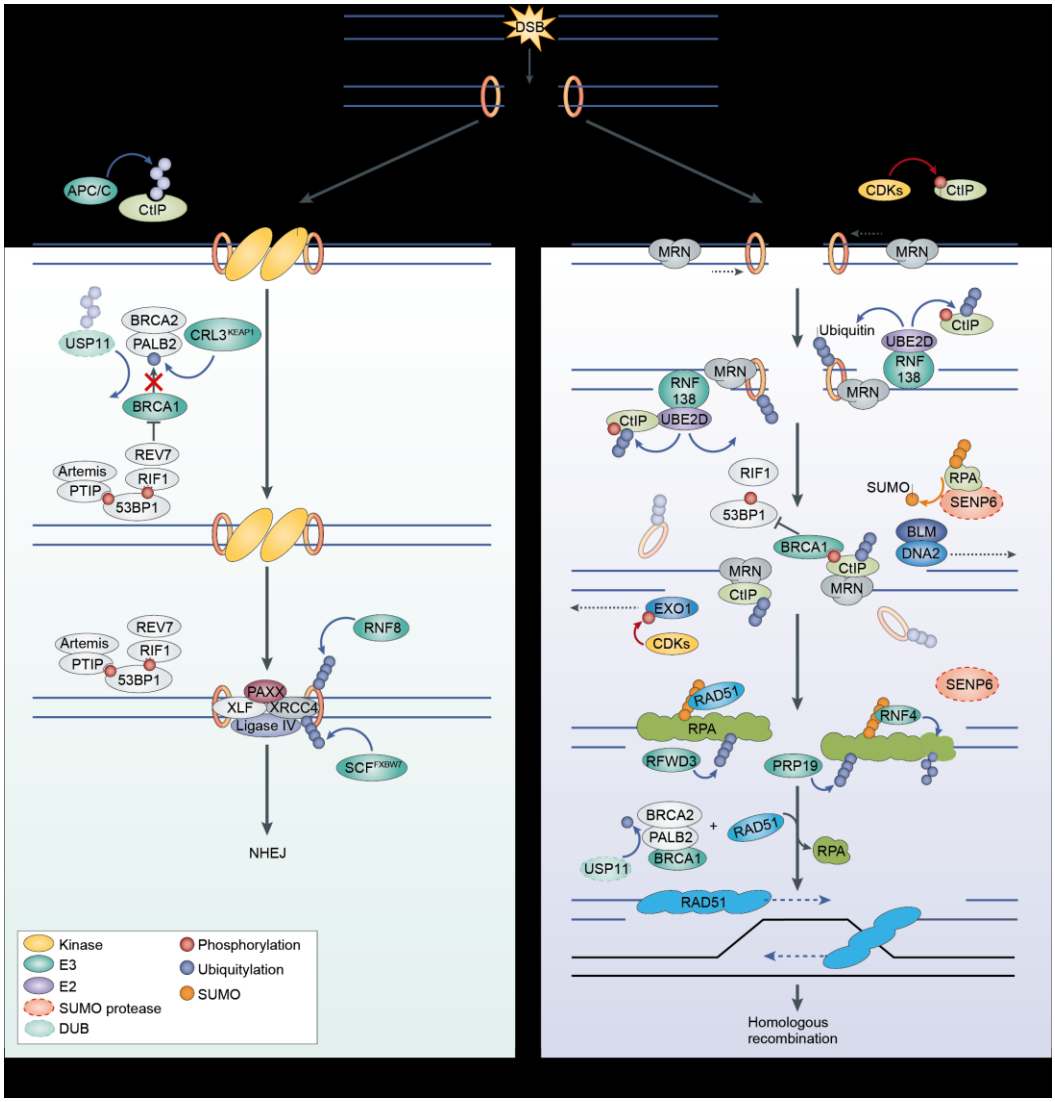

Figure 1.8: Model of post-translational modifications in DSB repair and pathway choice
DSB repair is a highly regulated process and the ubiquitin system is an important regulator. Depicted is ubiquitin-dependent signaling for NHEJ, HRR, and the choice between the pathways. NHEJ functions throughout the cell cycle, but HRR needs to be repressed in G_1 phase of the cell cycle, because no sister chromatid is available for recombination.
53BP1 antagonizes HRR through inhibition of BRCA1 recruitment. Therefore, 53BP1 forms a complex with RIF1 that binds the BRCA1-antagonizing factor REV7 and PTIP that binds the NHEJ nuclease Artemis. PALB2 localizes BRCA2 to DSBs and is ubiquitinated by a CRL3-KEAP1 complex, which prevents interaction with BRCA1 and thus HRR. The DUB USP11 that counteracts the PALB2 ubiquitination is ubiquitinated and degraded in G_1. In addition, CtIP is degraded upon ubiquitination by the anaphase-promoting complex. The NHEJ protein Ku80 is ubiquitinated by RNF8 in G_1 and in *X. laevis* by SCF^{FBXL12}. In S and G_2 phase, cyclin-dependent kinases phosphorylate and thereby activate CtIP and EXO1. The activation of nucleases promotes end resection and thus HRR. After initial end resection by the MRN complex, the E3 ligase RNF138 is recruited to ssDNA and, together with the E2 conjugating enzyme UBE2D, ubiquitinates Ku80 and CtIP. Ubiquitination of Ku80 promotes Ku release from DSBs. In contrast, CtIP ubiquitination enhances its retention at DSBs. BRCA1 binds to the site of the DSB via CtIP and excludes RIF1 and 53BP1 from the DNA. The single strand binding protein RPA is ubiquitinated by the E3 ligases RFWD3 and PRP19 to promote HRR. RPA70 is SUMOylated and this modification is elevated upon DSB induction, based on displacement of the SUMO protease SENP6 that usually removes SUMO from RPA. Rad51 and the STUbL RNF4 are recruited to SUMOylated RPA and RNF4 mediates the turnover of RPA, which promotes Rad51 filament formation and thereby HRR. Rad51 is loaded by BRCA2 that localized to BRCA1 via PALB2 and the interaction of this complex is enhanced by deubiquitination of PALB2 by USP11 in S/G_2. Figure from (Schwertman et al, 2016).

Besides ubiquitination, post-translational modifications with the small ubiquitin-like modifier (SUMO) are involved is DSB repair processes. SUMOylation of the NHEJ factor XRCC4 on K210 is required for nuclear localization of the protein (Yurchenko et al, 2006). SUMOylation regulates chromatin-modifying enzymes in response to DNA damage with positive, i.e. recruitment to damage sites, and negative, i.e. SUMO-induced degradation, effects (Hendriks et al, 2015).

The highly conserved ubiquitin E3 ligase RNF4 possesses a SUMO interaction motif (SIM) and belongs to the group of SUMO-targeted ubiquitin ligases (STUbLs). RNF4 is recruited to SUMOylated MDC1 and required for efficient HRR (Yin et al, 2012). RNF4 was found to control the amount of the Fanconi Anemia ID complex in interstrand crosslink repair (Gibbs-Seymour et al, 2015). Further, the mechanism of RNF4 recruitment and function in the FA pathway is an ideal example of the interplay of different PTMs in DNA repair. FANCI and FANCD2 form a complex (ID complex) that is phosphorylated by ATR in response to DNA damage. The phosphorylation triggers monoubiquitination of the ID complex by the FA core complex and the E2 enzyme UBE2T. Monoubiquitination licenses the ID complex for PIAS1/4-mediated SUMOylation and the STUbL RNF4 in turn recognizes the SUMO chains. RNF4 synthesizes polyubiquitination of the ID complex that is subsequently extracted by p97 in complex with DVC1. To fine-tune the regulation, the PTMs can be reversed and the DUB USP1 was found to antagonize ID monoubiquitination and the SUMO protease SENP6 cleaves SUMO chains from the complex.

1.16 Targeting of p97 and the UPS in research and therapy

p97 is upregulated in a number of cancers and high expression levels correlate with poor prognosis, e.g. in colorectal carcinomas (Yamamoto et al, 2004c), prostate cancer (Tsujimoto et al, 2004), non-small-cell lung carcinoma (Yamamoto et al, 2004b), and esophageal carcinoma (Yamamoto et al, 2004a). The reason of increased p97 expression in tumors is most likely a response to proteotoxic stress, which is caused by the abundance of misfolded proteins resulting from fast cellular growth in the context of a high mutational burden. Therefore, p97 is a potential target p97 for therapy, in which a decrease of protein degradation capacity is specifically toxic for cancerous cells. Small-molecule inhibitors of p97 were developed and shown to have antitumor effects. The non-competitive inhibitor NMS-873 (Magnaghi et al, 2013) and the competitive inhibitor CB-5083 (Anderson et al, 2015) were the most promising candidates, but they failed in clinical trials. Still, the inhibitors are a valuable tool for research and in this study both, NMS-873 and CB-5083, were used to block p97 function in cell culture experiments. In contrast, a significant correlation of low p97 expression and decreased survival was found in glioblastoma patients (Jiang et al, 2013). p97-mediated turnover of DNA-PK_{cs} was suggested as underlying mechanism.

Targeting mechanisms of proteostasis for cancer treatment can also be achieved by inhibition of the proteasome and the small-molecule inhibitor bortezomib is approved for treatment of multiple

myeloma and mantle cell lymphoma (reviewed in Deshaies, 2014). Other proteasome inhibitors were developed much earlier (reviewed in Lee & Goldberg, 1998) and in this study MG132 was used to block the proteasome function.

1.17 The aims of the thesis

At the starting point of this thesis, the ATPase p97 was found as a ubiquitin-directed segregase in the DSB repair pathways NHEJ and HRR (Meerang et al, 2011). This constituted a new molecular mechanism in the regulation of the two major DSB repair pathways. The aim of this thesis was to contribute on the one hand to the understanding of p97 physiology, with implications for p97 as a potential cancer target, and on the other hand to characterize p97 as a regulator of DSB repair.

The main focus was set on the analysis of the essential NHEJ protein Ku80 as potential p97 target for two reasons. First, Ku80 was described to be ubiquitinated with K48-linked chains in in vitro experiments (Postow et al, 2008) and K48-Ub is a modification that is targeted by p97 complexes. Second, Ku80 was identified as promising candidate in an in vitro mass spectrometry assay of our lab. The experiments of this thesis were performed in cells to complement and extend the results of the in vitro experiments. Recently described visualization techniques were applied to address the challenge of DSB-specific analysis of Ku80 (Britton et al, 2013). In addition, the goal was to describe the involved p97 cofactors. The experiments focused on Ufd1-Npl4 and FAF1, which were described as p97 cofactors on chromatin and were identified as potential cofactors in the mass spectrometry assay.

Further, the aim was to clarify whether Ku80 extraction is the possible basis for the role of p97 in HRR, as this repair pathway is blocked by Ku80. To test this hypothesis, DNA damage was induced with the topoisomerase I inhibitor camptothecin, which creates lesions that are specifically repaired by HRR. Finally, we set out to analyze Topoisomerase I cleavage complexes that are stabilized by CPT as potential p97 substrates.

2 Results

Previous studies showed that the essential ATPase p97 is involved in NHEJ and HRR, the most important DSB repair pathways. However, the underlying mechanisms were unknown. We therefore wanted to clarify the role of p97 in DSB repair by identifying its substrates at these lesions.

In a candidate approach, we investigated the essential NHEJ protein Ku80 as potential p97 target. Ku80 is a unique repair factor as it gets sterically trapped on chromatin during NHEJ repair and its removal requires unfolding of the protein. Another hint that led to the hypothesis were reports on Ku80 ubiquitination by K48-linked chains, a post-translational modification that is typical for p97 substrates.

In parallel to this study, experiments on Ku80 segregation by p97 were performed in *Xenopus laevis* egg extracts by J. van den Boom (see van den Boom et al, 2016). The first strong indication that p97 is involved in Ku80 extraction was obtained from mass spectrometry experiments. These results showed that Ku80 accumulates on DSBs upon p97 inhibition.

The results presented here focused on cell-based assays to gain evidence for p97-governed Ku80 extraction in living cells.

2.1 Visualization of DSB-bound Ku80

A prerequisite for analyzing Ku80 extraction by p97 in cells was to establish a visualization technique of DSB-bound Ku80 for microscopy experiments. Standard immunofluorescence staining was not suitable for visualization of DSB-bound Ku80, because Ku70/80 are abundant in the nucleus and also bind to RNA at specific sequences or via a C-terminal domain (Yoo & Dynan, 1998; Peterson et al, 2001). In 2013, Britton et al. had published a new method for imaging of Ku in U2OS cells (Britton et al, 2013) that was adopted for this study. The method utilizes enzymatic RNA digestion prior to fixation of the samples. The digestion enables washout of RNA-bound Ku, thereby leaving only the DSB-bound fraction of the protein.

To optimize this preextraction technique, a comparison of Ku80 binding to DSB sites and undamaged chromatin under identical conditions was required. Therefore, laser microirradiation was established and applied (see model in Figure 2.1 A). For laser microirradiation, the laser of a confocal spinning disc microscope was used to irradiate a precisely defined sub-nuclear area in living cells. DSBs induced by this technique allow a comparison of Ku80 binding to damaged and undamaged chromatin within the same nucleus.

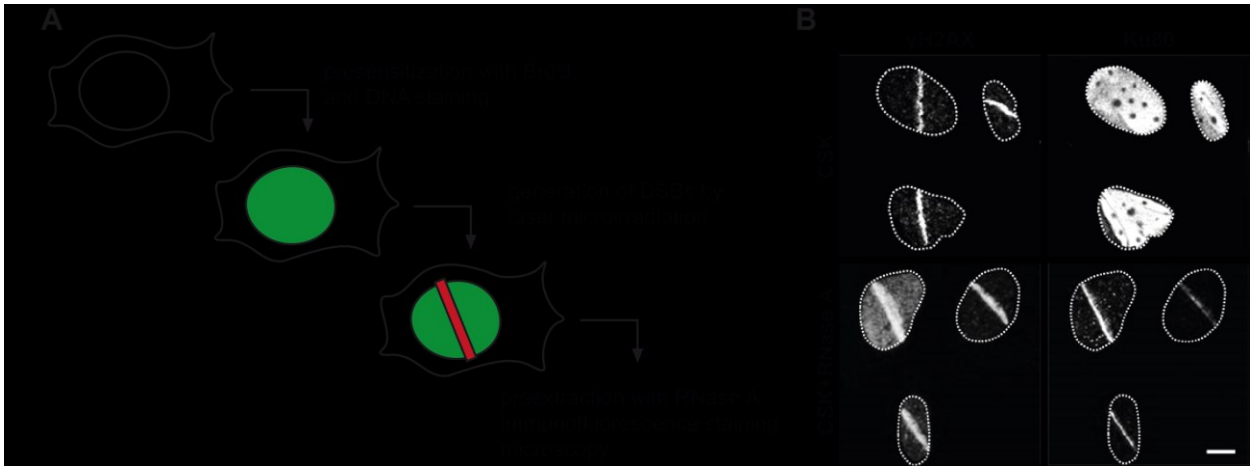

Figure 2.1: Specific visualization of DSB-bound Ku80 by CSK + RNase A preextraction after laser microirradiation.
A) Scheme of laser microirradiation experiments. U2OS cells were presensitized with BrdU for 24 h to be more susceptible for the laser irradiation, which yields higher amount of DSBs. The DNA of the living cells was stained with RedDot™1 dye (green) to define the laser tracks (red line) for microirradiation. After exposure to the 405 nm laser, the cells were subjected to a preextraction that included RNA digestion and processed for immunofluorescence imaging.
B) RNA digestion enables preextraction of Ku80 that is not bound to DSBs. Immunofluorescence images of microirradiated cells stained with γH2AX- and Ku80-specific antibodies. 60 min after microirradiation, cells were either preextracted with cytoskeleton buffer (CSK) or CSK containing 0.3 mg/ml RNase A and fixed with formaldehyde. After immunofluorescence staining, samples were visualized by confocal laser scanning microscopy. Nuclei (white lines) were defined by RedDot™1 staining (not shown). Scale bar = 10 µm.

Incorporation of the thymidine analog BrdU into one strand of the double helix during one completed S phase photosensitized the DNA and enabled to induce more DSBs with the laser. After microirradiation with a 405 nm laser and post-incubation, the cells were preextracted with cytoskeleton buffer (CSK; Figure 2.1 B). As expected, cells preextracted in CSK buffer without RNAse A exhibited a homogenous Ku80 staining in the nucleus that obscured the signal of DNA-bound Ku80. Notably, addition of RNAse A in the preextraction buffer strongly reduced this background and thus revealed DNA-bound Ku80 in the microirradiated area. Colocalization of the Ku80 signal with the DSB marker γH2AX confirmed that the DNA-bound Ku80 was specifically localized at sites of DSBs. Therefore, the preextraction technique with RNA digestion was well suited for the further microscopy-based investigation of Ku80 levels at DSBs.

2.2 p97 function is required for Ku80 release from DSBs

Laser microirradiation induces densely clustered damage and substantial amounts of other damage types besides DSBs (Reynolds et al, 2013). To apply a more physiological type of radiation, the samples were instead exposed to ionizing radiation, more specifically to hard X-rays (< 5 keV; X-IR), to generate DSBs. Choosing X-rays had further advantages, since no presensitization with BrdU was required and the ratio of DSBs to other radiation-induced DNA

damage, e.g. SSBs, 4,6-photoproducts, or 8-oxoguanine, was shifted in favor of DSBs (Reynolds et al, 2013).

2.2.1 Ku80 foci persist upon p97 inhibition

The DSB-specific visualization of Ku80 was applied on irradiated (X-IR) samples to study kinetics of Ku80. A super-resolution approach by 3D structured illumination microscopy (3D-SIM; lateral resolution ~90 nm) was necessary to resolve single Ku80 foci (Figure 2.2 A). These Ku80 foci had an approximate size of 200 nm, which was in agreement with the published value of 170 nm and each focus is associated to one DSB (Britton et al, 2013).

The number of Ku80 foci after exposure to 10 Gy of X-IR was quantified by automated image quantification. The mean number of foci/Gy was 23.0, which is in line with published data (24 Ku80 and γH2AX foci/Gy in U2OS cells; Britton et al, 2013). To analyze the function of p97, the ATPase was chemically inhibited with the allosteric small molecule inhibitor NMS-873. The IR-induced Ku80 levels were comparable in control samples and those with compromised p97, indicating that binding of Ku80 to DSBs was not altered upon p97 inhibition. After 60 min, the majority of Ku80 foci was resolved under control conditions (DMSO), but persisted in cells treated with the p97 inhibitor (NMS-873; Figure 2.2 B).

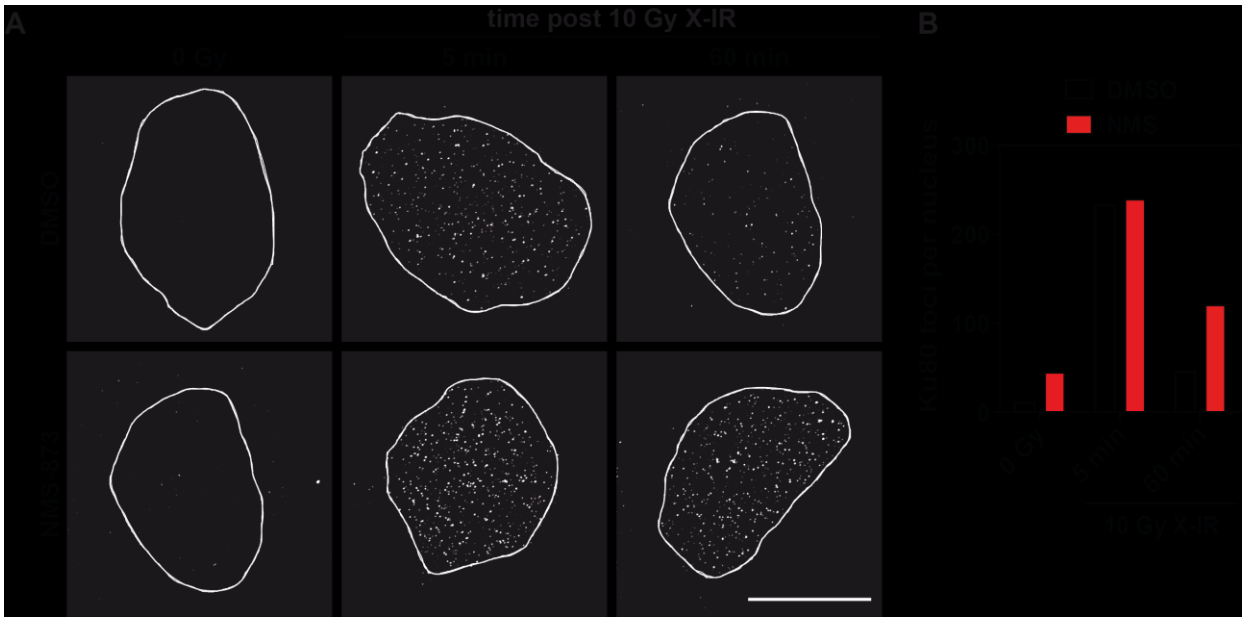

Figure 2.2: p97 is required for release of Ku80 from DSB sites.
A) Ku80 foci assay using super-resolution microscopy. U2OS cells were treated with the allosteric p97 inhibitor NMS-873 (10 µM) or vehicle control and exposed to 10 Gy of ionizing radiation (X-rays; X-IR) or mock treated (0 Gy). 5 or 60 min after irradiation the samples were processed with CSK + RNase preextraction and stained for Ku80. The cells were imaged in super-resolution by 3D structured illumination microscopy (3D-SIM). The images are maximum intensity projections and the white lines indicate the nuclei, as defined by DAPI staining. Scale bar = 10 µm.
B) Automated image quantification of A) using the CellProfiler software. The bars show mean number of Ku80 foci per nucleus of >5 cells per condition from one experiment.

Although 3D-SIM has superior resolution compared to confocal laser scanning microscopy, it is a slow technique and requires higher laser intensities that cause significant bleaching of the samples. Hence, further experiments were quantified by confocal laser scanning microscopy, to be able to analyze more time points and cells for Ku80 kinetics.

As expected, resolution of the laser scanning microscope was not sufficient to visualize Ku80 foci. Therefore, integrated intensities of the nuclear Ku80 signal were quantified instead and the area of the nuclei was defined by DNA staining with 4′,6-Diamidin-2-phenylindol (DAPI). A drawback of this measurement was that no information on the number of DSBs was available and the signal-to-noise ratio of the Ku80 staining was inferior to the super-resolution images (Figure 2.3 A). The samples were again exposed to 10 Gy of X-IR and post-incubated for up to 120 min. In control conditions, the amount of Ku80 decreased after 30 min and reached the level of non-irradiated control samples after 120 min (Figure 2.3 B). In contrast, chromatin-bound Ku80 levels of NMS-873-treated cells increased between 5 and 45 min post-irradiation. Even after 120 min, the amount of Ku80 was still slightly higher than 5 min after irradiation. Compared to DMSO controls, p97 inhibition entailed significantly more DSB-bound Ku80 after 45, 60, and 120 min. Thus, Ku80 persistence on chromatin of irradiated cells upon p97 inhibition with NMS-873 was consistent with the result from 3D-SIM.

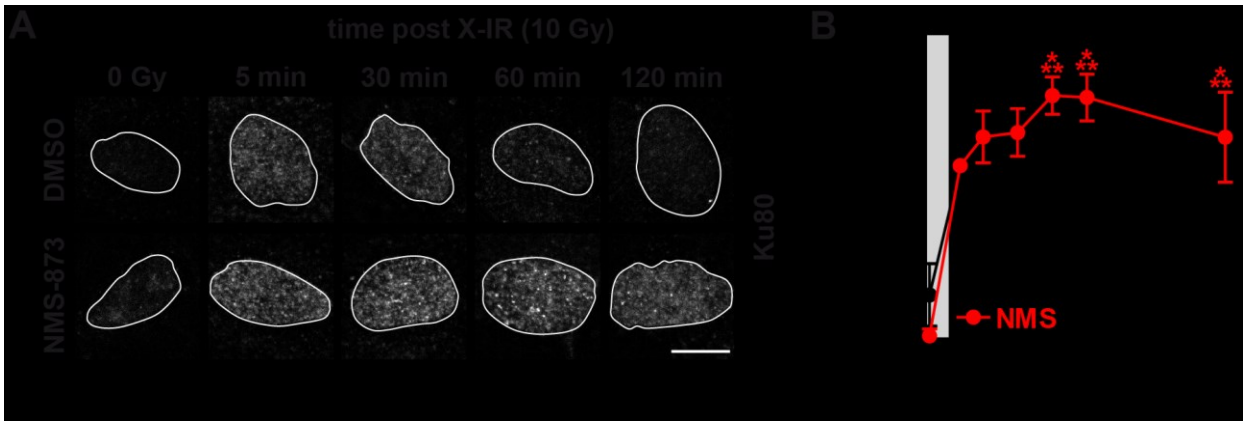

Figure 2.3: p97 mediates Ku80 release from damaged chromatin.
A) Time course of chromatin-bound Ku80 after DSB induction. U2OS cells were treated with or without 10 µM NMS-873 and irradiated with 10 Gy of X-IR or were mock treated (0 Gy). Cells were left to recover as indicated and then preextracted with CSK + RNase A and fixed. The samples were immunostained for Ku80 and imaged by confocal laser scanning microscopy. Nuclei are indicated by white outlines that were defined by DAPI staining. Scale bar = 10 µm.
B) Automated image quantification of nuclear Ku80 intensity from A) [plus 15 min and 45 min samples not shown in A)] using the CellProfiler software. The values are means ±SD of three independent experiments with at least 50 nuclei per experiment. Values were normalized to 5 min values. Gray background highlights the time of irradiation. Significance was tested by ANOVA with Tukey's post-hoc test. *** = $p<0.001$.

2.2.2 Dissociation of Nbs1 from DSBs is independent of p97

To test specificity of the impaired Ku80 extraction upon loss of p97 function, it was compared to another DNA repair protein. To this end, the release of Nbs1 from damaged chromatin was analyzed. Nbs1 is part of the MRN complex that is involved in early steps of DSB repair by HRR and, like Ku80, is ubiquitinated by the E3 ligase RNF8 (Lu et al, 2012).

Chromatin-bound Nbs1 was quantified similarly to Ku80 by immunofluorescence imaging with the established preextraction technique, but RNase A was omitted from CSK buffer, because RNA digestion was not required for visualization (Figure 2.4 A). The IR-induced increase of the DNA-bound Nbs1 fraction was comparable to the increase of DSB-bound Ku80 (signal intensities approximately doubled after exposure to X-IR), but Nbs1 release was slower. This was expected, because HRR has slower kinetics than NHEJ. 120 min after irradiation, more than half of the IR-induced fraction of Nbs1 on DNA was left, but, in contrast to Ku80 extraction, Nbs1 release was not impaired by p97 inhibition (Figure 2.4 B).

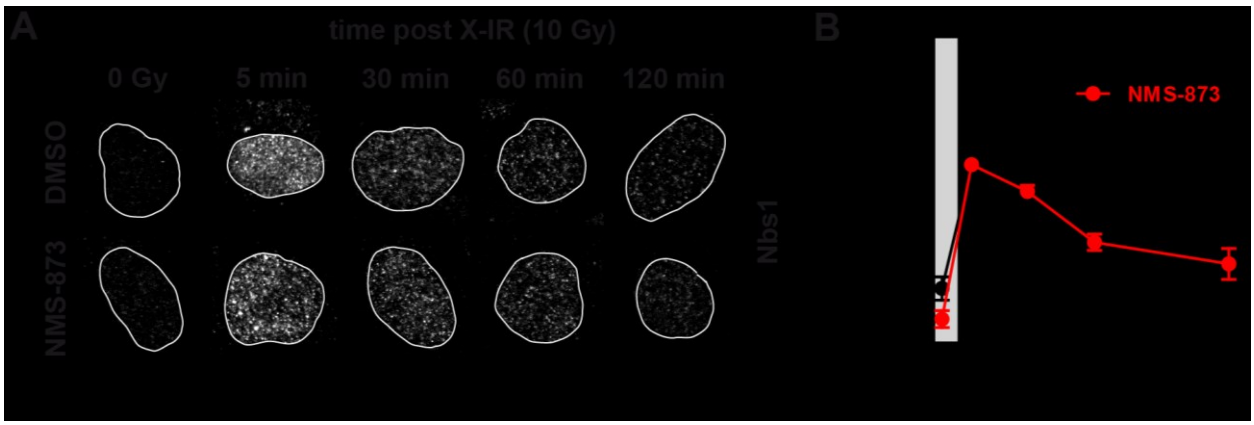

Figure 2.4: Release of the MRN component Nbs1 is independent from p97 function.
A) Time course of chromatin-bound Nbs1 after DSB induction. U2OS cells were treated with 10 µM NMS-873 or vehicle alone and exposed to 10 Gy of X-IR or to 0 Gy as control. Cells were allowed to recover for indicated time and then preextracted with CSK buffer and fixed. The samples were stained with Nbs1-specific antibody and imaged by confocal laser scanning microscopy. The white line marks the border of the nucleus, as defined by DAPI staining. Scale bar = 10 µm.
B) Automated image quantification of nuclear Nbs1 intensity from A) using the CellProfiler software. The values are means ±SD of three independent experiments with at least 50 nuclei per experiment. Values were normalized to 5 min values. Gray background highlights the time of radiation exposure. No significant differences were found by ANOVA with Tukey's post-hoc test.

2.2.3 NMS-873 treatment does not interfere with DSB signaling and DSB ligation

To exclude the possibility that the p97 inhibitor delays or inhibits DSB repair in general and that this causes Ku80 persistence, kinetics of the DSB marker γH2AX were analyzed by immunofluorescence (Figure 2.5 A). In control conditions, γH2AX peaked 30 min after X-IR and decreased afterwards to ~42 % (of 5 min value) at 120 min post-irradiation (Figure 2.5 B). In

NMS-873-treated samples, γH2AX intensity decreased after 45 min and was slightly (but not significantly) elevated compared to control samples.

In a second approach, a collaboration partner from the Iliakis lab measured the physical integrity of chromatin by pulsed-field gel electrophoresis (PFGE) to monitor the religation of DSBs under NMS-873 treatment. DSBs were repaired with the same kinetics in DMSO- and NMS-873-treated samples, as assessed by quantification as dose equivalents of reference samples. Thus, the p97 inhibitor had no influence on ligation of the DSBs. A small molecule inhibitor of the NHEJ kinase DNA-PK_{cs}, NU7441, served as positive control by inhibiting NHEJ repair and in these samples higher dose equivalents were measured at all time points (see Figure 3 I in van den Boom et al, 2016).

Together, these results establish p97 as factor for Ku80 extraction from sites of DNA damage in a process that is independent of DSB ligation.

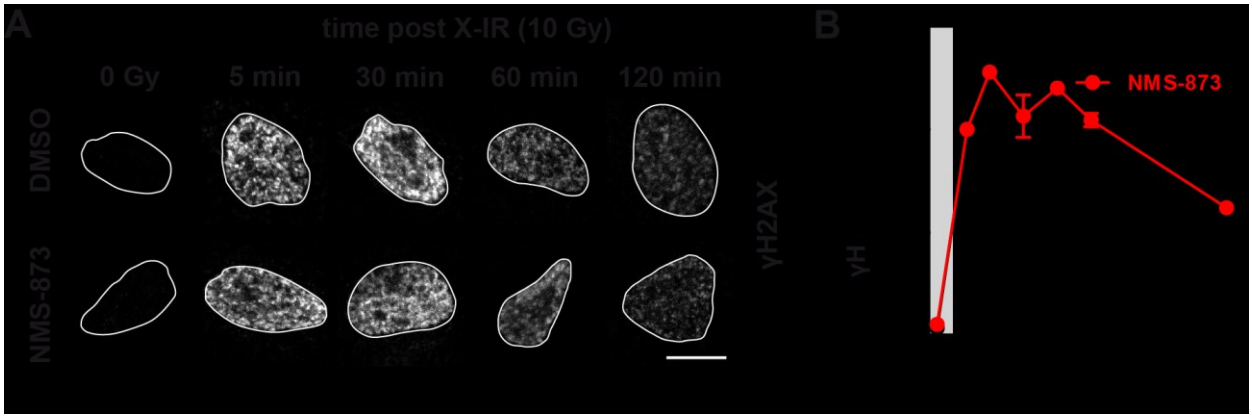

Figure 2.5: p97 inhibition by NMS-873 does not inhibit end-joining per se.
A) Time course of the DSB marker H2AX pS139 (γH2AX) after ionizing radiation. U2OS cells were treated with NMS-873 (10 μM) or DMSO as control and irradiated (10 Gy of X-IR) or were mock treated (0 Gy). Cells exposed to radiation were left to recover as indicated, then preextracted with CSK + RNase A and fixed. The cells were stained for γH2AX by immunocytochemistry and with DAPI to identify the nuclei (shown as white outlines) and imaged by confocal laser scanning microscopy. Scale bar = 10 μm.
B) Automated image quantification of nuclear γH2AX intensity from A) [plus 15 min and 45 min samples not shown in A)] using the CellProfiler software. The values are means ±SD of three independent experiments with at least 50 nuclei per experiment and values were normalized to 5 min. Gray background highlights the time of irradiation. Significance was tested by ANOVA with Tukey's post-hoc test and no significant differences were found.

2.3 Cofactors of p97 for Ku80 extraction

p97 interacts with a variety of cofactors and adaptor proteins to form functional complexes for the various cellular processes. Therefore, the next aim was to find the cofactors that form a complex with p97 for Ku80 extraction. Previous studies showed that the cofactors Ufd1-Npl4, UBXD7, DVC1, and FAF1 have known functions in chromatin-associated processes. Since Ufd1-Npl4 and FAF1 were enriched in label-free quantitative mass spectrometry (LFQ-MS) of *in vitro* samples

and the Ufd1-Npl4 heterodimer is involved in most described p97 processes on chromatin, we first analyzed if Ufd1 is required for efficient Ku80 extraction.

The role of Ufd1 was tested by RNAi in the established Ku80 extraction assay. The cofactor was depleted by transfection of specific siRNAs. In addition to Ufd1 depletion with two different oligonucleotides (siUfd1 s2 and -s6), two siRNAs targeting p97 (sip97 s3 and -s7) were used. 48 h after transfection, the samples were irradiated and processed. For this experiment only the initial Ku80 intensity (5 min post-irradiation) and the persistence after 120 min were analyzed (Figure 2.6 A).

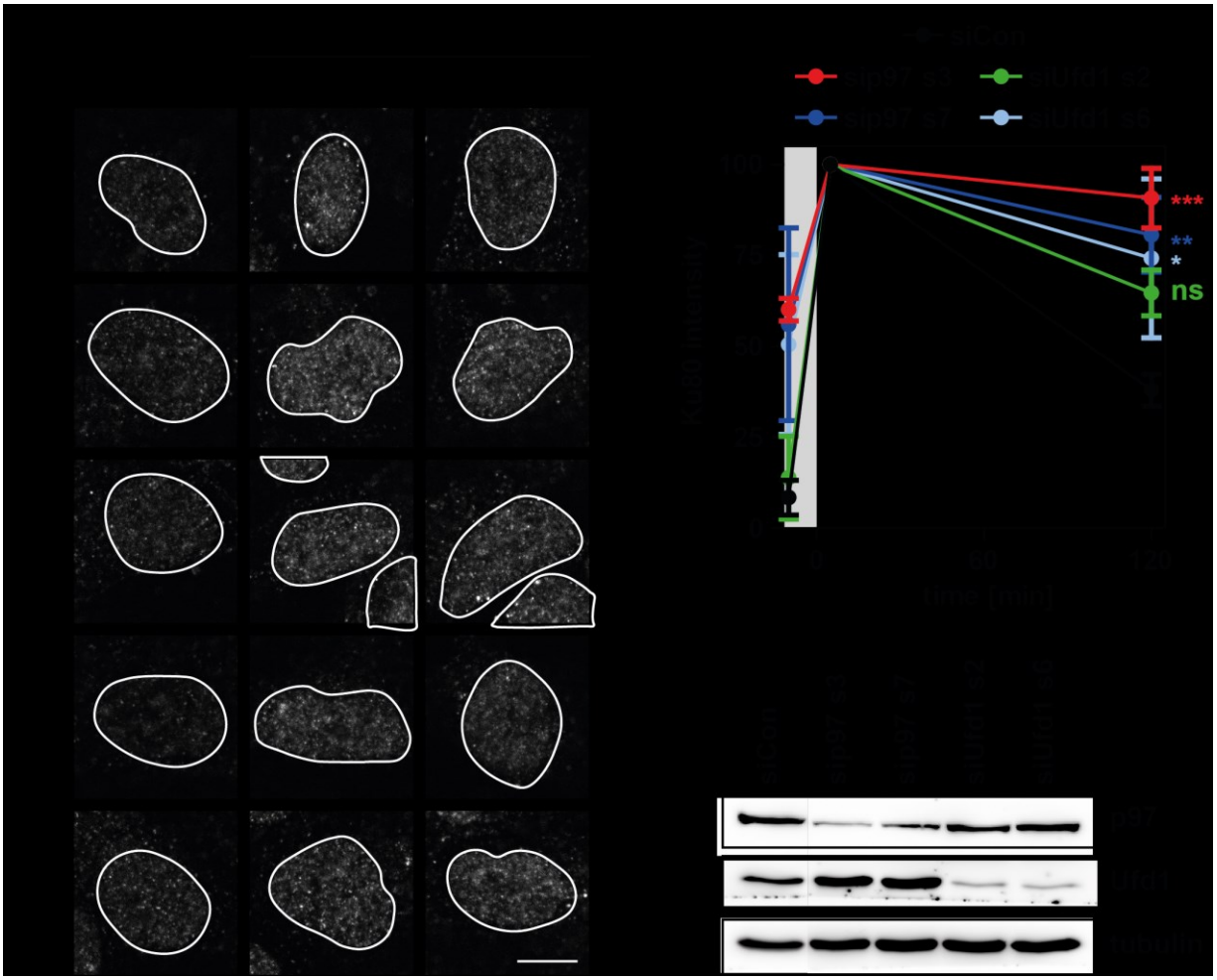

Figure 2.6: RNAi-mediated depletion of p97 or Ufd1 delays Ku80 release from DSBs.
A) Measurement of chromatin-bound Ku80 after DSB induction. U2OS cells were treated with or without 10 µM NMS-873 and irradiated with 10 Gy of X-IR or were mock treated (0 Gy). Cells were left to recover as indicated and then preextracted with CSK + RNase A and fixed. The samples were immunostained for Ku80 and imaged by confocal laser scanning microscopy. Position of the nuclei is depicted by a white outline that was defined by DAPI staining. Scale bar = 10 µm.
B) Automated image quantification of nuclear Ku80 intensity from A) using the CellProfiler software. The values are means ±SD of three independent experiments with at least 45 nuclei per experiment and sample. Values were normalized to 5 min value. Gray background highlights the time of radiation exposure. Significance was tested by ANOVA with Bonferroni post-hoc test. *** = $p<0.001$; ** = $p<0.01$; * = $p< 0.05$; ns = $p>0.05$.
C) Western blot for depletion control of p97 and Ufd1. U2OS cells were transfected as in B) and harvested after 48 h. Membrane was immunostained with antibodies specific for p97, Ufd1, and tubulin as loading control.

The control oligonucleotide (siCon) and siUfd1 s2 created only little background in non-irradiated samples, whereas samples transfected with Ufd1 s6 or the two p97 oligonucleotides had an elevated background signal of 50-60 %, which might result from intrinsic DNA damage that accumulated within the 48 h of knockdown. As expected, exposure to IR induced Ku80 binding to chromatin in all samples (Figure 2.6 B). While in control-depleted cells the Ku80 intensity decreased to 38 % after 120 min, knockdown (KD) with either p97 oligonucleotide or siUfd1 s6 significantly delayed Ku80 extraction. Moreover, the intensity was also increased in the siUfd1 s2 sample, but not significantly. In summary, Ufd1 or p97 depletion significantly reduced the Ku80 extraction rate, although the effect was not as strong as with the chemical p97 inhibitor NMS-873.The knockdown efficiency of p97 and Ufd1 was confirmed by Western blot with specific antibodies (Figure 2.6 C). The oligonucleotides targeting Ufd1 efficiently depleted the protein, as did sip97 s3. Slightly more p97 remained in the sample transfected with sip97 s7. Depletion with sip97 s3 inhibited Ku80 extraction more than knockdown with sip97 s7. Thus, the effect on Ku80 persistence correlated with the remaining amount of p97.

The parallel *in vitro* experiments found Ufd1 to accumulate on DNA with DSBs, and Ufd1 depletion delayed Ku80 extraction also in *Xenopus* egg extracts.

2.3.1 CRISPR/Cas9-mediated FAF1 knockout

Further RNAi studies were performed in the lab that included Npl4, UBXD7, and FAF1 KD (van den Boom et al, 2016). Only mild effects were observed, of which FAF1 depletion caused the strongest delay in Ku extraction. Interestingly, a codepletion of FAF1 and Ufd1 had synergistic effects. FAF1 was also enriched in the LFQ-MS screen and rendered FAF1 an interesting candidate for further analysis. To confirm the possible role of FAF1 in Ku80 extraction, a CRISPR/Cas9 knockout (KO) of FAF1 in U2OS cells was chosen. The advantage of this approach was the avoidance of potential problems with knockdown efficiency or sufficient function of residual amounts of the protein.

CRISPR-RNA (crRNA) sequences were required to target the Cas9 nuclease to the FAF1 gene. They were chosen based on the target sites, evaluation of cleavage efficiency and analysis of off-target activity, which were analyzed with tools from the Zhang and Root labs (Ran et al, 2013; Doench et al, 2016; see 4.3.1). Two oligonucleotides were designed to target Exon 1 or Exon 4 of the FAF1 locus (Figure 2.7 A). The cleavage site in Exon 1 disrupts the sequence very close to the 5' end (codon 11) and cleavage in Exon 4 is located after the sequence encoding the UBA domain. The additional cleavage site in Exon 4 was chosen, because its predicted efficiency and specificity was much higher. However, an expression of the FAF1 gene truncated after the UBA sequence might yield a protein with stable folding of this domain.

The crRNA was hybridized with trans-activating crRNA (tracrRNA) and the resulting hybrids were mixed with purified Cas9 protein to form ribonucleoprotein complexes that were transfected into U2OS cells. To confirm efficiency of the Cas9 cleavage at the target sites, genomic DNA was

isolated from a pool of transfected cells. The FAF1 locus was amplified by PCR and analyzed by Sanger sequencing. The resulting chromatograms were used to calculate the efficiencies with a decomposition algorithm (Brinkman et al, 2014). While the algorithm failed to calculate a result for Exon 1, cleavage efficiency of the Cas9 target site in Exon 4 was 48.1 % (Figure 2.7 B). Nevertheless, clones with homozygous KO were obtained for both target sites, as judged by Western blot. As the gene was disrupted further upstream with cleavage in Exon 1, two of these clones (FAF1 KO clone (cl.) 2 and cl. 4; Figure 2.7 C) were used for the following experiments.

2.3.2 Generation of a FAF1-specific antibody

In parallel, full-length His-FAF1 was purified in our lab and used to raise a custom-made FAF1 antibody in rabbits. This was necessary, because the commercial antibodies did not work in our hands. The purified His-FAF1 was used to enrich the FAF1 antibody from sera by affinity purification. The eluate was used to probe Western blots and a strong band was detected in the range of the expected molecular weight of 74 kDa (Figure 2.7 C wt). Specificity was confirmed by samples of the two FAF1 KO clones, in which the protein was not detectable. Two unspecific bands were visible, but clearly distinguishable from the specific signal, as they appeared at smaller molecular weight and persisted in the KO samples.

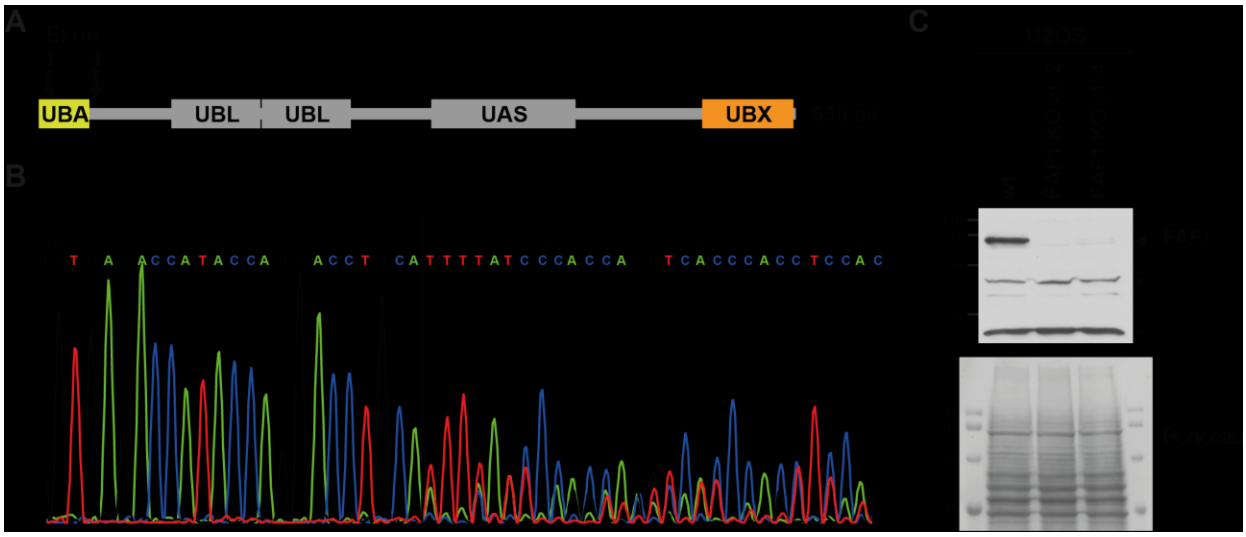

Figure 2.7: CRISPR-Cas9 knockout of the p97 cofactor FAF1.
A) Schematic representation of the FAF1 domain structure with indicated truncations resulting from the Cas9 target sites in Exon 1 and Exon 4 of the FAF1 gene. The cleavage site in Exon 4 is after the UBA domain.
B) U2OS cells were transfected with ribonucleoprotein complexes of purified Cas9 and gRNA targeting the FAF1 gene (Exon 1 or Exon 4). Genomic DNA was extracted from the cells after 48 h. The FAF1 locus was amplified by PCR and analyzed by Sanger sequencing. The figure shows an exemplary sequencing chromatogram from cells with Cas9 cleavage site (labeled by black line) in Exon4. Cleavage efficiency was calculated with the TIDE tool (Brinkman et al, 2014).
C) Western blot analysis of U2OS wild type (wt) and two FAF1 knockout (KO) clones (2 and 4) that were isolated from the sample with Cas9 cleavage in Exon1. The blot was stained with Ponceau S as loading control and a custom-made and affinity purified FAF1 antibody. * marks unspecific bands.

2.3.3 FAF1 knockout does not influence survival after exposure to ionizing radiation

As first characterization of the U2OS FAF1 KO clones, long-term survival of the cells after radiation exposure was tested by colony formation assay. For this, a defined number of cells was seeded on 10 cm dishes, was irradiated 4 h later and was incubated for 14 days. Colonies (≳50 cells) were stained with crystal violet and counted. Plating efficiency of the cells with knockout was reduced by one third compared to wild type cells (Figure 2.8 A). However, the surviving fractions of wild type and knockout cells were equal (Figure 2.8 B). This indicates that the lack of FAF1 does not impair survival after exposure to X-IR or can be compensated.

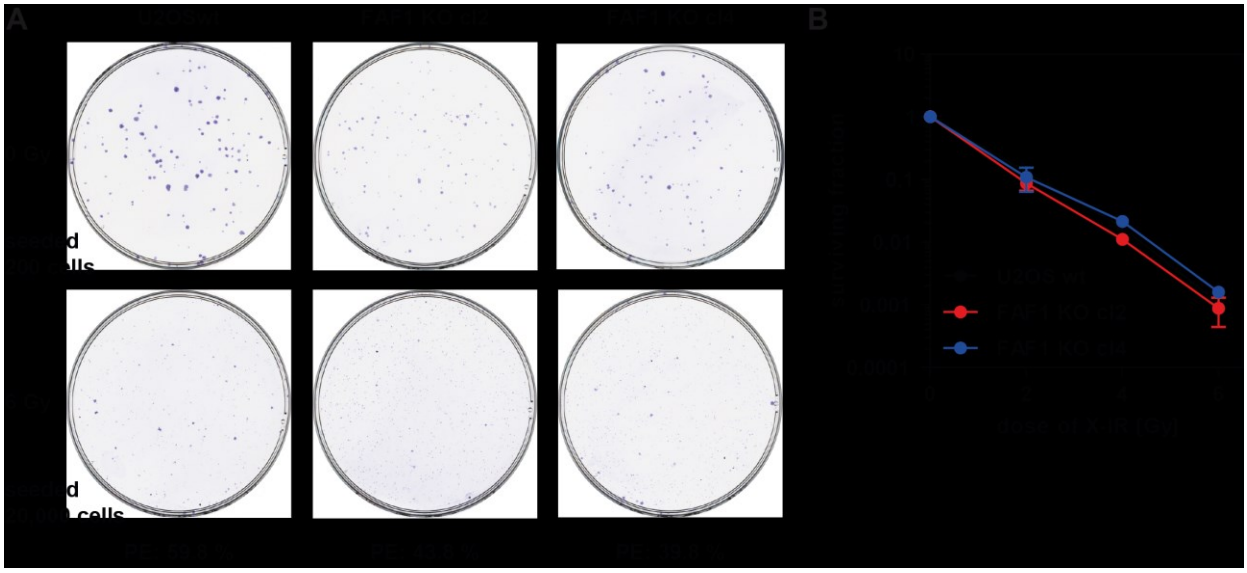

Figure 2.8: FAF1 KO does not impair long-term survival of U2OS cells after exposure to IR.
A) Colony formation assay of U2OS wt and FAF1 KO clones 2 and 4. The number of cells seeded depended on the dose of X-IR. 200 cells were seeded for mock irradiation, 500 cells for a radiation dose of 2 Gy, 2,000 cells for a dose of 4 Gy, and 20,000 cells for a dose of 6 Gy. The cells were irradiated 4 h after plating and incubated for 14 days. The samples were then stained with crystal violet and colonies were counted. Exemplary pictures of samples exposed to 0 Gy or 6 Gy. PE = plating efficiency.
B) Quantification of the surviving fraction in the colony formation assay shown in A) from three independent experiments. Values are means ±SD normalized to 0 Gy. No significant differences were found by ANOVA with Tukey's post-hoc test.

2.3.4 FAF1 is involved in Ku80 extraction, but hypostatic to Ufd1

Next, Ku80 extraction from DSBs was analyzed in the FAF1 KO clones. For this, Ku80 was analyzed by immunofluorescence in U2OS wt and FAF1 KO cells. This was combined with Ufd1 knockdown (KD), as we had observed synergistic effects in our RNAi experiments (van den Boom et al, 2016 Figure 3 H). Ku80 binding in non-irradiated cells, which is an indicator of intrinsic DSBs, was not detectable in FAF1 KO clones (Figure 2.9 A). DSB induction was equal in wild type and knockout samples, as demonstrated by Ku80 binding upon radiation exposure. However, different amounts of Ku80 remained bound to the DNA 60 min post-irradiation (Figure 2.9 B). The FAF1 KO alone (+ siCon) affected Ku80 extraction only marginally compared to U2OS

wt (+ siCon) cells. In contrast, Ufd1 KD in U2OS wt cells caused persistence of Ku80 on chromatin. Notably, Ku80 levels were further increased upon Ufd1 depletion in FAF1 KO clones. At the later time point (120 min after X-IR), the DSB-bound fraction of Ku80 was decreased in all conditions and the differences between the samples were smaller than after 60 min. Ufd1 KD still caused increased Ku80 levels in comparison with the control-depleted samples, but no difference was observed between FAF1 KO clones and U2OS wt cells.

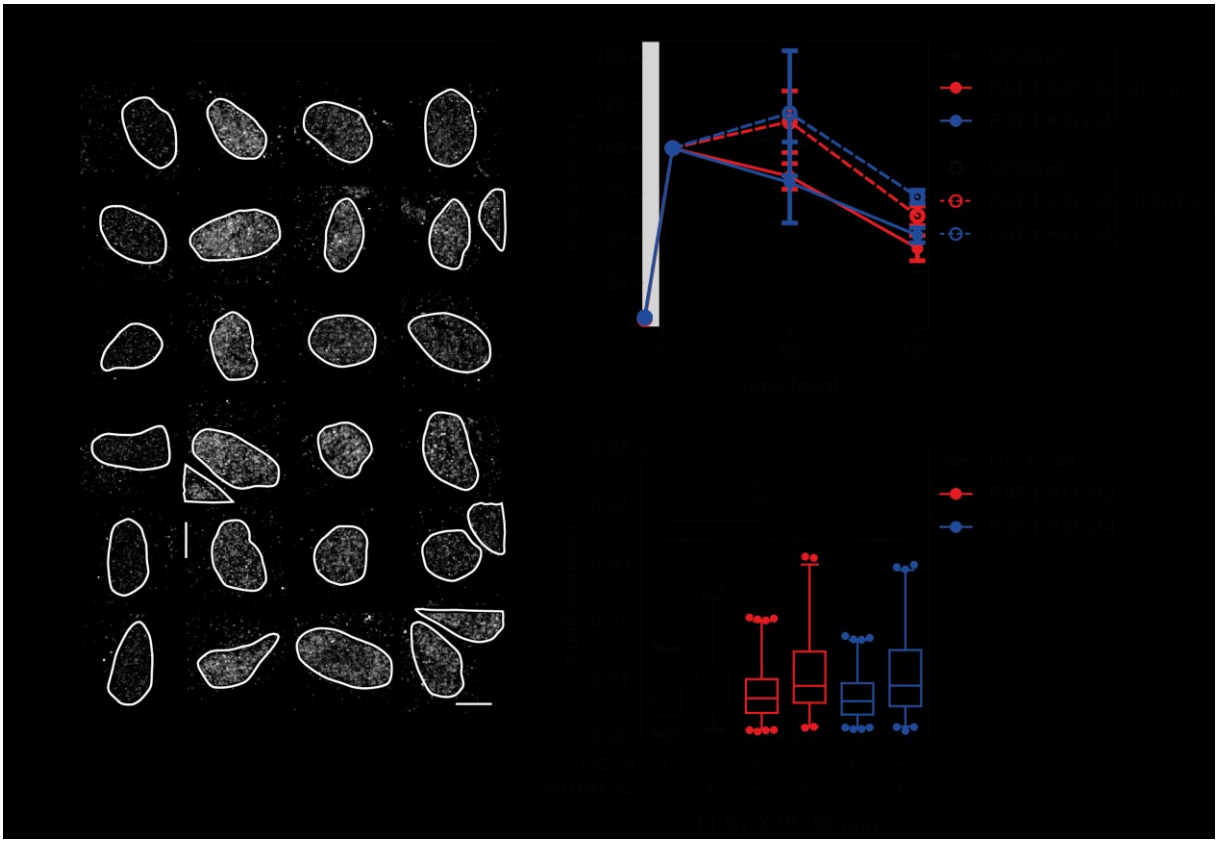

Figure 2.9: Knockdown of Ufd1 and FAF1 delays Ku80 extraction from DSBs, whereat Ufd1 is epistatic to FAF1.
A) Time course of chromatin-bound Ku80 after DSB induction. U2OS wt and FAF1 KO cells were transfected with siRNA targeting Ufd1 (siUfd1 s2) or control (siCon). 48 h after transfection the samples were irradiated with 10 Gy of X-IR or sham irradiated (0 Gy). The cells were left to recover for the indicated time and then preextracted with CSK + RNase A and fixed. Ku80 was stained by immunocytochemistry and images were acquired with a confocal laser scanning microscope. The nuclei were defined by co-staining with DAPI and are highlighted by a white line.
Scale bar = 10 µm.
B) Automated image quantification of nuclear Ku80 intensity from A) using the CellProfiler software. The values are means ±SD of three independent experiments with >90 nuclei per sample and experiment, normalized to 5 min values. Gray background highlights the time of irradiation.
C) Box-and-whisker plot of raw values from 60 min time point of the automated image quantification. Significance was tested by ANOVA with Tukey's post-hoc test. *** = p<0.001; ** = p<0.01; * = p<0.05.

Thus, we focused on the interesting differences 60 min after irradiation and samples of this time point were analyzed again with pooled values of the nuclei (Figure 2.9 C). This revealed that Ufd1 KD caused significantly increased Ku80 persistence in U2OS wt and both FAF1 KO clones.

Moreover, FAF1 KO alone caused significantly different Ku80 removal only in cl. 2 with $p<0.05$. The combination of Ufd1 KD and FAF1 KO significantly increased the chromatin bound Ku80 compared to Ufd1 KD alone in both FAF1 KO clones. The synergistic effect was in line with the delayed Ku removal after co-depletion of Ufd1 and FAF1 (van den Boom et al, 2016 Figure 3 H).

In summary, Ku80 extraction was delayed by loss of Ufd1 and FAF1, whereat the effect of Ufd1 depletion was stronger. CRISPR/Cas9-mediated KO of Ufd1 was performed to analyze Ku80 extraction without residual amounts of Ufd1 protein. However, the experiment did not yield any clones with a homozygous KO, indicating that Ufd1 is an essential gene and a homozygous KO is lethal.

2.4 Ku80 as substrate for K48-linked polyubiquitination at DSB sites

p97 targets substrates that are ubiquitinated and many p97 cofactors have ubiquitin-binding domains to mediate binding of the ATPase to the substrate. Ufd1 is able to bind to ubiquitin with its UT3 domain and FAF1 binds to ubiquitin chains with the UBA. Previous experiments in *Xenopus laevis* egg extracts showed that Ku80 is polyubiquitinated with K48-linked chains upon DNA binding and this ubiquitination is required for efficient Ku80 removal from chromatin (Postow et al, 2008; Postow & Funabiki, 2013). The DNA damage-induced ubiquitination cascade of RNF8 and RNF168 has been described for human cells (Doil et al, 2009; Stewart et al, 2009) and RNF8 was described to ubiquitinate Ku80 and primarily synthesize K48-linked chains (Feng & Chen, 2012). Therefore, we wanted to test whether K48-linked polyubiquitin accumulates at DSB sites, if Ku80 extraction is blocked by p97 inhibition.

Laser microirradiation was used to confirm elevated K48-linked poly-ubiquitination at DSBs (Figure 2.10 A). The assay was performed as in Figure 2.1 A, but another, RNAse A-free, preextraction buffer was used (Meerang et al, 2011). The cells were fixed 30 min after laser microirradiation and stained for immunofluorescence with an antibody specific for K48-linked polyubiquitin chains. The level of this post-translational modification was clearly increased on microirradiated chromatin (Figure 2.10 A).

In the following experiment, the influence of p97 inhibition on the ubiquitin levels was analyzed to assess the extent of Ku80 modification with K48-linked polyubiquitin. As before, p97 function was inhibited by NMS-873 treatment and DSBs were induced by exposure to X-IR. RNAi-mediated knockdown of Ku80 was used to estimate the ubiquitinated fraction of this protein and the immunofluorescence was measured by laser scanning microscopy (Figure 2.10 B). 60 min after radiation exposure, K48-linked ubiquitin chains were not generally increased by irradiation, but polyubiquitin accumulated in all conditions with NMS-873 treatment (Figure 2.10 C). This was expected because of the described role for p97 in chromatin associated degradation (Vaz et al, 2013). In control-depleted cells, radiation exposure significantly increased the ubiquitin signal in cells with compromised p97. Importantly, this increase was abolished by Ku80 depletion.

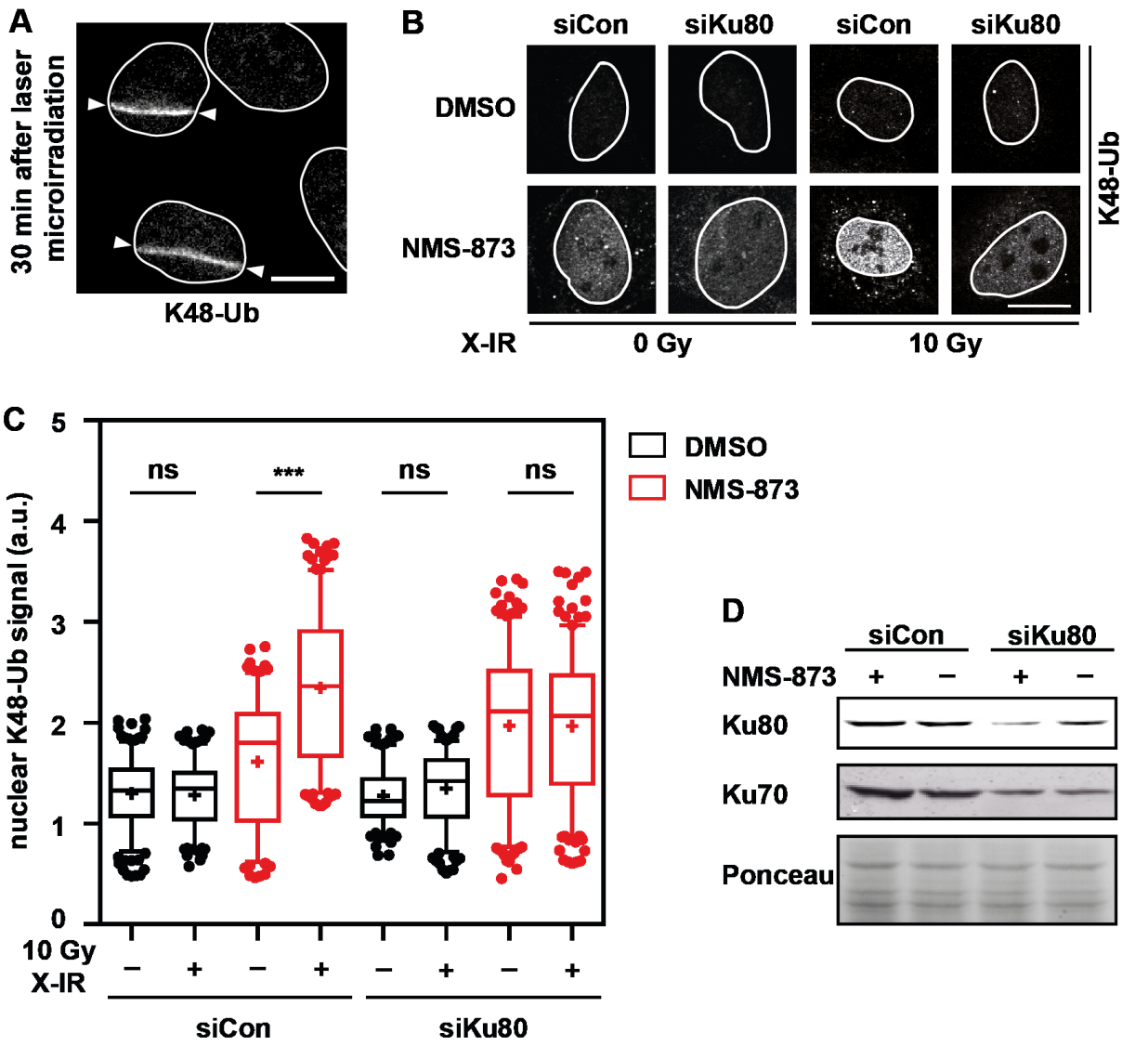

Figure 2.10: Ku80 is a major p97 substrate at DSBs and modified with K48-linked polyubiquitin chains.

A) K48-linked polyubiquitin chains are increased at sites of DSBs. U2OS cells were presensitized with BrdU for 24 h microirradiated with a 405 nm laser along a line in the nucleus (highlighted by white arrowheads). The cells were preextracted with preextraction buffer, fixed 30 min after microirradiation, and stained for K48-linked polyubiquitin. Imaging was done with a confocal laser scanning microscope. The white lines encircle the area of each nucleus, as defined by DAPI staining. Scale bar = 10 µm.
B) K48-linked polyubiquitin levels are increased upon p97 inhibition and in addition by irradiation. U2OS cells were transfected with siRNAs targeting Ku80 (siKu80) or with control siRNA (siCon). After 48 h the cells were treated with NMS-873 (10 µM) or DMSO control and exposed to 10 Gy of X-IR or left unirradiated (0 Gy). 60 min after irradiation the cells were preextracted, fixed, and stained with a K48-linked polyubiquitin specific antibody. Images were acquired with a confocal laser scanning microscope. DAPI staining was used to identify the area of the nuclei (white outlines). Scale bar = 10 µm.
C) K48-linked polyubiquitin levels are significantly increased by irradiation upon p97 inhibition with NMS-873 and this effect is abolished by Ku80 depletion. Automated image quantification of B) using the CellProfiler software. The values are integrated intensities of each nucleus from four independent experiments with >60 cells per experiment and sample. Whiskers indicate the 5th and 95th percentile and **+** indicates means. Significance was tested by ANOVA with Tukey's post-hoc test. *** = p<0.001.
E) Depletion efficiency of Ku80. U2OS cells were transfected with siRNAs targeting Ku80 (siKu80) or with control siRNA (siCon). After 48 h the cells were treated with NMS-873 (10 µM) or DMSO control for 60 min and lysed. The Western blot was stained with Ponceau as loading control and with Ku70- and Ku80-specific antibodies.

Knockdown of Ku80 was proven by immunoblotting (Figure 2.10 D), and, as expected, a codepletion of Ku70 was observed. Although the experiment does not prove a K48-Ub modification of Ku80, the results are in line with the idea that Ku80 accounts for a large fraction of the K48-polyubiquitinated proteins at DSBs. Further, it indicates that Ku80 is a major substrate of p97 in the context of DNA damage.

These findings are in line with results from the experiments in *X. laevis* egg extracts. The *in vitro* experiments demonstrated that p97 targets Ku80 modified with K48-linked chains, but not K11- or K63-linked chains.

2.5 p97 in homologous recombination repair

We assumed that the rapid occupation of DSB ends by Ku could inhibit end resection at breaks to be repaired via HRR. The hypothesis was that p97 extracts Ku80 to enable end resection and HRR repair. After exposure to ionizing radiation, the cell repairs DSBs via all three pathways and it is difficult to discriminate them. Therefore, the aim was to set up assays that enable specific analysis of HRR and test if p97 function is required for this pathway.

2.5.1 Reporter assay indicates roles for p97 and Ufd1 in HRR

The first experiment was a reporter assay to analyze if p97 function is required for HRR. For this endeavor, the DR-GFP recombination reporter system was chosen (Pierce et al, 1999). The reporter construct is stably integrated into the genome of cultivated cells and GFP expression is restored by HRR repair of a DSB induced by transient transfection of the endonuclease I-SceI. This repair event occurs with an efficiency of 5-6 % in positive controls.

For this study, U2OS cells with a stable integration of the reporter were used (U2OS DR-GFP). The cells were cultivated for 24 h before I-SceI transfection and for additional 72 h afterwards. Flow cytometry was used to measure GFP fluorescence of living single cells (Figure 2.11 A). In this assay, p97 was compromised by RNAi mediated knockdown and the cofactor Ufd1 was depleted as well (Figure 2.11 B). An siRNA targeting Rad51, a factor that is essential for HRR, served as positive control and abolished HRR. As expected, U2OS DR-GFP cells that were transfected with the empty vector (–I-SceI) exhibited no GFP fluorescence. In contrast, restoration of GFP fluorescence in the U2OS DR-GFP cells occurred with the expected efficiency of 5-6 % of the gated events. Importantly, depletion with both siRNAs of each target, p97 and Ufd1, significantly decreased the percentage of GFP positive cells (Figure 2.11 C).

The DR-GFP reporter assay pointed out that p97 and Ufd1 might be required for HRR and this was consistent with previous reports (Bergink et al, 2013). Nevertheless, as this was an endpoint assay, it remained unknown at which step of the HRR pathway p97 is involved. Thus, another experiment was needed to test the hypothesis of Ku80 segregation at an early step in the HRR pathway.

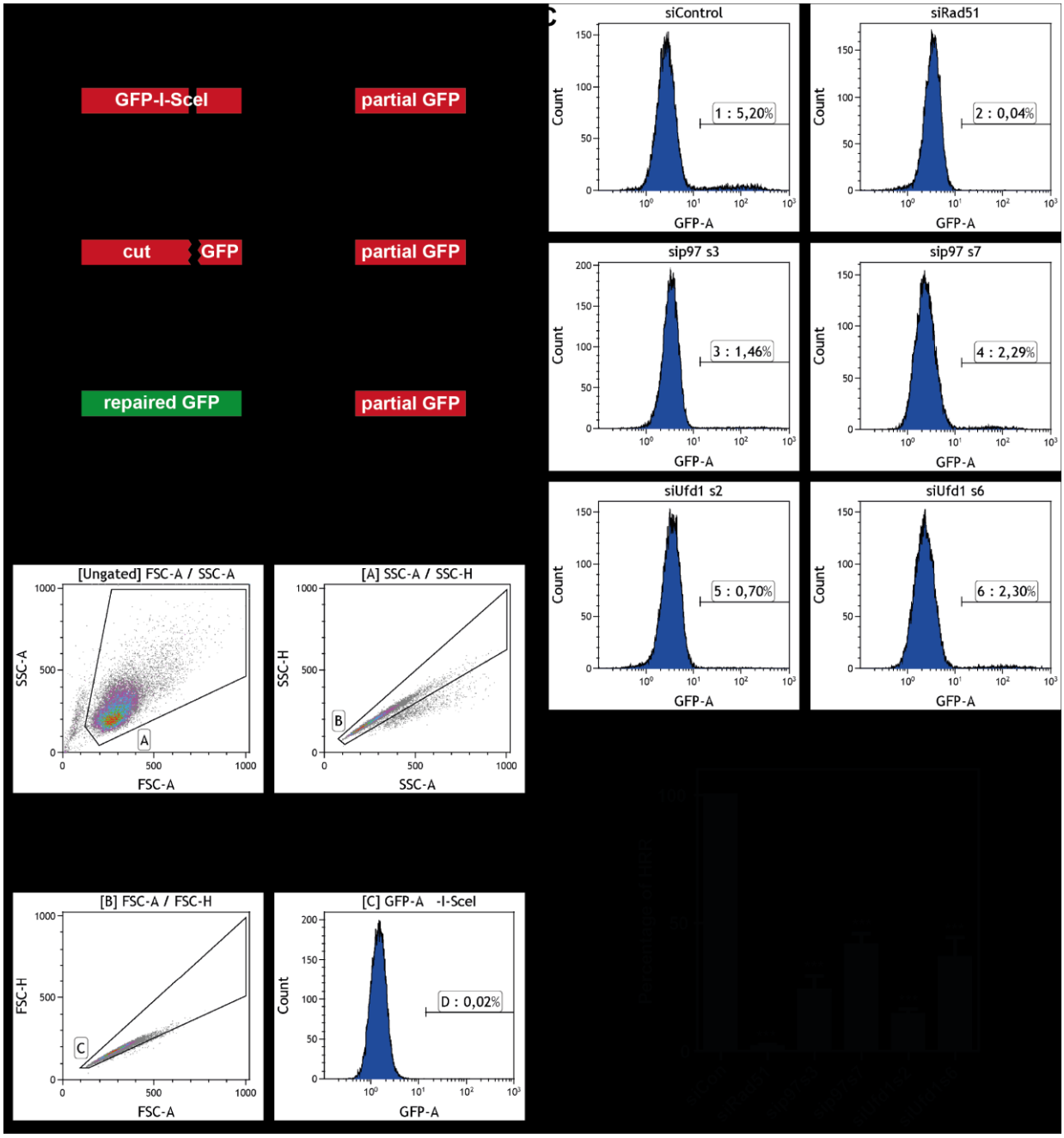

Figure 2.11: Homologous recombination repair (HRR) is reduced upon depletion of p97 or its cofactor Ufd1.

A) Flow cytometry plots of U2OS cells with stably integrated DR-GFP reporter to measure HRR. The plots depict the general gating strategy for the flow cytometric measurements. First, dead cells and debris were excluded and from these living cells, doublets were excluded twice. The histogram shows the GFP fluorescence of the living single cells in the sample transfected with an empty vector (–I-SceI). The gate is set to measure GFP positive events.

B) U2OS DR-GFP cells were transfected with siRNAs targeting the Rad51 recombinase (positive control), p97 (two oligos), Ufd1 (two oligos), or control. After 24 h, cells were transfected with a plasmid encoding the endonuclease I-SceI to induce a DSB in the reporter sequence. Additional 48 h later, the cells were analyzed by flow cytometry. Gating was performed as described in A) and shown are exemplary histograms of the GFP fluorescence with gating for GFP positive cells (percentage of living single cells). Note that restoration of the GFP sequence generally has a low efficiency.

C) Summary of three independent experiments with 20,000 gated events per sample and experiment. Error bars show means ±SD of GFP positive fractions normalized to siControl. Statistical significance was tested with repeated measures ANOVA with Tukey's post-hoc test. *** = $p<0.001$.

2.6 p97 in the repair of CPT-induced DNA damage

2.6.1 Camptothecin induces seDSBs that are repaired by HRR

To generate a situation in which the DSBs are exclusively repaired by HRR, we used camptothecin (CPT) treatment instead of X-IR to induce DNA damage. CPT is a small molecule inhibitor of topoisomerase I (Top1) and acts by stabilizing the usually transient covalent bond between the enzyme and a DNA strand, called topoisomerase cleavage complexes (Top1ccs). The nick in one strand of the DNA double helix is propagated into a single ended DNA double strand break by the encountering replication machinery during S-phase of the cell cycle. As there is no second free double-stranded DNA terminus, end-joining pathways are not able to repair the break, but recombination with the already replicated part of the DNA is used for repair of the seDSBs.

2.6.2 Camptothecin treatment induces DSBs in S-phase of the cell cycle

To prove that CPT induced seDSBs specifically in S phase of the cell cycle, immunofluorescence microscopy of the DSB marker γH2AX was performed (Figure 2.12 A). To visualize S phase cells, two independent marker were chosen. First, incorporation of the thymidine analog 5-Ethynyl-2'-deoxyuridine (EdU) into the newly synthesized DNA was used and detected by a click chemistry reaction. Second, proliferating cell nuclear antigen (PCNA), a processivity factor of DNA polymerases δ and ε that shows a characteristic pattern during S phase was stained with a specific antibody. Based on the PCNA pattern, cells could be categorized in early, mid, or late S phase and in the EdU labeling, a distinct pattern was observed as well. In early S phase, the protein was equally distributed in the nucleus and the EdU signal is homogenous. In mid S phase, PCNA foci formed and the protein accumulated at the nuclear lamina, which was visible at the rim of the nucleus. The EdU signal was still very strong in these cells, but more heterogeneous. In late S phase, less but larger PCNA foci could be seen and EdU incorporation was strong at these foci and reduced in the other areas. Some γH2AX foci were visible especially in mid S phase, which are most likely unrelated to DSBs but instead induced by ATR at sites of stalled replication (Ward & Chen, 2001).

Upon treatment with CPT, the PCNA and EdU pattern was not changed but signal intensities were generally reduced. This was expected, because CPT-stabilized Top1ccs blocked replication. A strong H2AX phosphorylation was induced in all stages of S phase but not in cells outside of S phase (white arrowhead in Figure 2.12 A). During 1 h of CPT treatment, the fraction of EdU-positive cells was not altered (Figure 2.12 B). γH2AX intensity was significantly increased in EdU-positive and CPT treated cells compared to background level in other samples. This demonstrates that CPT induces DSBs specifically in S phase.

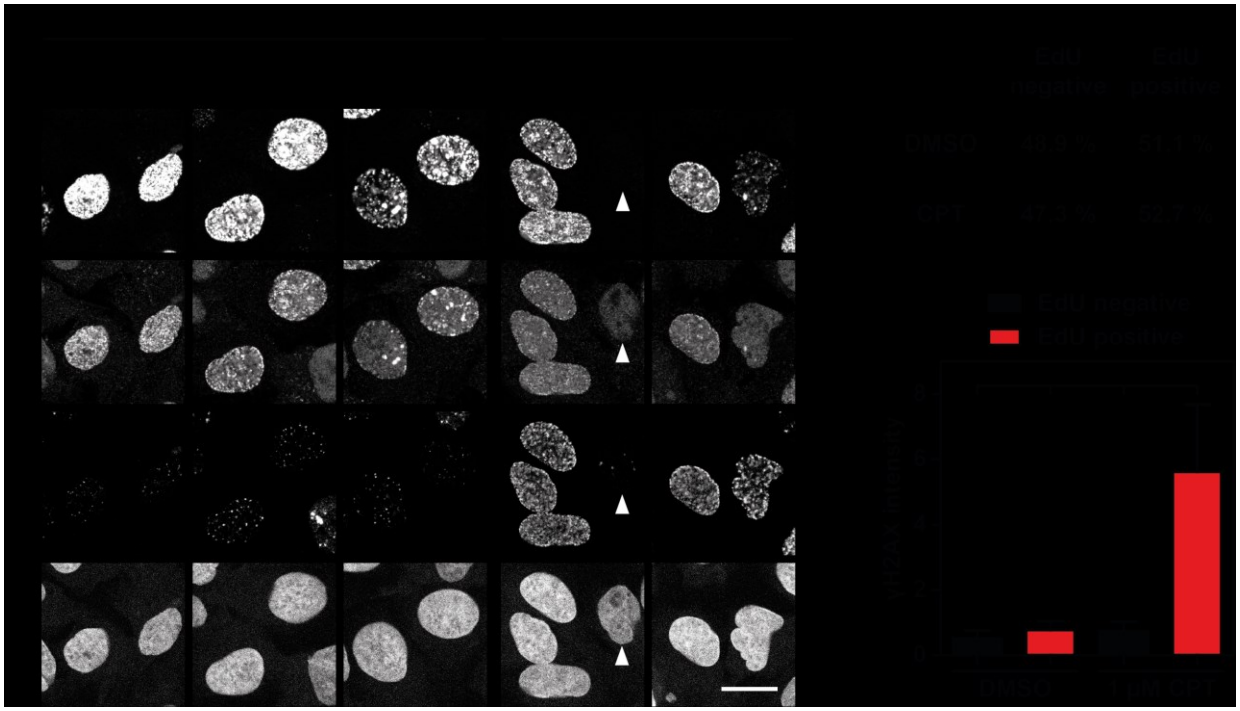

Figure 2.12 DSB induction by camptothecin is dependent on replication
A) Immunofluorescence imaging of CPT-induced DSBs and cell cycle marker for S phase cells. U2OS cells were treated with 1 µM CPT or DMSO as control for 1 h and in parallel with 5 µM EdU. Cells were fixed and EdU was labeled with a fluorophore by click chemistry. PCNA and γH2AX were stained with specific antibodies and DAPI was used to visualize DNA (nuclei). Images were acquired by confocal laser scanning microscopy. The white arrowheads point to a cell that is not in S phase. Scale bar = 20 µm.
B) Automated image quantification of A) using the CellProfiler software. The nuclei were categorized based on their EdU intensity as negative (no DNA synthesis – cells not in S phase) or positive (DNA synthesis – cells in S phase) and γH2AX intensity was quantified. Error bars show means ±SD of >50 cells/sample. Significance was tested with ANOVA and Tukey's post-hoc test. *** = $p<0.001$

2.6.3 Ku80 release from seDSBs is facilitated by MRE11 and CtIP but not by p97

The immunofluorescence-based Ku80 segregation assay was combined with CPT treatment of U2OS cells and p97 was inhibited with NMS-873 as before (Figure 2.13 A). As CPT treatment induces DSBs only during S-phase of the cell cycle, costaining for γH2AX was used to visualize the DNA damage burden. Knockdown of CtIP and MRE11 was used as positive control, because recent publications described a function of these end resection factors for Ku release from seDSBs (Chanut et al, 2016; Myler et al, 2017). After 1 h of CPT treatment, 55 % of the cells were γH2AX positive (in siCon DMSO) with a mean of about 170 γH2AX foci per nucleus (data not shown). This was in a comparable range to the irradiation-induced foci (IRIF), where 10 Gy yield around 240 foci per nucleus in U2OS cells (Britton et al, 2013). However, the Ku80 signal was much weaker after CPT than after irradiation. Additional NMS-873 treatment did not significantly change the amount of chromatin-bound Ku80. In contrast, knockdown of CtIP or MRE11 increased Ku80 levels in γH2AX-positive cells and this effect was significant for the MRE11 depletion. NMS-873 in combination with CtIP or MRE11 knockdown did not further

increase the Ku80 intensity. Instead, significantly less Ku80 was measured in the MRE11-depleted sample compared to DMSO treatment.

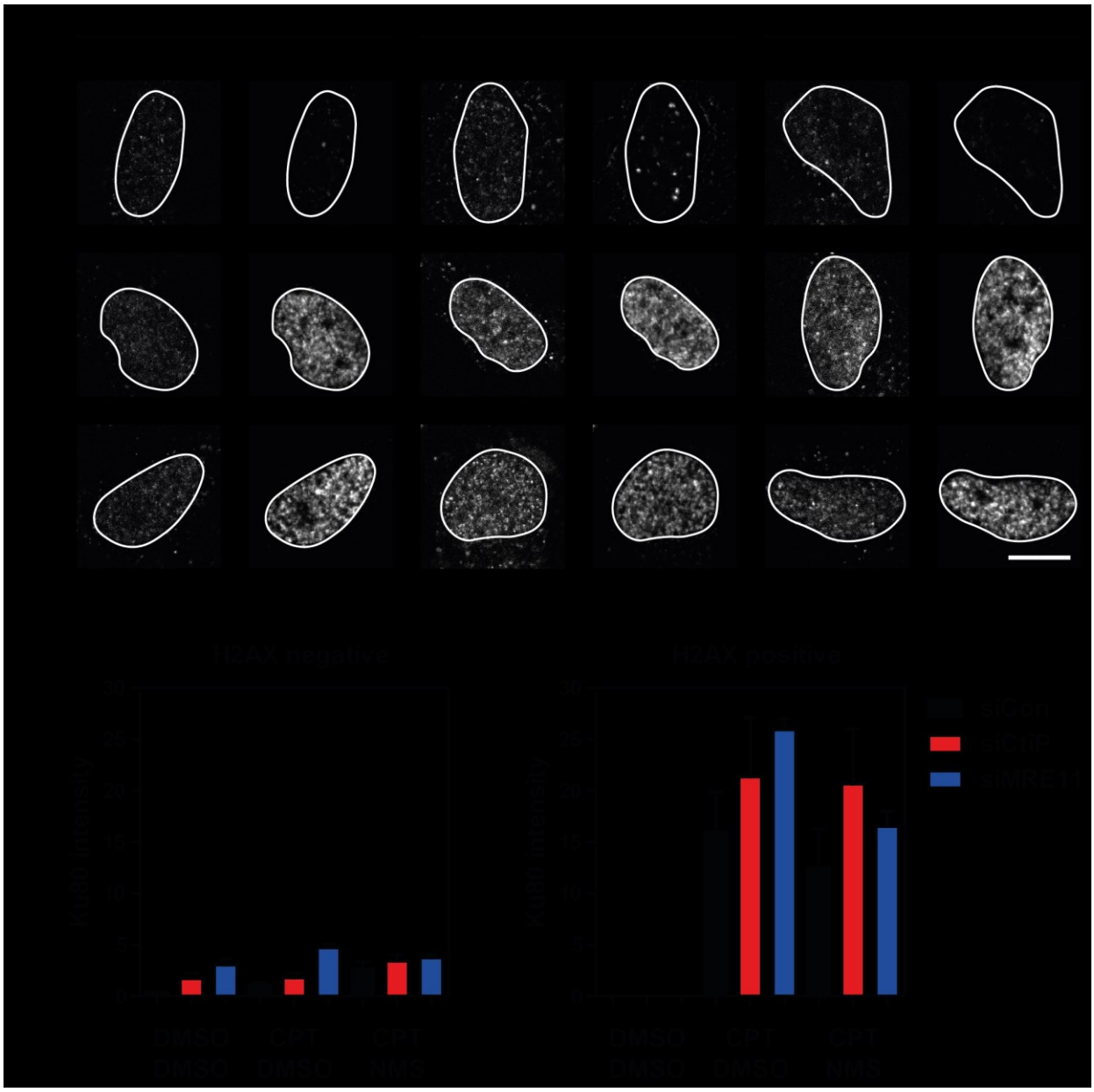

Figure 2.13: Ku80 is not extracted by p97 during repair of camptothecin (CPT)-induced DNA damage, but MRE11 and CtIP are required for efficient Ku80 removal.
A) Measurement of chromatin bound Ku80 after CPT treatment. U2OS cells were treated with or without 1 µM CPT and in addition with or without 10 µM NMS-873 for 1 h. Cells were then preextracted with CSK + RNase A, fixed and immunostained for Ku80 and γH2AX. Images were acquired by confocal laser scanning microscopy. Nuclei (white lines) were defined by DAPI staining. Scale bar = 10 µm.
B) Automated image quantification of A) using the CellProfiler software. As CPT induces significant amount of DNA damage only in S-phase cells, the nuclei were categorized based on their γH2AX intensity as negative (no damage) or positive (with DNA damage) and Ku80 intensity was measured. Error bars show means ±SD of three independent experiments. Significance was tested with ANOVA and Tukey's post-hoc test. * = $p<0.05$

In summary, the described function of CtIP and MRE11 could be confirmed, but p97 did not extract Ku80 from seDSBs, not even when CtIP or MRE11 were compromised.

An immunofluorescence-based analysis that was performed in our lab (see van den Boom et al, 2016 Figure 4 A + B), revealed that NMS-873 treatment strongly decreases the amount of phosphorylated RPA (pSer4/pSer8) bound to CPT-induced DNA damage sites. Further, in the experiment above (Figure 2.13) NMS-873 treatment reduced the number of γH2AX positive cells from 55 % to 43 % (in siCon samples).

2.6.4 p97 inhibition reduces CPT-induced seDSBs

We therefore set out to analyze γH2AX kinetics of seDSBs induced by CPT in combination with compromised p97 (Figure 2.14 A). In parallel to NMS-873, the competitive small molecule inhibitor CB-5083 was used to block p97 function. The inhibitors were added 15 min before CPT treatment and kept during the recovery time of up to 4 h. As established before, EdU incorporation was used as an independent marker to label cells in S-phase of the cell cycle and applied together with the CPT treatment. After fluorescent labeling of the EdU by click chemistry, the samples were stained with a γH2AX-specific antibody and DAPI and images were acquired by confocal laser scanning microscopy.

EdU incorporation was decreased by CPT treatment, but not due to p97 inhibition (Figure 2.14B). This was expected as the CPT-induced Top1ccs block replication forks and thereby DNA synthesis. In contrast, the γH2AX levels were significantly decreased by either p97 inhibitor (Figure 2.14 C) at the 0 h recovery time point. In the vehicle control, phosphorylation of the histone was induced within the 15 min of CPT treatment and reduced to less than 50 % at 4 h of recovery. Interestingly, with compromised p97, the induction of γH2AX by CPT was largely inhibited and the residual signal decreased over time.

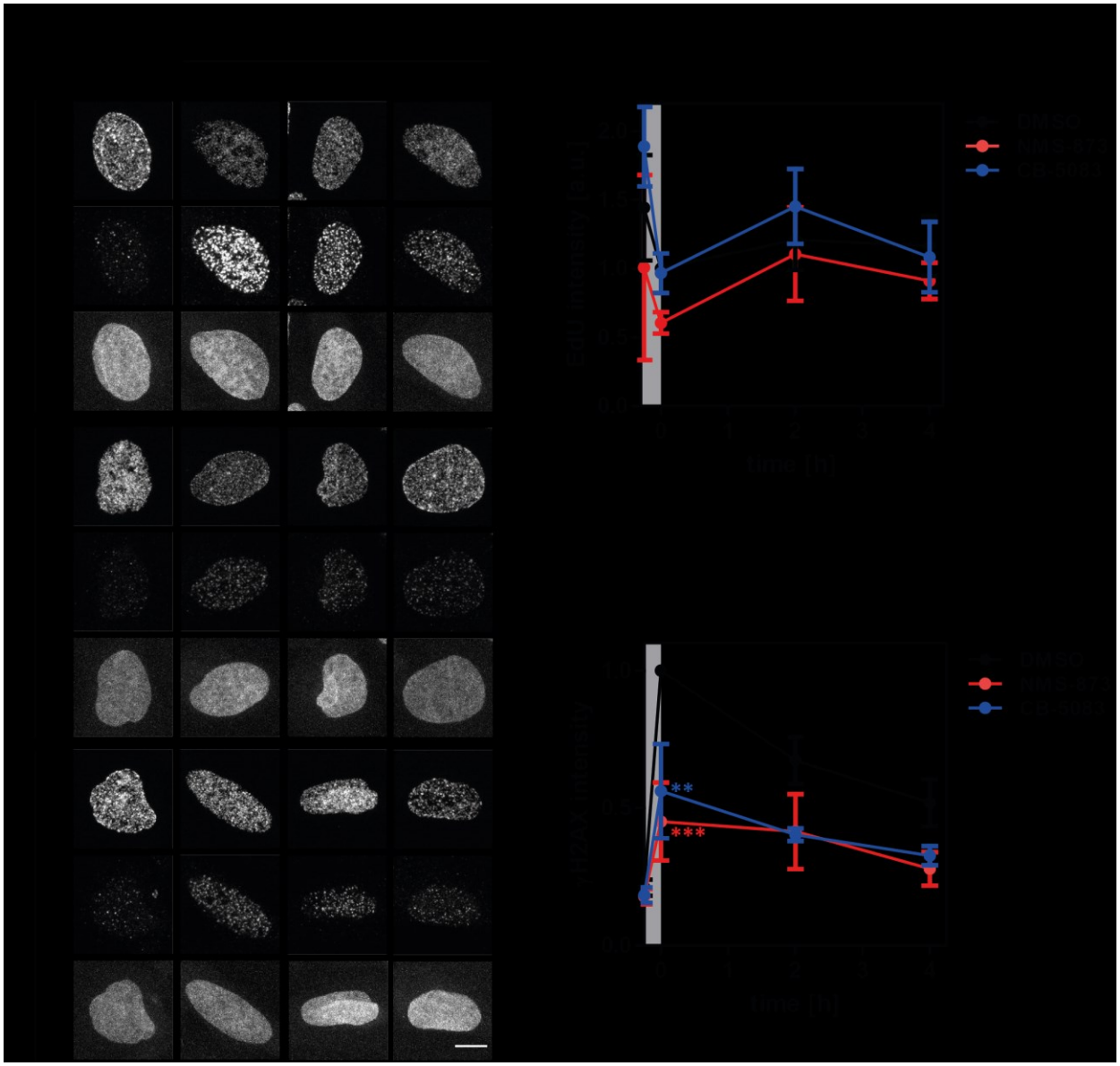

Figure 2.14: CPT-induced γH2AX levels are decreased with compromised p97.
A) Time course of γH2AX after CPT treatment. U2OS cells were pre-incubated with 10 µM NMS-873, 5 µM CB-5083, or DMSO as control for 15 min and then additionally treated with 5 µM EdU and 1 µM CPT or DMSO for another 15 min. Cells were then allowed to recover in the presence of NMS-873 or CB-5083 and fixed at the indicated time points. Samples were processed with a click chemistry reaction to label the EdU fluorescently and stained with Ku80-specific antibody and DAPI to visualize DNA. Images were acquired by confocal laser scanning microscopy. Scale bar = 10 µm.
B) Automated image quantification of EdU from A) using the CellProfiler software. Values are means ±SD of three independent experiments normalized to DMSO 0 h. Gray background highlights the time of CPT treatment. Significance was tested by ANOVA with Tukey's post-hoc test.
C) Automated image quantification of γH2AX from A) using the CellProfiler software. Values are means ±SD of three independent experiments normalized to DMSO 0 h. Gray background highlights the time of CPT treatment. Significance was tested by ANOVA with Tukey's post-hoc test. *** = p<0.001; ** = p<0.01.

2.6.5 CPT-induced topoisomerase 1-clevage complexes are not resolved by p97

To understand the mechanism of the reduced seDSB induction in p97 compromised conditions, the substrate of p97 at these lesions has to be identified. In a first hypothesis-driven approach, Top1 and Top1ccs were tested as potential substrates of p97. Top1 binds to chromatin by encircling the DNA helix and in the Top1ccs the protein is covalently attached to the DNA and cannot simply dissociate (Figure 1.5). This covalent tyrosyl-phosphodiester bond is known to be cleaved by a specialized enzyme, tyrosyl-DNA phosphodiesterase 1 (TDP1), but this might require structural changes, e.g. partial unfolding, to make the DNA-protein crosslink accessible. To analyze whether p97 is involved in the process of Top1cc removal or rather Top1 extraction, DNA slot blotting followed by immunostaining with Top1- and Top1cc-specific antibodies was performed.

CPT treatment induced Top1 binding to DNA, and inhibition of p97 by NMS-873 or CB-5083 or the proteasome by MG132 did not interfere with this effect (Figure 2.15 A). In fact, CPT-induced Top1 levels were increased upon p97 or proteasome inhibition and for MG132 this was significant (Figure 2.15 B). Top1 binding was reversed in all conditions within 10 min after CPT washout. Top1ccs were detected separately with an antibody specific for the phosphodiester bond (Figure 2.15 C). Only samples that were lysed directly after CPT treatment exhibited detectable Top1ccs. 10 min after washout of CPT, all Top1ccs were resolved, which was expected as the total Top1 protein was also released at this time point. However, no influence of p97 or proteasome inhibitors could be observed compared to control samples (Figure 2.15 D). Thus, the inhibitors showed a difference in their effect on Top1ccs and the total chromatin-bound Top1 protein.

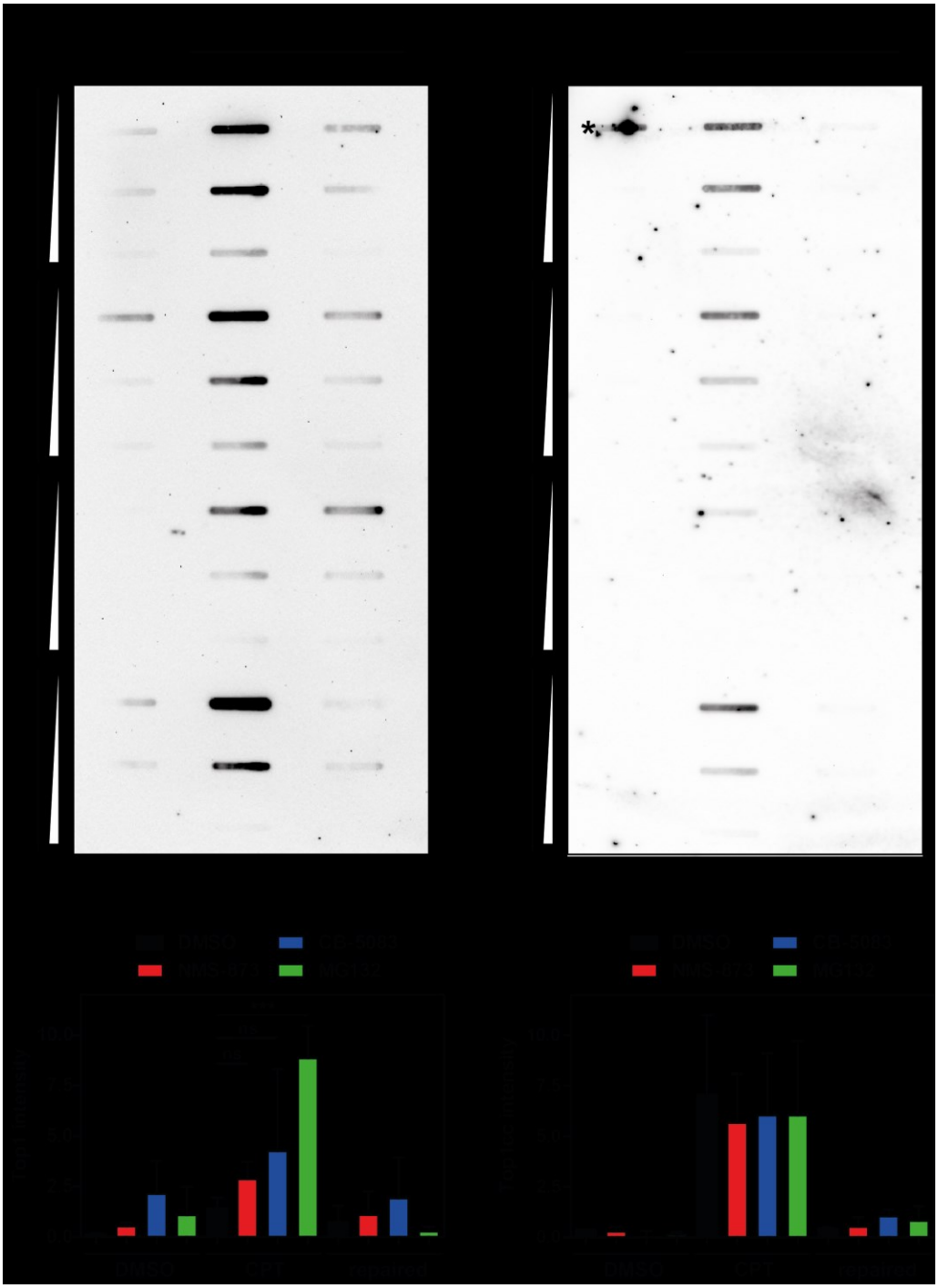

Figure 2.15: p97 does not target Top1ccs for extraction, but Top1 extraction from chromatin is influenced by p97 and dependent on the proteasome.
A) DNA slot blot immunostained for topoisomerase 1 (Top1). HEK293T cells were treated with 10 µM NMS-873, 5 µM CB-5083, 20 µM MG132, or DMSO as control and additionally with 1 µM CPT or DMSO for 1h. Cells were lysed directly or after they were allowed to recover for 10 min without CPT, but in the presence of the other inhibitors. DNA was precipitated from the lysates and 10, 5, or 2.5 µg of DNA were transferred to nitrocellulose membrane by slot blotting. The DNA-bound fraction of Top1 protein was detected by immunostaining with Top1-specific antibody.
B) Quantification of A) using TotalLab Quant software. Bars represent means ±SD from three independent experiments. Statistical significance was tested by ANOVA with Tukey's post-hoc test. *** = $p<0.001$.
C) DNA slot blot from A) immunostained with a topoisomerase I cleavage complex (Top1cc) specific antibody. The asterisk * marks an artefact that was excluded from the analysis (see D))
D) Quantification of A) using TotalLab Quant software. Bars represent means ±SD from three independent experiments (DMSO only n=2). Statistical significance was tested by ANOVA with Tukey's post-hoc test.

3 Discussion

This study aimed at defining the function of the essential ATPase p97 in the important pathways of DSB repair by identification of DSB-associated p97 substrates. Cell-based assays were performed and, together with parallel *in vitro* approaches by Johannes van den Boom, Ku80 was identified as substrate of p97. Our results demonstrate that p97 extracts sterically trapped Ku80 after NHEJ repair. This depends on K48-ubiquitination and ubiquitin-adaptor proteins.

Further, a role of p97 in response to CPT-induced DNA damage was found. CPT induces Top1ccs that yield seDSBs during replication. Loss of p97 function significantly reduced the CPT-induced γH2AX levels and the effect occurred independent of replication progression and Top1cc removal, which were not affected.

3.1 p97-mediated Ku80 extraction

3.1.1 p97 extracts Ku80 from DNA double strand breaks

The experiments presented here show that the essential NHEJ protein Ku80 is a substrate of p97. To enable specific analysis of DSB-bound Ku80, a sophisticated preextraction and immunofluorescence technique was established at localized DSBs that were induced by laser microirradiation (Figure 2.1). Using this technique, super-resolution imaging by 3D structured illumination microscopy was performed (Figure 2.2). Imaging with 3D-SIM enabled visualization of single DSB sites (Britton et al, 2013) and was combined with inhibition of p97 (Figure 2.2). Ku80 foci persisted upon loss of p97 activity, suggesting that p97 facilitates extraction of Ku80 from DSBs. This result was investigated more comprehensively with confocal laser scanning microscopy, in which the total amount of DSB-bound Ku80 was measured (Figure 2.3). Ku80 bound rapidly to IR-induced DSBs and was then removed from chromatin within two hours. Strikingly, acute inhibition of the ATP hydrolysis of p97 by NMS-873 completely abolished Ku80 release. This result confirmed observations from the 3D-SIM experiments and lead to the conclusion that the p97 ATPase facilitates the extraction of Ku80 from DSBs. Notably, no p97-independent mechanism compensated for loss of p97 function in that process.

The *in vitro* experiments in *Xenopus laevis* egg extracts showed Ku accumulation in response to compromised p97 by label-free quantitative mass spectrometry (LFQ-MS) and by a release assay that measured removal of ^{35}S-labled Ku80 from DSB-containing DNA beads (van den Boom et al, 2016). Together, the results demonstrated that removal of Ku80 from DSBs depends on functional p97.

The IF measurement of DSB-bound Ku80 showed that upon p97 inhibition, Ku80 levels even increased compared to the initial amount after exposure to IR (Figure 2.3). Ku binding to DSBs occurs within one second and increases for ~10 s after DSB induction (Hartlerode et al, 2015; Yang et al, 2018), which excludes an increase due to slow occupation of the DNA ends by Ku. Therefore, the increase was probably caused by DSBs that occurred temporally delayed. Such

breaks are called indirect DSBs and are generated by enzymatic processing of IR-induced lesions, e.g. processing of base damage opposite to a SSB on the complementary strand (Schipler & Iliakis, 2013). Another possible reason for the increasing Ku80 levels is that lesions in densely packed heterochromatin might not immediately be accessible for the Ku protein, but require chromatin remodeling during the DDR (Price & D'Andrea, 2013), which delays Ku binding. These processes probably also occurred in the control conditions, but ongoing p97-mediated extraction masked the effect.

3.1.2 Ku gets sterically trapped during NHEJ and is extracted after religation

Ku binds rapidly to DSBs by sliding on the DNA with a preformed channel and initiates NHEJ repair. Ku recruits many factors of this pathway and remains DNA-bound also during the ligation step of NHEJ (Figure 1.2). Thus, after religation of the breaks, Ku is sterically trapped on the DNA strand due to its ring-shaped form. Further, the molecule has no clasp to open for dissociation by a conformational change. This is a unique binding mode among the described DNA repair proteins and among the known p97 substrates.

Recently, a resection-dependent NHEJ pathway was identified that is active in G_1 phase of the cell cycle and performed by exonucleases (Biehs et al, 2017). At DSBs that are processed by this pathway, the resection only occurs from the DNA end, is not blocked by Ku, and Ku is pushed inwards, i.e. ahead of the exonucleases. In contrast to end resection in G_2 phase, which results in HRR, the subsequent steps are accomplished by NHEJ. Thus, Ku is also trapped at the end of this DSB repair pathway.

We performed assays to analyze whether p97 extracts the sterically trapped Ku80 after NHEJ or facilitates extraction upstream of the religation step. Measurement of γH2AX after irradiation and NMS-873 treatment showed that the γH2AX kinetics were not significantly different upon p97 inhibition (Figure 2.5). The progressing decrease of γH2AX levels in NMS-873-treated samples indicated that DSBs were repaired even without functional p97.

In addition, the persistence of DSBs upon loss of p97 was measured by pulsed-field gel electrophoresis (PFGE; van den Boom et al, 2016). This assay is a physical measurement of the amount of DSBs and revealed that the repair efficiency was not influenced by the NMS-873 treatment. In the *in vitro* experiments, DSBs were repaired by the *X. laevis* egg extract that contained radiolabeled Ku. Of note, these extracts were not able to repair DSBs via HRR. Next, the DNA was isolated and subjected to a high salt wash to remove DNA-bound proteins. Finally, the release of radiolabeled Ku was measured. Indeed, the salt wash was able to remove Ku80 from unrepaired, DSB-containing beads, but not from beads that were incubated to allow DSB repair. Ku80 was detected on those beads even after the high-salt wash, which indicated that it was sterically trapped, and Ku80 release from the DNA depended on p97 (van den Boom et al, 2016). Importantly, DSB religation in the egg extracts also occurred upon loss of p97 function.

In summary, the breaks were religated upon loss of p97 and Ku80 was sterically trapped on chromatin. The results lead to the conclusion that Ku80 is primarily extracted after religation of DSBs by NHEJ. Our conclusion is in line with the published data, which showed that Ku80 promotes the ligation step of NHEJ by recruitment of factors of the ligation complex (Nick McElhinny et al, 2000; Yano et al, 2008).

In comparison to Ku80 extraction, the release of an independent DSB repair factor, Nbs1, from chromatin was tested in combination with p97 inhibition (Figure 2.4). In contrast to Ku80, Nbs1 did not persist on chromatin and the release was not impaired upon loss of p97 function. Nbs1 is part of the MRN complex that has important functions in end processing, promotes HRR, and, like Ku, binds rapidly to DSBs. Nbs1 is not sterically trapped on chromatin during DSB repair, but it is ubiquitinated by the same E3 ligase as Ku80 (RNF8; Lu et al, 2012). Nevertheless, the results suggested that Nbs1 is not a substrate of p97 and indicated the specificity of the effects of NMS-873 treatment on Ku80 extraction without affecting DNA repair in general.

3.1.3 Ku80 is a major substrate for DSB-induced K48-linked polyubiquitination

Binding of Ku to DNA triggers Ku80 ubiquitination (Postow et al, 2008). Ku80 ubiquitination occurs at multiple positions and mutations of 19 lysine residues did not abolish ubiquitination (Ishida et al, 2017). Different E3 ubiquitin ligases have been described for Ku80 ubiquitination: RNF 8 (Feng & Chen, 2012), RNF 126 (Ishida et al, 2017), RNF138 (Ismail et al, 2015) and SCF^{FBXL12} (Postow & Funabiki, 2013). Except for RNF138, the ligases were described to form K48-linked polyubiquitin chains (the chain type of Ku80 ubiquitination by RNF138 was not reported). The RNF ligases were found in human cells, whereas SCF^{FBXL12} was identified in *X. leavis*.

In this study, DSB-induced and chromatin-bound K48-linked polyubiquitination was analyzed in U2OS cells by immunofluorescence, which revealed that IR-induced K48-Ub is largely reduced upon Ku80 knockdown (Figure 2.10). This suggested that a large fraction of DSB-associated K48-linked ubiquitin chains occur on Ku80. Further, K48-Ub accumulated upon p97 inhibition (Figure 2.10), which indicates that the modified form of Ku80 is extracted by p97.

In the *in vitro* assays, K48R ubiquitin mutants, which are unable to form K48-linked chains, reduced Ku ubiquitination (van den Boom et al, 2016). Moreover, the experiments revealed that the interaction of p97 and Ku80 depends on K48-linked polyubiquitin.

Taken together, our results show that Ku80 is a major substrate for DSB-induced modification with K48-linked ubiquitin chains and that this modification is important for the interaction with p97 and leads to extraction from chromatin.

3.1.4 Roles of the p97 cofactors Ufd1 and FAF1 in Ku80 extraction

p97 interacts with a variety of cofactors, which recruit the ATPase to its substrates and modulate the function of the complex. Results of this study show that the functional complex for Ku80 extraction contains p97 and Ufd1(-Npl4) and might additionally contain FAF1. Alternatively, p97 and FAF1 could act in a separate complex with minor role in Ku80 extraction.

In the aforementioned LFQ-MS experiment, the p97 cofactors Ufd1-Npl4 and FAF1 were enriched at DSBs upon p97 inhibition (van den Boom et al, 2016). In a subsequent RNAi approach, knockdown of Ufd1 had the strongest effect among the cofactor depletions and depletion of FAF1, the cofactor that was most enriched in the LFQ-MS, did not significantly reduce Ku80 extraction. In the experiments of this study, the effect of Ufd1 knockdown on Ku80 extraction was not as strong as the effect of p97 knockdown, although depletion efficiency was lower for p97 (Figure 2.6).

A genomic knockout of FAF1 was chosen to analyze the function of the cofactor in Ku80 extraction, since the knockdown had insignificant effects. The homozygous knockout of FAF1 was achieved by CRISPR/Cas9 in U2OS cells (Figure 2.7). FAF1 KO alone had no effect on long-term survival of U2OS cells after exposure to IR (Figure 2.8) and a mild effect on Ku80 extraction (Figure 2.9). Importantly, a synergistic effect on Ku80 extraction was observed in combination with Ufd1 knockdown (Figure 2.9). The results confirmed data of in the *in vitro* assay, in which Ufd1 depletion significantly delayed Ku80 release (van den Boom et al, 2016).

Our findings were in line with the other reported p97-dependent processes on chromatin that found in nearly all cases the complex of p97-Ufd1-Npl4 (1.14). Structural studies revealed a quaternary complex of p97-Ufd1-Npl4-FAF1 with a stoichiometry of 6:1:1:1 (Hänzelmann et al, 2011) and a quaternary complex was also found in other studies (Lee et al, 2013; Ewens et al, 2014). The published data suggest functions of the quaternary complex in ERAD (Lee et al, 2013). Additionally, the structure of a FAF1 trimer that binds above the D1 domain ring of the p97 hexamer was solved (Ewens et al, 2014) and binding in this stoichiometry is probably mutually exclusive with binding of a Ufd1-Npl4 heterodimer for steric reasons. Thus, at least three complexes are possible (p97-Ufd1-Npl4, p97-Ufd1-Npl4-FAF1, p97-FAF1) and our data are sufficient to conclude that the p97-FAF1 complex is dispensable for Ku80 extraction in wild type conditions (Figure 2.9). However, the data are not sufficient to determine whether FAF1 is part of the p97-Ufd1-Npl4 complex that acts in Ku80 extraction or part of a distinct p97-FAF1 complex that acts in a backup pathway upon loss of Ufd1.

A p97-dependent process on chromatin that involves Ufd1-Npl4 and FAF1 is release of the CMG helicase, which is facilitated by ubiquitination and p97-mediated extraction of the Mcm7 subunit. In a study using frogs and worms, Sonneville et al. revealed that Ufd1-Npl4 is required for the p97- and ubiquitin-dependent extraction of the helicase after replication termination (Sonneville et al, 2017). Upon perturbed Mcm7 ubiquitination, CMG persists on chromatin after replication and is removed during mitosis by a second pathway that depends on FAF1. A comparable backup function of FAF1 for Ku80 extraction would be in line with the data of this study, since Ufd1 was epistatic to FAF1 (Figure 2.9). The data were obtained from non-synchronized cells and a potential cell cycle-specific requirement of the cofactors, like for CMG extraction, needs to be addressed by further analyses.

3.1.5 Protein unfolding as a possible mechanism of p97-mediated Ku80 extraction

The unique DNA binding mode of Ku presupposes unfolding of the Ku80 molecule to be extracted from DNA. Indeed, p97 meets this requirement, since it can unfold its substrates by a recently described mechanism. It was shown that substrate processing by p97 involves threading through the central channel of the hexamer and therefore entails substrate unfolding (Bodnar & Rapoport, 2017). For Ku80 extraction, this potential mode of action is in line with our results that described the requirement of unfolding due to steric trapping of Ku and identified Ufd1-Npl4 as cofactor for Ku80 extraction (Figure 2.6; van den Boom et al, 2016).

Additionally, efficient threading through the central channel of p97 was shown to rely on deubiquitination (Bodnar & Rapoport, 2017). p97 has three known cofactors with DUB activity (VCIP135, YOD1, Ataxin3) and they are all recruited to sites of DNA damage (Nishi et al, 2014) and could therefore deubiquitinate Ku80 that is threaded through p97. Knockdown of the DUBs did not interfere with ligation of DSBs (Nishi et al, 2014). This is resembled by p97 inhibition that did not interfere with DSB religation, as discussed above (3.1.2). Thus, published data and results of this study are in line with a function of DUBs in p97-mediated Ku80 extraction after NHEJ and this needs to be addressed in future studies.

The mechanism of threading through the p97 hexamer is supported by a recent study that investigated the structure of a fungal Cdc48-Ufd1-Npl4 complex (Bodnar et al, 2018). They found the Ufd1-Npl4 heterodimer positioned above the D1 ring and substrates that bind to Ufd1-Npl4 can be delivered to the central channel of p97 for threading and unfolding. Substrate binding is mediated by ubiquitin that is recognized by the UT3 domain of Ufd1 and the CTD and MPN domains of Npl4. Their results render Ufd1-Npl4 an ideal cofactor to assist translocation through the central channel of p97 and support the possibility that Ku80 is unfolded by this pathway. In this thesis, not only Ufd1 was identified as cofactor for Ku80 extraction, but also FAF1 was found to be involved in the extraction, although the effects were hypostatic to Ufd1 (Figure 2.9). However, whether FAF1 can contribute to the mechanism of threading substrates into the D1 pore of p97 is unknown.

3.1.6 Regulation of p97-mediated Ku80 extraction

p97-mediated Ku80 extraction is a ubiquitin-dependent process and therefore Ku80 ubiquitination is the major regulator of the extraction. *In vitro,* Ku80 ubiquitination is triggered by DNA binding (Postow et al, 2008), which in turn enables recognition by the p97-Ufd1-Npl4(-FAF1) complex(es). As Ku is essential for NHEJ repair, a regulating mechanism that restricts extraction of ubiquitinated Ku80 before religation would be beneficial for efficient NHEJ repair. This could include restriction of Ku ubiquitination to the end of NHEJ or blocking access of the p97 complex to Ku before ligation. The fact that different E3 ligases ubiquitinate Ku80 indicates that the modification is required in various situations, e.g. different repair pathways or cell cycle phases, which are presumably regulated differently. Indeed, it was shown that Ku80 is ubiquitinated by

RNF8 in G_1 phase (Feng & Chen, 2012) and by RNF138 in S and G_2 phase (Ismail et al, 2015). Further, RNF138 is recruited to ssDNA that is generated by initial end resection and promotes HRR (Ismail et al, 2015). In contrast to inhibition of p97, loss of RNF8 and RNF126 did not only impair Ku80 extraction but also compromised DSB repair by NHEJ (Feng & Chen, 2012; Ishida et al, 2017), which might still be independent of Ku80 ubiquitination and extraction.

Aside from Ku80 ubiquitination, additional regulatory mechanisms of p97-mediated Ku80 extraction are possible. A potentially interesting modification of p97 in this context is the DSB-induced phosphorylation close to the C-terminus at S784 by DNA-PK_{cs} (Livingstone et al, 2005). Although the relevance of this modification is unknown, it might be related to the function of p97 at DSBs. Another C-terminal phosphorylation that modulates p97 activity was identified at Y805, the penultimate amino acid, and shown to block the interaction with the cofactors peptide:N-glycanase (PNGase) and Ufd3 (PLAA in humans; Zhao et al, 2007). This inhibits the function of p97 in ERAD (Li et al, 2008).

Ku interacts with several proteins and recruits factors for NHEJ, which could limit interaction with ubiquitin ligases or p97 complexes during NHEJ and postpone the extraction to a point after dissociation of the non-trapped repair factors. Another possibility that could prevent early Ku extraction would include regulating protein-protein interactions of factors that bind to Ku and to p97, e.g. DNA-PK_{cs} (Walker et al, 2001; Livingstone et al, 2005) and WRN (Cooper et al, 2000; Partridge et al, 2003). Further, Ku80 extraction could be regulated by kinetics, i.e. a competition between completion of NHEJ repair that relies on DNA-bound Ku and Ku80 extraction from DNA. This would imply that if NHEJ fails within a certain time frame, Ku is removed to allow initiation of alternative DNA repair pathways. The aforementioned hypotheses need to be addressed by experiments to get a better understanding how Ku80 ubiquitination and extraction is regulated.

3.1.7 p97-independent mechanisms of Ku release

Hypothetical possibilities to remove the ring-shaped Ku protein independent of p97-mediated extraction include proteolytic cleavage, e.g. in the bridge region or nucleolytic cleavage of the Ku-bound DNA. At least in *Xenopus* egg extracts, it was shown that Ku extraction is a separate step upstream of proteolytic processing by the proteasome (Postow et al, 2008) and in the *in vitro* experiments, Ku80 was detected as full-length protein after extraction (van den Boom et al, 2016). This renders proteolytic cleavage for Ku removal from chromatin unlikely. Detection of full-length Ku80 after extraction indicates another intriguing scenario, in which Ku80 might be refolded after extraction instead of being degraded by the proteasome. Ku80 removal by nucleolytic cleavage is not suitable after DSB religation, as it would reintroduce a DSB. However, such a nucleolytic cleavage is possible at open DSBs and is discussed below.

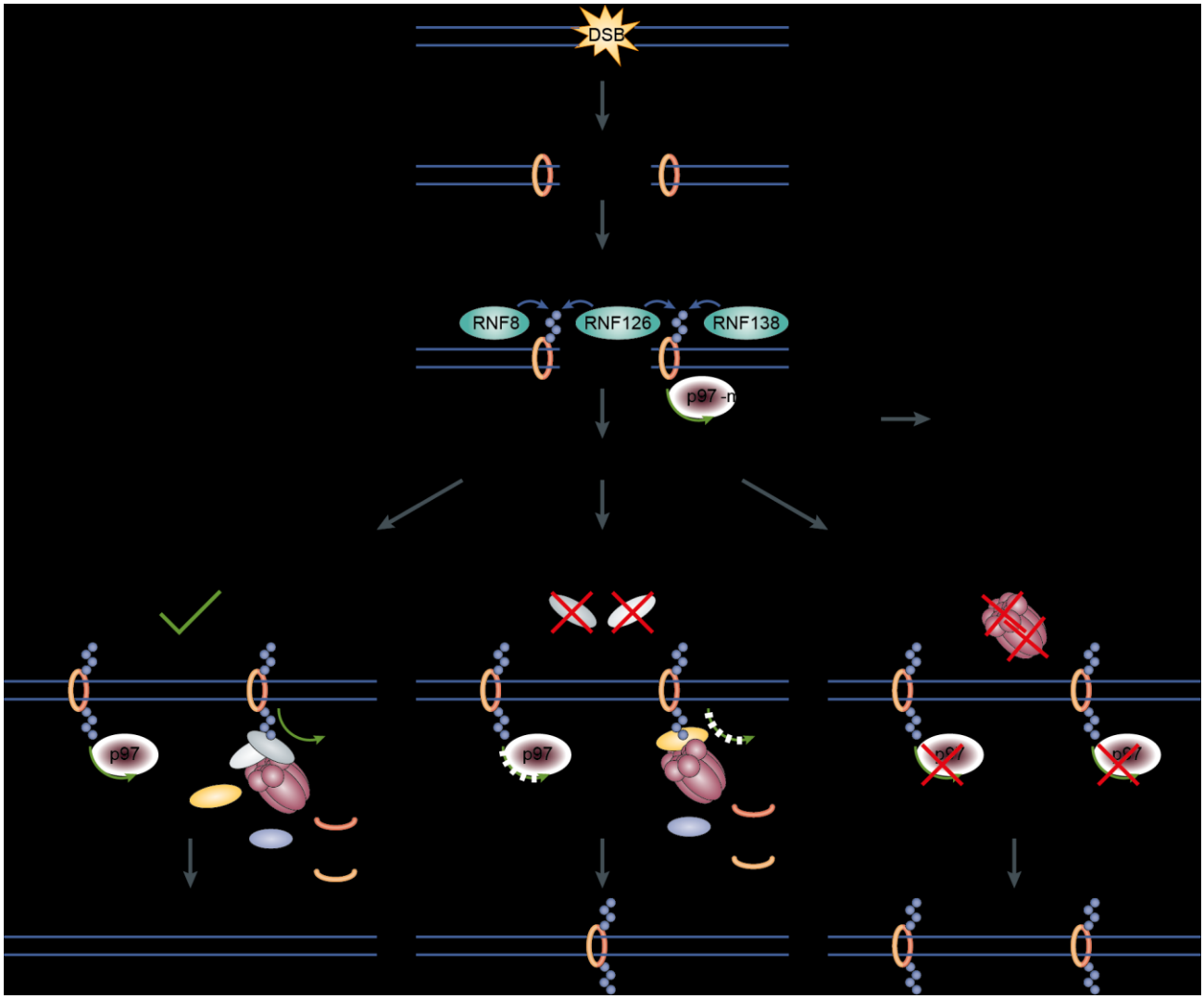

Figure 3.1: Model of p97-mediated Ku80 extraction during DSB repair.
A) A DNA double strand break (DSB) is rapidly bound by the Ku70/80 heterodimer, that has a ring shaped form and slides onto the double helix from the end. Upon DNA binding, Ku80 is modified with K48-linked polyubiquitin chains (depicted in blue). E3 ubiquitin ligases that mediate Ku80 ubiquitination were identified and shown to function cell cycle specific. RNF8 is predominantly active in G_1 phase and activity of RNF138 is restricted to S and G_2 phase. Additionally, RNF126 was described, but a cell cycle regulated function is unknown. The present study identified Ku80 is extracted from chromatin by the p97 ATPase. This might take place at open DSBs and would probably promote homologous recombination repair (HRR). DSB repair via non-homologous end-joining (NHEJ) requires DNA-bound Ku and upon religation of the DSB, Ku is sterically trapped on chromatin.
B) p97 targets ubiquitinated Ku80 and extracts it from chromatin. p97 acts in a complex with its cofactors Ufd1-Npl4 that might also contain FAF1. The cofactors can bind to the ubiquitin chains and thereby function as substrate adaptors for p97. Ufd1-Npl4 was shown to be required for a substrate processing mechanism in which the client proteins are threaded through the central channel of p97. The substrates are unfolded by this mechanism and extraction of the sterically trapped Ku requires substantial unfolding. Further, ubiquitin chains need to be removed for efficient extraction and therefore, Ku removal might involve deubiquitinating enzymes (DUBs). Whether Ku70 is extracted concomitantly or by other mechanisms is unknown.
C) In our experiments, depletion of Ufd1 and Npl4 caused reduced or delayed Ku80 extraction. However, this might be compensated by a backup pathway in which Ku80 extraction can be facilitated by a complex of p97 and FAF1. This pathway could also include additional factors, e.g. DUBs.
D) In the absence of functional p97, sterically trapped Ku persists on DNA. In the assays of this study, no other pathway could compensate for the loss of p97. Ku persistence will interfere with chromatin processes like transcription and replication. Some elements of the model were adopted from Schwertman et al, 2016.

The cell-based experiments presented here concentrated on the remaining chromatin-bound Ku80 and therefore conclusions regarding protein folding, potential proteolytic or nucleolytic cleavage, and proteasomal degradation cannot be drawn. However, if a proteolytic or nucleolytic pathway for Ku release exists in U2OS cells, it is not impaired by NMS-873 treatment and can compensate the loss of p97 function at least partially. As mentioned before, in our experiments no other mechanism compensated for the loss of p97 in extraction of Ku80 from chromatin (Figure 2.3). Therefore, the results indicate that p97-independ Ku removal by proteases and nucleases is also unlikely in human cells and establish p97-mediated extraction of Ku80 as the main – if not the only – pathway in NHEJ.

In other situations, e.g. at open DSB ends or during HRR, different mechanisms for Ku removal cannot be excluded. In fact, recent reports described a mechanism of Ku removal from seDSBs that depends on DSB resection by the MRN complex and CtIP (Chanut et al, 2016; Myler et al, 2017). The seDSBs were induced by CPT and seemed to trigger a different damage response than deDSBs. seDSBs can only repaired by HRR and Ku blocks repair by this pathway (Sun et al, 2012). MRN and CtIP nucleolytically release a short piece of DNA with Ku bound to it (Chanut et al, 2016) and therefore this mechanism is restricted to Ku80 release from open DSBs and not possible after NHEJ.

The results of this study are in line with the reported mechanism for Ku80 release from seDSBs. In particular, Ku80 release from CPT-induced breaks was affected by Mre11 and CtIP knockdown, but not by p97 inhibition (Figure 2.13). This is in contrast to the striking effects of p97 inhibition at IR-induced deDSBs, at which Ku80 release is completely blocked (Figure 2.3). The MRN complex itself was found to be released together with Ku in the nucleolytic pathways (Myler et al, 2017). Here, the immunofluorescence-based comparison of chromatin-bound Ku80 and the MRN component Nbs1 revealed different kinetics at IR-induced, i.e. double-ended, DSBs in control and p97-inhibited conditions (Figure 2.4). In the NMS-873-treated samples, Nbs1 was released slightly faster than in control conditions, but Ku80 largely persisted compared to DMSO. This suggests that the mechanism of Ku80 release from seDSBs has no major role at deDSBs. Thus, the MRN- and CtIP-dependent processes are likely restricted to HRR of seDSBs or possibly general HRR, but cannot function as general backup mechanism for Ku80 removal after p97 inhibition.

An independent observation is that phosphorylation of Ku70 decreases the binding affinity to DNA, which was suggested to be sufficient for Ku release from open DNA ends (Lee et al, 2016). Phosphorylation and ubiquitination often occur in parallel or even regulate each other, e.g. in the Fanconi anemia pathway (Gibbs-Seymour et al, 2015). Ku70 phosphorylation was not addressed by our experiments, but the results did not exclude presence of this modification. Release of Ku70 is also discussed below (3.1.10).

3.1.8 p97-mediated Ku80 extraction from open DSBs

The aforementioned Ku release from open seDSBs was described as an p97-independent mechanism (Chanut et al, 2016), which is in line with results of this study (Figure 2.13). However, it is possible that p97-mediated Ku80 extraction is an additional process at unrepaired deDSBs and the mechanism would probably resemble extraction of trapped Ku80 after NHEJ repair.

Ku80 ubiquitination is triggered by binding of the protein to dsDNA, irrespective of the repair status of the DSB (Postow et al, 2008). Results from FRAP experiments (Mari et al, 2006) and our *in vitro* experiments (unpublished data) suggested that p97 is able to extract ubiquitinated Ku80 also from open DSBs. The results reported here are in line with that idea, although none of the experiments can prove the hypothesis. At first glance, Ku extraction from open DNA ends is counterintuitive, because Ku is required for the whole NHEJ pathway including the ligation step. Nevertheless, NHEJ shows rapid kinetics and recruitment of the NHEJ factors to the break is probably faster than Ku80 extraction. The extraction from open non-repaired DSBs might be relevant upon failure of NHEJ, to enable the switch to another repair pathway. More generally, p97-mediated Ku80 extraction might generate a layer of kinetic regulation for NHEJ repair, in which NHEJ-promoting recruitment of repair factors competes with NHEJ-compromising Ku extraction.

3.1.9 Implications of Ku80 extraction for repair pathway choice and early steps of HRR

Pathway choice is a critical process in DSB repair and determines if the break is repaired by HRR or one of the end-joining pathways. Except for the possibility of crossovers, the use of HRR is beneficial due to error-free restoration of the DNA, but it has certain requirements (Wright et al, 2018). The repair via HRR requires a homologous sister chromatid that is only available after replication and it involves long-ranged resection, which might be hindered by the chromatin structure around the break. Commitment to (extensive) end resection is a critical step in repair pathway choice and Ku inhibits EXO1-mediated long-ranged end resection (Sun et al, 2012). In contrast, Ku is a critical factor for NHEJ and therefore, regulation of its removal from open deDSBs might be a mechanism of pathway choice.

As mentioned above, MRN-CtIP-mediated end resection was shown to remove Ku at seDSBs (Chanut et al, 2016), but it is unknown whether this mechanism removes Ku from deDSB prior to HRR. However, for efficient EXO1-mediated end resection, Ku needs to be removed from these lesions. A p97-mediated Ku80 extraction from open DSBs would therefore not only regulate NHEJ, but also create a bias towards HRR. The aforementioned ubiquitin ligase RNF138 is recruited to ssDNA which is generated by the initial MRN-CtIP-mediated end resection, and ubiquitinates Ku80 specifically in the S/G_2 phase of the cell cycle (Ismail et al, 2015). This supports the idea of ubiquitin-dependent Ku removal upstream of extensive end resection and it is likely that p97 can facilitate this extraction.

In this study, all experiments were performed in non-synchronized cells and consequently deDSBs that allow pathway choice were only present in irradiated cells. The preextraction technique allowed specific analysis of DSB-bound fraction of Ku80, but an isolated analysis of the minority of breaks that are repaired by HRR was not feasible. Thus, no conclusions on repair pathway choice by p97-mediated Ku80 extraction can be drawn from our data.

In the HRR reporter assay performed in this study, loss of p97 strongly reduced the number of successful HRR events (Figure 2.11). This suggested an important role of p97 in the HRR repair pathway, although the underlying mechanism is still elusive due to the fact that DR-GFP is an endpoint assay. Although reporter assays entail different limitations, reporter assays that enable simultaneous measurement of NHEJ and HR are available (traffic light reporter from Certo et al, 2011 and SeeSaw reporter 2.0 from Gomez-Cabello et al, 2013). These systems are suitable to measure changes in the ratio between NHEJ and HRR upon p97 inhibition and indicate a potential p97-dependent repair pathway choice. However, p97 was already implicated in HRR (Bergink et al, 2013; Ali et al, 2018) and thus a conclusion whether (p97-mediated) Ku80 extraction is a mechanism of pathway choice would still require additional approaches that analyze the distinct steps in the repair pathways.

3.1.10 Extraction of Ku70

The focus of this thesis was the p97-mediated Ku80 extraction. However, as Ku is a stable heterodimer of Ku70 and Ku80 with a large interface between both proteins (Walker et al, 2001), the question arises how Ku70 is extracted. Ubiquitination of Ku70 at K114 has been identified (Brown et al, 2015), but it is weaker than Ku80 polyubiquitination that occurs at multiple sites (Ishida et al, 2017), which renders p97-mediated Ku70 extraction unlikely. Additional described PTMs of Ku70 include SUMOylation in budding yeast (Hang et al, 2014) and several phosphorylations, especially in the bridge region that encircles DNA, in human cells (Lee et al, 2016). SUMOylation of yKu70 is connected to increased affinity for DNA and is therefore rather inhibitory for Ku extraction. The reported phosphorylations decrease the affinity of Ku70 towards DNA ends and are sufficient for Ku release from open DNA ends *in vitro*. Ku70 phosphorylation can probably occur together with Ku80 ubiquitination and might even support Ku80 extraction. However, a decreased affinity is not sufficient for removal of trapped Ku rings and therefore Ku70 phosphorylation alone cannot release Ku after NHEJ. Ku70 and Ku80 form a tightly-bound dimer also in solution, which stabilizes the proteins (Walker et al, 2001). Here, knockdown of Ku80 led to destabilization and codepletion of Ku70 (Figure 2.10). Therefore, unfolding of DNA-bound Ku80 by p97 might destabilize the associated Ku70 molecule, but it remains unclear whether Ku70 is unfolded and removed together with Ku80.

3.2 Functions of p97 in HRR and in processing of CPT-induced DNA lesions

3.2.1 HRR is compromised upon loss of p97

In yeast, p97 and Ufd1 have reported functions during HRR at the step of Rad52-mediated Rad51 filament formation and the authors suggested similar functions in U2OS cells (Bergink et al, 2013). p97 facilitates removal of the HRR-inhibiting factor RYBP and loss of p97 leads to accumulation of RYBP, which impairs HRR (Ali et al, 2018). The reporter assay performed in this study (Figure 2.11) suggests functions of p97 and Ufd1 in HRR. As mentioned above, measuring fluorescence of the DR-GFP reporter is an endpoint assay and the known functions of p97 will have an impact on the results. Therefore, we were interested in a more specific analysis of Ku80 extraction at early steps of HRR and aimed at generating damage that is exclusively repaired by HRR.

3.2.2 seDSBs induced by CPT treatment are repaired specifically by HRR

We decided for treatment with the topoisomerase I inhibitor camptothecin (CPT), which stabilizes the usually transient Top1ccs. During S phase, the nicks at Top1ccs are propagated into seDSBs and can only be repaired by HRR, as no second end is available for repair via end joining pathways. The situation of an approaching replisome to a Top1cc can vary. Either the nick is on the leading strand and the Mcm helicase runs off, which yields a seDSB, or the nick is on the lagging strand, which stalls the helicase. The latter situation is probably solved by Mus81-dependent cleavage that then also yields seDSBs (Regairaz et al, 2011).

CPT treatment strongly induced γH2AX specifically during S phase (Figure 2.12). Ku80 bound to the CPT-induced seDSBs and, as discussed above, the amount did not increase upon loss of p97 (Figure 2.13).

3.2.3 p97 inhibition reduces CPT-induced γH2AX levels

During the analysis of Ku80, we noticed reduced levels of CPT-induced γH2AX in NMS-873-treated samples and elaborated on this with a second p97 inhibitor (CB-5083; Figure 2.14). Further, the levels of pRPA, Rad51 (van den Boom et al, 2016), and RPA were significantly decreased. The published work on p97 functions in HRR can help to explain the reduction of (p)RPA and Rad51, but not reduced γH2AX levels. Upon loss of p97, RYBP accumulated and reduced end resection (Ali et al, 2018). Thus, the effect was upstream of (p)RPA and Rad51 binding. Further, if the p97-Ufd1-mediated regulation of Rad51 filament formation exists in cells (Bergink et al, 2013), it can additionally account for reduced Rad51 levels in samples with compromised p97.

H2AX is phosphorylated quickly in response to DSB induction and is significantly decreased upon p97 inhibition (Figure 2.14), which can have at least two causes. Either the DSB signaling including H2AX phosphorylation or the induction of seDSBs from Top1ccs is impaired by p97 inhibition. Unspecific effects of the inhibitors can be excluded, because the significant reduction of γH2AX was observed independently with NMS-873 and CB-5083. H2AX can be

phosphorylated by all of the three major DDR kinases (ATM, ATR and DNA-PK) that are activated by different mechanisms in response to DSBs (Blackford & Jackson, 2017). It is highly unlikely that NMS-873 and CB-5083 block all three pathways of DSB signaling upstream of γH2AX. This supports the possible explanation that seDSB induction by CPT treatment is a p97-dependent process. This possibility is also in line with the other results, such as significantly reduced amounts of pRPA, RPA, Rad51 (van den Boom et al, 2016) and, in combination with MRE11 knockdown, Ku80 (Figure 2.13).

The induction of seDSBs via stabilized Top1ccs requires ongoing replication and impaired replication fork progression in the absence of functional p97 could explain the observed effects. Reduction of replication forks progression in response to p97 inhibition has also been discussed in the literature (Mouysset et al, 2008). In this study, quantification of EdU incorporation confirmed unperturbed progression of replication in samples treated with p97 inhibitors (Figure 2.14), which excludes impaired replication from constituting the underlying mechanism of the γH2AX reduction.

p97 is a ubiquitin-dependent segregase that has functions on chromatin. Thus, the most likely mechanism how the ATPase contributes to seDSB induction is the extraction of proteins from DNA upon collisions of Top1ccs and replication forks. Alternatively, formation of Top1ccs could be impaired upon loss of p97, which is unlikely. p97 is an important factor of the UPS and in line with the effects of p97 inhibition, proteasome inhibition by MG-132 treatment reduces CPT-induced RPA, 53BP1 and DNA-PK_{cs} phosphorylation and these effects are also resembled by a block of replication progression with hydroxyurea (Sakasai et al, 2010). In summary, the probable function of p97 upstream of γH2AX induction is extraction of (so far unidentified) proteins, whose extraction sets free seDSBs.

3.2.4 Potential p97 substrates at sites of CPT-induced DNA damage

In order to understand the function of p97 at CPT-induced DNA damage, we aimed at identifying the substrates at these lesions. In a candidate approach, p97-dependent removal of the topoisomerase I and Top1ccs were tested by DNA slot blotting (Figure 2.15). CPT-induced Top1cc levels were not influenced by inhibition of p97 or the proteasome and Top1cc removal was neither affected. Reversal of the 3'-phosphotyrosyl DNA bond for repair of stabilized Top1ccs is achieved by the enzyme TDP1 (Yang et al, 1996). The total level of DNA-bound Top1 was significantly increased upon proteasome inactivation and elevated upon p97-inhibition in CPT-treated samples. However, the effects of NMS-873 and CB-5083 treatments were not significant and could therefore not explain the strong reductions of γH2AX. Thus, other substrates of p97 need to be identified in further experiments, e.g. by an unbiased approach using mass spectrometry.

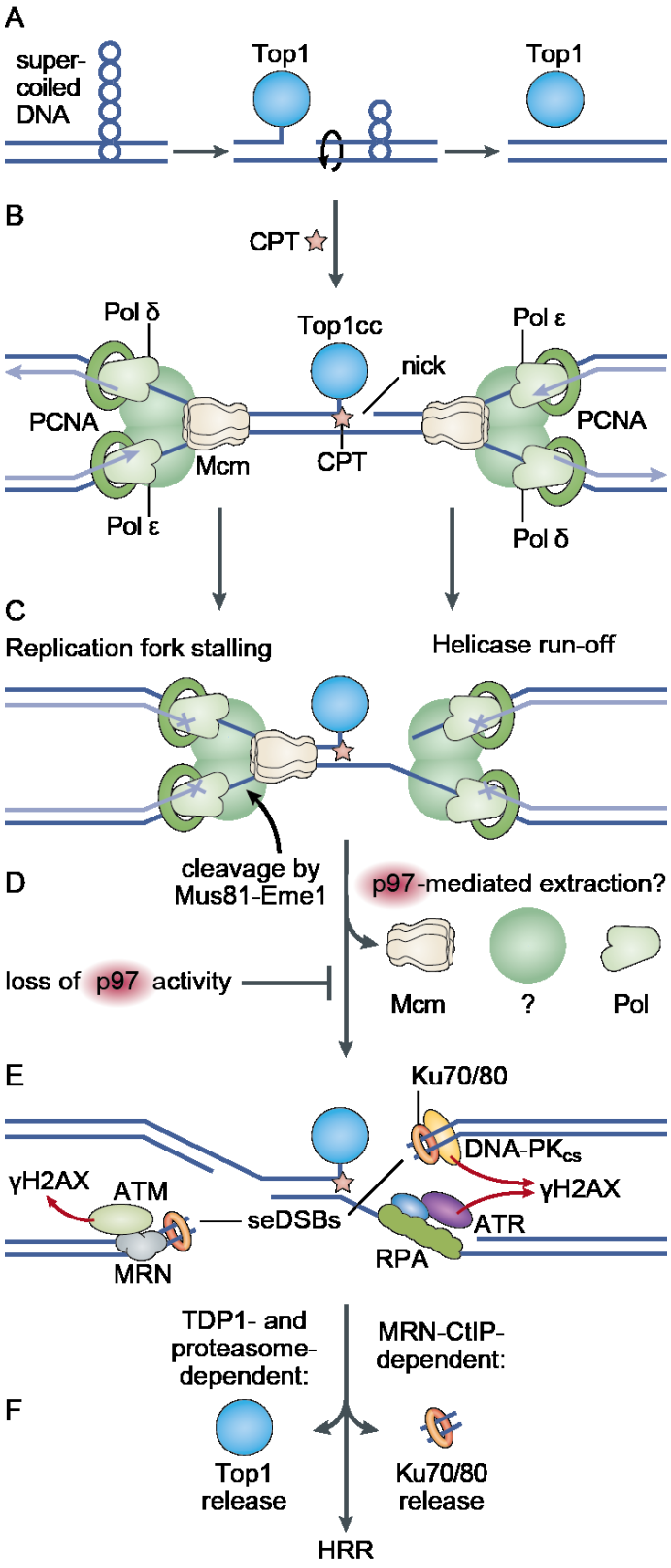

Figure 3.2: Model of CPT-induced seDSBs and the possible functions of p97.

A) Replication and other sources cause positive supercoiling of the DNA, which can be released by topoisomerase I (Top1). Top1 binds covalently to one DNA backbone, which induces a nick. Top1 binding is transient and the nick enables relaxation of the supercoiling.

B) Camptothecin (CPT) inhibits Top1, which stabilizes the covalently bound form, called Top1 cleavage complex (Top1cc), and the nick. Top1ccs are DNA-protein crosslinks and form a barrier for replication. During S phase, replication forks that are composed of the Mcm helicase, DNA polymerases (Pol δ, Pol ε), PCNA, and other factors approach the Top1cc.

C) Top1ccs were described to stall replication forks and induce single ended DNA double strand breaks (seDSBs) due to run-off of the Mcm helicase at the nick. CPT-induced replication fork stalling activates the structure specific endonuclease Mus81-Eme1 and the nucleolytic cleavage induces seDSBs as well.

D) Results of this study indicate that p97 is involved in CPT-dependent seDSB induction. A possible function of p97 is extraction of replisome components including the Mcm helicase, DNA polymerases, and unknown factors (?). This might be required to set seDSBs free, as acute inhibition of p97 suppressed the induction of histone H2AX phosphorylation.

E) seDSBs are bound by the Ku70/80 heterodimer that recruits and activates the DNA-PK$_{cs}$ kinase. RPA coats single stranded DNA sections and is bound by ATRIP, which recruits and activates the ATR kinase. Additionally, the MRN complex can bind to seDSBs and recruit the ATM kinase via its subunit Nbs1. All three kinases are able to phosphorylate (red arrows) histone H2AX at S129 (γH2AX).

F) A specialized enzyme, Tyrosyl-DNA phosphodiesterase 1 (TDP1), resolves the covalent Top1-DNA-bond and in experiments of this study, Top1 removal from DNA was proteasome-depended. The MRN complex and CtIP facilitate Ku release from seDSBs, which was independent of active p97 in our experiments. Subsequent, seDSBs are specifically repaired by homologous recombination repair (HRR).

Some elements of the model were adopted from Gaillard et al, 2015 and Schwertman et al, 2016.

Further candidates include proteins of the replisome, which is a large multi-protein complex and several factors might be substrates of p97. Mcm7, a part of the replicative helicase, is ubiquitinated and extracted by p97 during replication termination (Maric et al, 2014) and interstrand crosslink repair (Fullbright et al, 2016), which could be similar at CPT-induced lesions.

In summary, it was shown that p97 has a role in processing of CPT-induced DNA lesions, but the substrate and the underlying mechanism remains elusive. At these lesions, Ku80 was not extracted by p97, but removed during MRN- and CtIP-mediated end resection of seDSBs. Top1ccs that were stabilized by CPT were not targeted by p97 or the proteasome and reports showed that Top1ccs are dissolved by TDP1. However, extraction of Top1 from chromatin seems to be a separate process, for which the proteasome is required. Upon p97 inhibition, the levels of γH2AX, pRPA, and, in combination with MRE11 KD, Ku80 were significant reduced. These results suggest a role of p97 in an early step of the processing of CPT-induced lesions, most likely before the seDSBs are set free, which could include extraction of replisome components.

4 Materials and Methods

4.1 Materials

Table 1: Media, buffers, and solutions used in this study

Name	Component	Concentration	Source
Medium for: U2OS wild type U2OS FAF1 KO HEK293T	DMEM FCS penicillin streptomycin	 10 % 100 U/ml 100 mg/ml	all PAN Biotech GmbH
Medium for: U2OS DR-GFP	McCoy's 5A FCS penicillin streptomycin L-glutamine	 10 % 100 U/ml 100 µg/ml 2 mM	all PAN Biotech GmbH
Trypsin/EDTA (without Ca^{2+} and Mg^{2+})	PBS Trypsin EDTA	 0.05 % 0.02 %	PAN Biotech GmbH
Cytoskeleton buffer (CSK; preextraction for Ku80 IF)	PIPES pH 7.0 (NaOH) NaCl sucrose $MgCl_2$ Triton X-100	10 mM 100 mM 300 mM 3 mM 0.7 % (v/v)	Sigma Aldrich GmbH AppliChem GmbH AppliChem GmbH Acros Organics AppliChem GmbH
Preextraction buffer (for K48-Ub IF)	HEPES pH 7.5 NaCl EDTA $MgCl_2$ sucrose Triton X-100	25 mM 50 mM 1 mM 3 mM 300 mM 0.5 % (v/v)	AppliChem GmbH AppliChem GmbH AppliChem GmbH Acros Organics AppliChem GmbH AppliChem GmbH
PBS	Na_2HPO_4 pH 7.4 NaH_2PO_4 NaCl	10 mM 2.17 mM 154 mM	all AppliChem GmbH

Name	Component	Concentration	Source
PBS for cell culture	KCl KH_2PO_4 NaCl Na_2HPO_4	200 mg/l 200 mg/l 8 g/l 1,15 g/l	PAN Biotech GmbH
IP buffer (cell lysis)	150 mM KCl 50 mM Tris pH 7.4 $MgCl_2$ glycerol Triton X-100 β-mercaptoethanol	150 mM 50 mM 5 mM 5 % 1 % 2 mM	 AppliChem GmbH Acros Organics Sigma Aldrich GmbH
6x SDS sample buffer	Tris pH 6.8 glycerol (87%) SDS DTT bromophenol blue	350 mM 30 % 10 % 600 mM 0.02 %	AppliChem GmbH AppliChem GmbH AppliChem GmbH AppliChem GmbH Riedel-de Haën AG
SDS-PAGE buffer	Tris pH 8.8 glycine SDS	25 mM 190 mM 0.1 %	all AppliChem GmbH
Wet blot buffer	Tris pH 8.3 glycine SDS methanol	25 mM 192 mM 0.04 % 20 % (v/v)	AppliChem GmbH AppliChem GmbH AppliChem GmbH VWR Chemicals
Ponceau S solution	Ponceau S acetic acid	0.2 % (w/v) 5 % (v/v)	Sigma Aldrich GmbH Fisher Scientific
slot blot lysis buffer	guanidine thiocyanate sodium citrate pH 7.0 N-laurosylsarcosine 2-mercaptoethanol	4 M 25 mM 0.5 % (w/v) 100 mM	AppliChem GmbH Sigma Aldrich GmbH Sigma Aldrich GmbH Sigma Aldrich GmbH
6x SSC solution	NaCl trisodium citrate	900 mM 90 mM	all AppliChem GmbH

Table 2: Recipes for handcasted SDS polyacrylamide gels (amount for one gel)

stock solutions	7.5 % gel	10 % gel	18 % gel	5 % stacking gel
water	2.19 ml	1.69 ml	0.085 ml	1.75 ml
1 M Tris pH 8.8	2.25 ml	2.25 ml	2.25 ml	(pH 6.8) 305 µl
30 % PAA	1.5 ml	2 ml	3.6 ml	410 µl
10 % SDS	60 µl	60 µl	60 µl	25 µl
10 % APS	30 µl	30 µl	30 µl	25 µl
TEMED	3 µl	3 µl	3 µl	5 µl

Table 3: Oligonucleotides used in this study

The final concentrations were specific for each assay (IF: immunofluorescence; reporter: DR-GFP reporter)

Name	Sequence	Reference	Final concentration	Database entry
siCon	UUCUCCGAACGUGUCACGUTT	(Dobrynin et al, 2011)	10-20 nM depending on the experiment	714
siCtIP	GCTAAAACAGGAACGAATCTT	(Chanut et al, 2016)	20 nM	1519
siKu80	GGAUGGAGUUACUCUGAUUTT	(Ma et al, 2012)	20 nM	1485
siMRE11	GAGCATAACTCCATAAGTATT	(Chanut et al, 2016)	20 nM	1520
sip97 s3	AAGUAGGGUAUGAUGACAUUGTT	(Wójcik et al, 2004)	10 nM IF 15 nM reporter	740
sip97 s7	CAAUAAACGUUGGGUCAAATT	(Zhou et al, 2013)	10 nM IF 15 nM reporter	1389
siRad51	GGGAAUUAGUGAAGCCAAATT	(Meerang et al, 2011)	15 nM	1168
siUfd1 s2	GUGGCCACCUACUCCAAAUTT	(Dobrynin et al, 2011)	10 nM IF 15 nM reporter	594
siUfd1 s6	CCCAAUCAAGCCUGGAGAUAUTT	(Li et al, 2014)	10 nM IF 15 nM reporter	1263

Table 4 Primary and secondary antibodies used in this study

Primary antibodies				
Antigen	**Species**	**Source**	**Dilution IF**	**Dilution blot**
α-tubulin	mouse	Sigma	-	1:10,000
FAF1	rabbit	Eurogentec, custom made	-	1:500
γH2AX	rabbit	abcam, ab11174	1:1,000	-
γH2AX	mouse	BioLegend, clone 2F3	1:5,000	-
K48-Ub	rabbit	Merck Millipore, clone Apu2	1:800	-
Ku70	mouse	abcam, clone N3H10	-	1:500
Ku80	mouse	Thermo Scientific, clone 111	1:100	-
Ku80	rabbit	Aviva Systems Biology, OAAN01591	-	1:800
Nbs1	rabbit	Novus Biologicals, NB100-143	1:100	-
p97	mouse	Fitzgerald Ind., clone 58.13.3	-	1:1,000
PCNA	rabbit	abcam, clone EPR3821	1:100	-
Top1	rabbit	abcam, clone EPR5375	-	1:10,000
Top1cc	mouse	TopoGEN, TG2017	-	1:1,000
Ufd1	mouse	C. Brasseur, 5E2, purified	-	1:500
Secondary antibodies				
Antigen	**Species**	**Source**	**Dilution IF**	**Dilution blot**
HRP anti-mouse	goat	BioRad	-	1:10,000
HRP anti-rabbit	goat	BioRad	-	1:10,000
Alexa 488 anti-mouse	goat	Life Technologies	1:500 or 1:250 (SIM)	-
Alexa 488 anti-rabbit	goat	Life Technologies	1:500	-
Alexa 568 anti mouse	goat	Life Technologies	1:500	-
Alexa 568 anti-rabbit	goat	Life Technologies	1:500	-

Table 5 Chemicals used in this study

Chemical	Source	Final concentration
BrdU	Sigma Aldrich	10 µM
Camptothecin (CPT)	Sigma Aldrich	1 µM
CB-5083	Selleckchem	5 µM
DAPI	Roche	0.5 µg/ml
DMSO	Sigma Aldrich	variable
EdU	abcam	5 µM
MG132	ApexBio	20 µM
NMS-873	Sigma Aldrich	10 µM
RedDot 1	Biotium	1:1000 from stock

4.2 Cell culture and treatments

4.2.1 General culturing of cells

All cell lines were cultivated in humidified atmosphere containing 5 % CO_2 at 37 °C. Medium was depending on the cell line (Table 1). For passaging, the cells were washed with PBS and detached with Trypsin/EDTA. Cells were counted with a Neubauer counting chamber before seeding to achieve equal cell numbers for each experiment.

For long-term storage, cells were resuspended in DMEM supplemented with 40 % FCS and 10 % DMSO, cooled down to -80 °C with a rate of 1 °C/min, and stored in vapor phase of liquid nitrogen (~160 °C).

4.2.2 Transfections

siRNA oligonucleotides (Table 3) were transfected by lipofection with Lipofectamine RNAiMAX according to the manufacturer's instructions. The ratio of Lipofectamine RNAiMAX:siRNA was 1 µl : 10 pmol and the final siRNA concentrations are listed in Table 3. The oligonucleotides were purchased from Microsynth Seqlab GmbH.

DNA plasmids were transfected by polyfection with jetPRIME according to the manufacturer's protocol, using a ratio of 2 µl jetPRIME : 1 µg plasmid DNA.

4.2.3 Chemical treatments

For chemical treatments, the substances were prediluted in pH- and temperature-equilibrated medium (~10 % of the final volume) and added to the cultivated cells. To wash out chemicals, samples were rinsed with PBS or medium and fresh equilibrated medium was added. Substances and concentrations are listed in Table 5.

4.2.4 Irradiation with x-rays

The X-ray source for exposure of cells to X-IR was a Philips MCN 165 with 3 mm Al filter at 130 kV and 16 mA yielding a dose-rate of 1.2 Gy/min. Cells were kept in medium during irradiation.

4.3 CRISPR/Cas9 knockout

4.3.1 crRNA design

Two crRNA sequences were designed with tools from the Zhang lab (http://crispr.mit.edu/; Ran et al, 2013) and the Root lab (https://portals.broadinstitute.org/gpp/public/analysis-tools/sgrna-design; Doench et al, 2016). The tools use data from a genome-wide gRNA screen (Wang et al, 2015). The target genome was “human hg38” or “human GRCh38”, respectively and the FAF1 genomic sequence (NCBI GeneID: 11124; Ensembl: ENSG00000185104) was used as input. Cas9 enzyme of *Streptococcus pyogenes* with the protospacer adjacent motif (PAM) NGG was used.

The selected sequences were targeting exon 1 and exon 4 of the FAF1 gene:

FAF1 Exon1: GGA CCG GGA GAU GAU CCU GGG UUU UAG AGC UAU GCU

FAF1 Exon4: UGA CUU GCU GGA UUA AAU GCG UUU UAG AGC UAU

Cas9 cleavage site in exon1 was in codon 11 and after codon 65 in exon4. The UBA domain is encoded by codons 1–47.

4.3.2 RNP generation and transfection

crRNA and tracrRNA were mixed in nuclease-free duplex buffer at a final concentration of 30 µM. The mix was heated to 95 °C for 5 min and allowed to cool for 15 min. The crRNA:tracrRNA hybrids were diluted to 1 µM with duplex buffer and purified Cas9 (*S. pyogenes*)-3NLS protein was diluted to a concentration of 1 µM in OptiMEM. Both components were mixed with OptiMEM in a ratio of 1:1:15 and incubated at RT for 10 min to form ribonucleocomplexes (RNPs). RNPs were diluted with OptiMEM (1:1) and Lipofectamine RNAiMAX was added (1:40). After incubation for 20 min at RT, the RNPs were mixed with U2OS cells at a final concentration of 10 nM.

4.3.3 Purification of gDNA, PCR and sequencing

Genomic DNA was purified from cultured cells with a NucleoSpin Tissue kit (MACHEREY-NAGEL GmbH & Co. KG) and DNA concentration was measured. Exons 1 and 4 of FAF1 were amplified from gDNA by PCR (sample mix and thermocycle in Table 6).

The PCR mix was loaded on an agarose gel (1 %) and separated by electrophoresis. PCR products were purified from the gel with a NucleoSpin Gel and PCR Clean-up kit (MACHEREY-NAGEL GmbH & Co. KG) and sent to GATC Biotech AG for Sanger sequencing. The PCR primer were also used as sequencing primer.

Table 6: Sample mix and thermocycle for FAF1 amplification from genomic DNA

Mix		
Component	**for 50 µl reaction**	**Final concentration**
5X Phusion HF buffer	10 µl	1X
10 mM dNTPs	1 µl	200 µM
100 µM forward primer	0.5 µl	1 µM
100 µM reverse primer	0.5 µl	1 µM
Template DNA	100 ng	2 ng/µl
Nuclease-free water	to 50 µl	
Phusion DNA Polymerase	0.5 µl	0.02 units/µl
Thermocycle		
Step	**Temperature**	**Time**
Initial denaturation	98 °C	30 s
30 cycles	98 °C	7 s
	66 °C	15 s
	72 °C	30 s
Final extension	72 °C	5 min
Hold	10 °C	∞

4.3.4 TIDE analysis

Chromatograms from Sanger sequencing (.ab1-files) of control and KO samples and the crRNA sequence were uploaded to the TIDE tool (Tracking Indels by DEcomposition), which is available online (https://tide.nki.nl/). The algorithm reconstructs the occurring insertions and deletions and reports their frequency (Brinkman et al, 2014).

4.4 Cell-based assays

4.4.1 Colony formation assay

The protocol for colony formation was adopted from Munshi et al, 2005 and Franken et al, 2006. U2OS wt and FAF1 KO cells were seeded in 10 cm dishes for colony formation assay after X-IR doses up to 6 Gy. Triplicates of each sample were analyzed in each experiment and the following amounts of cells were plated and irradiated after 4 h:

0 Gy – 200 cells; 2 Gy – 500 cells; 4 Gy – 2000 cells; 6 Gy – 20000 cells.

The samples were incubated for two weeks. Then, the medium was aspirated and the plates were rinsed once with PBS. Cells were stained and fixed with 0.5 % crystal violet in 20 % ethanol. Plates were washed in tap water several times, dried and colonies were counted.

The average plating efficiency of each sample (from n=3) was calculated (Equation 1) and normalized, setting the non-irradiated wild type sample to 100 %.

Equation 1: Calculating the plating efficiency

$$plating\ efficiency = \frac{number\ of\ colonies}{number\ of\ plated\ cells} * 100\ \%$$

The surviving fraction was determined (Equation 2) and plotted on a logarithmic axis against the radiation dose (**Fehler! Verweisquelle konnte nicht gefunden werden.**).

Equation 2: Calculating the surviving fraction

$$surviving\ fraction = \frac{plating\ efficiency\ of\ irradiated\ sample}{plating\ efficiency\ of\ nonirradiated\ control} * 100\ \%$$

4.4.2 DR-GFP reporter assay measured by flow cytometry

For each sample, 200,000 U2OS DR-GFP cells were plated into six-well plates with reverse depletion (4.2.2). 24 h later, the I-SceI-expressing plasmid was transfected with fresh medium (1 µg/well; 4.2.2) and the medium was changed again 24 h after this transfection. The samples were analyzed after additional 48 h (72 h after plasmid transfection). For this, the cells were trypsinized, resuspended in medium to stop the reaction, spun down (900*g/3 min), and resuspended in PBS on ice. The samples were measured on a MACSQuant VYB (Miltenyi Biotec GmbH) with the following settings: FSC 240 V, SSC 235 V, GFP 400 V, IFP 440 V (these values were changed slightly by calibration procedures performed before every experiment with MACSQuant Calibration Beads (Miltenyi Biotec GmbH)); fast flow rate; sample premixing; stop after 20,000 gated events. Gating was done for living cells (FSC-A/SSC-A) and doublets were excluded twice (SSC-A/SSC-H and FSC-A/FSC-H; Figure 2.11).

Data was analyzed with the Kaluza flow cytometry software (Beckman Coulter GmbH) and gates for GFP fluorescence were set based on negative control (siCon) samples. Values are presented in percent of gated events and normalized to negative control, which was set to 100 %.

4.5 Microscopy-based assays

4.5.1 Laser microirradiation

48 h before the laser microirradiation experiments, U2OS wt cells were seeded in µ-slide 8 well (#1.5 with ibiTreat; ibidi GmbH) with 25,000 cells/well in 300 µl medium. Alternatively, 150,000 cells were cultivated in 2 ml medium on µ-dish 35mm low grid-500 (#1.5 with ibiTreat; ibidi

GmbH). After 24 h, 10 µm BrdU was added to presensitize the cells. RedDot 1 was added shortly before the experiment (~10 min; 1:1,000 from 200x stock solution) to visualize the nuclei.

The prepared samples were subjected to laser microirradiation on an Eclipse Ti-E inverted microscope (Nikon) with an Andor AOTF Laser Combiner, a CSU-X1 Yokogawa spinning disk unit and an iXon3 897 single photon detection EMCCD camera (Andor Technology). A CFI Apo TIRF 100×/1.49 NA oil immersion objective (Nikon) and a continuous wave diode laser with 405 nm and 100 mW combined with a Revolution FRAP and Photo Activation illumination system (FRAPPA; Andor Technology) were used for irradiation. The RedDot 1 dye was visualized with a continuous wave diode laser with 640 nm (max. 100 mW). The system was controlled by Andor IQ3 software (Andor Technology). Additionally, the microscope was equipped with a live cell imaging chamber that was set to 37 °C and 5 % CO_2 during the experiment.

A line with a width of 8 px (1.12 µm) was defined as ROI for each nucleus and irradiated 10 times for 200 µs with 50 mW (50 % power). Each sample was microirradiated for 5 min, which yielded ca. 40 irradiated nuclei. Sample processing (4.5.2) and imaging (4.5.4) is described below.

4.5.2 Processing of microscopy samples

For imaging experiments, 70,000-90,000 U2OS cells were seeded in 12 well plates on 18 mm 1.5H glass cover slips and (optionally) transfected with siRNAs. After 48 h, cells were treated with inhibitors and/or ionizing radiation as described. Further processing steps were determined by the targets for immune staining. If not stated differently, all reagents were kept at room temperature and the incubation steps were performed at room temperature and in the dark.

Preextraction techniques for immunofluorescence of DSB-bound Ku80 were based on the procedure described by Britton et al, 2013. The cover slips were transferred into a clean multiwall plate with PBS, washed with PBS twice, and preextracted 2x 3 min with CSK buffer containing 0.3 mg/ml RNase A (Sigma R4875). The samples were washed 3x 1 min with PBS and fixed with 4 % formaldehyde in PBS for 15 min.

For staining of K48-Ub, cells were rinsed with PBS, preextracted with preextraction buffer for 1 min on ice, washed with PBS and fixed with 4 % formaldehyde in PBS for 15 min.

For staining of other epitopes, cells were not preextracted and fixed directly after short PBS wash. Therefore, the samples were incubated for 15 min with 4 % formaldehyde in PBS. The slides were washed 3x 1 min with PBS and permeabilized with 0.5 % Triton X-100 in PBS for 10 min.

Subsequent steps were identical in all immunofluorescence assays. The cells were washed 3x 1 min in blocking buffer (PBS, 0.05 % Tween-20, 4 % BSA) and blocked for 1 h in blocking buffer. Primary antibodies were diluted in blocking buffer and incubated with the samples for 2 h. Samples were rinsed and then washed 3x 5 min with blocking buffer, followed by 1-2 h incubation of the secondary antibodies that were also diluted in blocking buffer. Samples were rinsed and washed 3x 5 min with blocking buffer and fixed in 2 % formaldehyde/PBS for 10 min. Finally, the

samples were rinsed with PBS, dipped into ultra-pure water and mounted in ProLong Gold antifade reagent (Thermo Fisher Scientific) on microscope slides. Cover slips of 3D-SIM samples were sealed with nail polish to avoid curing of the ProLong Gold. Samples were imaged within two days and stored at 4 °C.

To label incorporated EdU by click chemistry (Presolski et al, 2011), the cells were processed with a EdU-Click 647 kit (Baseclick GmbH; volumes differed from manual as stated below). After permeabilization and before incubation of the primary antibodies, the cells were incubated 30 min in the click reaction mix. This mix was prepared in the following order and directly before use (volumes per 18 mm cover slip): 125 µl ultra-pure water, 12.5 µl reaction buffer (from 10x stock), 6.25 µl catalyst solution (contains $CuSO_4$), 0.25 µl Eterneon-Red 645 azide solution (contains azide-coupled fluorophore), and 12.5 µl buffer additive (from 10x stock, contains reducing agent). After fluorescent labeling of EdU by click chemistry, the samples were washed with blocking buffer twice and blocked in blocking buffer for 30 min. The following steps for antibody staining were performed as described above.

4.5.3 3D structured illumination microscopy

Images were acquired on a Zeiss ELYRA PS.1 Super-resolution Microscope with Structured Illumination (SIM) equipped with an edge sCMOS camera (PCO), an alpha Plan-Apochromat 100×/1.46 NA oil immersion DIC M27 Elyra objective (Zeiss). A 405 nm diode laser (max 50 mV) was used for excitation of DAPI and a 488 nm OPSL laser (max 200 mV) for Alexa Fluor 488. Band pass beam splitter filtered the emission to ranges of 420-480 nm (DAPI) and 495-575 nm (Alexa Fluor 488). ZEN black software (Zeiss) was used to control the microscope and image acquisition. Images had a size of 1280x1280 px with a bit depth of 16 bit and were averaged from two frames. Five SIM rotations (72 °) with a SIM grating of 42 µm were used and 14 or 15 Z-stacks with a spacing of 101 nm were recorded. Quantification was done with CellProfiler (4.5.5) after calculation of the super-resolution images and maximum intensity projection with ZEN black software.

4.5.4 Confocal laser scanning microscopy

Immunofluorescence images were acquired on a TCS SP8 HCS confocal laser scanning system controlled by LAS X software (Leica Microsystems). An HC PL APO 63×/1.4 NA CS2 oil immersion objective was used and the fluorophores were excited with a 405 nm diode laser (50 mW; for DAPI), an argon laser line 488 nm (20 mW; for Alexa Fluor 488), a 561 nm diode-pumped solid-state laser (20 mW; for Alexa Fluor 568), and a 633 nm helium-neon laser (10 mW; for RedDot 1 and Eterneon-Red 645). Signals were detected with a Hybrid detector (HyD) in a 1024x1024 px or 2048x2048 px format (1x zoom) with a bit depth of 12 bit. Z stacks were acquired with the SuperZ Galvo stage with a spacing of 300 µm. Quantification was done with CellProfiler (4.5.5) after maximum intensity projection with LAS X software.

4.5.5 Image analysis

Images were processed and analyzed with Fiji (Schindelin et al, 2012), a distribution of ImageJ (Rueden et al, 2017). Automated image quantification was done with CellProfiler (versions 2.1, 2.2, and 3.0; Carpenter et al, 2006). The pipelines were specific for the assay, but followed a basic scheme: Identify nuclei (DAPI or RedDot 1) with identify primary objects, measure object intensity (Ku80, γH2AX, EdU, K48-Ub) and optionally had further modules, e.g. classify objects (positive/negative) or use identify objects to define foci. Analysis was done in Excel 2013 (Microsoft Corporation) and GraphPad Prism 5 (Graphpad Software Inc.). Figures were built with Adobe Illustrator CC 2018 (Adobe Systems).

4.6 Biochemical assays

4.6.1 Preparation of cell lysates and measurement of protein concentration

Cell lysates were prepared on ice and all buffers and reagents were kept at 0 °C. Cells were rinsed with PBS and IP buffer supplemented with cOmplete EDTA-free protease inhibitor (Roche) was added. Cells were detached using a cell scraper, collected in 1.5 ml reaction tubes, and incubated for 15 min. The lysates were centrifuged at 17,000 – 21,100 *g (max. speed) at 4 °C for 15 min. The supernatant was transferred into new tubes and protein concentration was determined by bicinchoninic acid assay (BCA protein assay; Interchim) according to the manufactures manual. The lysates were snap frozen and stored at -80 °C or analyzed directly.

4.6.2 SDS-PAGE and blotting

Protein samples were separated by sodium dodecyl sulfate polyacrylamide gel electrophoresis (SDS-PAGE). For this, 30-50 µg of protein/sample (determined by BCA assay) were boiled with 2x SDS sample buffer (diluted 1:3 from 6x) at 95 °C for 5 min. Polyacrylamide gels (10 % or 7.5-18 % gradient; recipes in Table 2) were casted with a Mini-PROTEAN Tetra Handcast System (BioRad) and electrophoresis was done in the Mini-PROTEAN Tetra Cell with SDS-PAGE buffer and a current of 20 mA/gel generated by an EPS 601 power supply (GE Healthcare). Transfer to a nitrocellulose membrane (Amersham Protran Premium 0.45 µm, GE Healthcare Life Sciences) was done by wet blot in the Mini Trans-Blot cell (BioRad) using wet blot buffer and 400 mA for 3 h at 4 °C. The membrane was stained with Ponceau S solution and destained with 5 % acetic acid. The staining was documented and washed out with 0.05 % Tween 20 in PBS (PBS-T). The membrane was then developed by immunostaining (4.6.4).

4.6.3 DNA slot blotting

For each sample, 300,000 HEK293T cells were plated into six-well plates. After two days, cells were treated with inhibitors and recovered as described (Figure 2.15). Sample processing included cell lysis, DNA precipitation, solubilization, slot blotting, and immunostaining.

To lyse the cells, the medium was aspirated and 750 µl of slot blot lysis buffer were added to each well. Using cell scrapers, the lysate was collected in 15 ml tubes and DNA was precipitated

by addition of 1.5 ml ethanol (absolute). After careful but thorough mixing, the samples were centrifuged at 12,000 *g for 2 min at room temperature. The DNA pellet was washed twice in 1 ml 70 % ethanol and, after complete removal of the ethanol, solubilized in 450 µl 8 mM NaOH. 50 µl of 100 mM HEPES (free acid) were added and the DNA was sheared by processing with a Bioruptor Plus (Diagenode SA, Belgium) for 5 min at high intensity and an 30 s on/30 s off interval. The DNA concentration was determined photometrically on a NanoDrop 2000 (Thermo Fisher Scientific). The DNA samples (10, 5, and 2.5 µg) were prepared in 250 µl buffer (10 mM HEPES-NaOH pH 7.8) per slot. Slot blotting of DNA was done with a Minifold I vacuum device (Schleicher & Schuell). For this, two filter papers (Grade 3MM Chr Cellulose, GE Healthcare Life Sciences) were moistened in 6x SSC solution and placed on the membrane support plate. A nitrocellulose membrane (Amersham Protran Premium 0.45 µm, GE Healthcare Life Sciences) was incubated for 10 min in 6x SSC solution and placed on the filter papers. The sample template was placed on top and the apparatus connected to vacuum. Each slot was washed with 500 µl TE buffer (1 mM EDTA, 10 mM Tris-HCl pH 8.0) before samples (250 µl/slot) were loaded. After sample application, each slot was washed with 500 µl 2x SSC solution (diluted from 6x SSC solution). The membrane was removed from the apparatus and rinsed twice with 2x SSC solution and once with TBS-T (1.5 M NaCl, 100 mM Tris pH 7.6, 0.1% Tween 20). The DNA-bound proteins were detected by immunostaining (4.6.4).

4.6.4 Immunostaining, development and quantification

The nitrocellulose membranes were blocked in 5 % non-fat dry milk/PBS-T and for 30-60 min and washed 3x 5 min with PBS-T. The primary antibodies were diluted in 3 % BSA/ NaN_3/PBS-T and incubated at 4 °C overnight or for 2 h at room temperature. The membranes were washed 3x 5 min in PBS-T and incubated with the horseradish peroxidase-coupled secondary antibodies that were diluted in 3 % BSA/PBS-T for 1-2 h. Primary and secondary antibodies and the dilutions are described in Table 4. The membranes were washed 3x 5 min and incubated with SuperSignal West Pico ECL substrate (Thermo Scientific) or ECL Prime Western Blotting detection reagent (GE Healthcare). The chemiluminescence signals were detected on Super RX films (Fujifilm) developed with a Cawomat 2000 IR (Agfa-Gevaert HealthCare GmbH) or recorded with a Chemostar ECL Imager (INTAS Science Imaging Instruments GmbH).

4.6.5 Affinity purification of FAF1 antibody

The custom-made polyclonal rabbit FAF1 antibody from Eurogentec was affinity purified using full-length His-FAF1 (made by Johannes van den Boom), which was also used for immunization. The antigen was coupled to a matrix and the used to enrich FAF1-specific antibodies from the serum.

1 ml Affi-Gel 15 (Bio-Rad) was filled into a 10 ml filter column and washed with cold water several times. 10 mg of purified His-FAF1 in 3 ml coupling buffer (0.1 M cabonate buffer [Na_2CO_3 /$NaHCO_3$ pH 8.3], 0.5 M NaCl; pH 8.3) were added and incubated for 4 h at 4 °C (slowly rotating).

100 µl of 1 M ethanolamine HCl (pH 8) were added and incubated for 1 h at 4 °C (slowly rotating). The matrix was resuspended in coupling buffer and the column was stored at 4 °C. 7 ml of the rabbit serum that was delivered from Eurogentec were transferred to a 15 ml tube. It was spun at full speed for 5 min and the supernatant (had no visible pellet) was heat inactivated for 30 min at 56 °C. The prepared column was washed with 5 ml PBS, then with 3x 1.5 ml elution buffer (200 mM Glycine-HCl pH 2.8), and again with 5 ml PBS. The prepared antiserum was loaded on the column and incubated for 2 h at 4 °C (slowly rotating). The antiserum was reapplied after flowthrough and collected after the second flowthrough. The column was washed with 5 ml PBS, then with 5 ml 1 M NaCl (buffered to pH 7.4), and again with 5 ml PBS. To elute the antibody, 5x 250 µl elution buffer were pipetted into the coloum and each fractions was collected in a 1.5 ml tube containing 100 µl neutralization buffer (1 M KCl and 20 µl Tris-HCl pH 8.8). Each fraction was mixed and then centrifuged for 2 min at full speed. The protein concentration was measured photometrically (Eppendorf BioPhotometer) and the protein-containing fractions were pooled. Finally, the pooled fractions were dialyzed over night at 4 °C against PBS and the purified antibody was stored at -20 °C.

5 References

Acs K, Luijsterburg MS, Ackermann L, Salomons FA, Hoppe T & Dantuma NP (2011) The AAA-ATPase VCP/p97 promotes 53BP1 recruitment by removing L3MBTL1 from DNA double-strand breaks. *Nat. Struct. Mol. Biol.* **18:** 1345–1350

Alexandru G, Graumann J, Smith GT, Kolawa NJ, Fang R & Deshaies RJ (2008) UBXD7 binds multiple ubiquitin ligases and implicates p97 in HIF1alpha turnover. *Cell* **134:** 804–816

Ali MAM, Strickfaden H, Lee BL, Spyracopoulos L & Hendzel MJ (2018) RYBP Is a K63-Ubiquitin-Chain-Binding Protein that Inhibits Homologous Recombination Repair. *Cell reports* **22:** 383–395

Anand RP, Lovett ST & Haber JE (2013) Break-induced DNA replication. *Cold Spring Harbor perspectives in biology* **5:** a010397

Anderson DJ, Le Moigne R, Djakovic S, Kumar B, Rice J, Wong S, Wang J, Yao B, Valle E, Kiss von Soly S, Madriaga A, Soriano F, Menon M-K, Wu ZY, Kampmann M, Chen Y, Weissman JS, Aftab BT, Yakes FM & Shawver L et al (2015) Targeting the AAA ATPase p97 as an Approach to Treat Cancer through Disruption of Protein Homeostasis. *Cancer Cell* **28:** 653–665

Arnoult N, Correia A, Ma J, Merlo A, Garcia-Gomez S, Maric M, Tognetti M, Benner CW, Boulton SJ, Saghatelian A & Karlseder J (2017) Regulation of DNA repair pathway choice in S and G2 phases by the NHEJ inhibitor CYREN. *Nature* **549:** 548–552

Balakirev MY, Mullally JE, Favier A, Assard N, Sulpice E, Lindsey DF, Rulina AV, Gidrol X & Wilkinson KD (2015) Wss1 metalloprotease partners with Cdc48/Doa1 in processing genotoxic SUMO conjugates. *eLife Sciences* **4**

Banerjee S, Bartesaghi A, Merk A, Rao P, Bulfer SL, Yan Y, Green N, Mroczkowski B, Neitz RJ, Wipf P, Falconieri V, Deshaies RJ, Milne JLS, Huryn D, Arkin M & Subramaniam S (2016) 2.3 Å resolution cryo-EM structure of human p97 and mechanism of allosteric inhibition. *Science (New York, N.Y.)* **351:** 871–875

Baranes-Bachar K, Levy-Barda A, Oehler J, Reid DA, Soria-Bretones I, Voss TC, Chung D, Park Y, Liu C, Yoon J-B, Li W, Dellaire G, Misteli T, Huertas P, Rothenberg E, Ramadan K, Ziv Y & Shiloh Y (2018) The Ubiquitin E3/E4 Ligase UBE4A Adjusts Protein Ubiquitylation and Accumulation at Sites of DNA Damage, Facilitating Double-Strand Break Repair. *Molecular Cell* **69:** 866-878.e7

Bebeacua C, Förster A, McKeown C, Meyer HH, Zhang X & Freemont PS (2012) Distinct conformations of the protein complex p97-Ufd1-Npl4 revealed by electron cryomicroscopy. *Proc. Natl. Acad. Sci. U.S.A.* **109:** 1098–1103

Bennardo N, Gunn A, Cheng A, Hasty P & Stark JM (2009) Limiting the persistence of a chromosome break diminishes its mutagenic potential. *PLoS Genet.* **5:** e1000683

Bergink S, Ammon T, Kern M, Schermelleh L, Leonhardt H & Jentsch S (2013) Role of Cdc48/p97 as a SUMO-targeted segregase curbing Rad51-Rad52 interaction. *Nat Cell Biol* **15:** 526–532

Biehs R, Steinlage M, Barton O, Juhasz S, Kunzel J, Spies J, Shibata A, Jeggo PA & Lobrich M (2017) DNA Double-Strand Break Resection Occurs during Non-homologous End Joining in G1 but Is Distinct from Resection during Homologous Recombination. *Molecular Cell* **65:** 671-684.e5

Blackford AN & Jackson SP (2017) ATM, ATR, and DNA-PK: The Trinity at the Heart of the DNA Damage Response. *Molecular Cell* **66:** 801–817

Blier PR, Griffith AJ, Craft J & Hardin JA (1993) Binding of Ku protein to DNA. Measurement of affinity for ends and demonstration of binding to nicks. *J. Biol. Chem.* **268:** 7594–7601

Blythe EE, Olson KC, Chau V & Deshaies RJ (2017) Ubiquitin- and ATP-dependent unfoldase activity of P97/VCP•NPLOC4•UFD1L is enhanced by a mutation that causes multisystem proteinopathy. *Proc. Natl. Acad. Sci. U.S.A.* **114:** E4380-E4388

Bodnar NO, Kim KH, Ji Z, Wales TE, Svetlov V, Nudler E, Engen JR, Walz T & Rapoport TA (2018) Structure of the Cdc48 ATPase with its ubiquitin-binding cofactor Ufd1–Npl4. *Nature Structural & Molecular Biology* **25:** 616

Bodnar NO & Rapoport TA (2017) Molecular Mechanism of Substrate Processing by the Cdc48 ATPase Complex. *Cell* **169:** 722-735.e9

Boersma V, Moatti N, Segura-Bayona S, Peuscher MH, van der Torre, Jaco, Wevers BA, Orthwein A, Durocher D & Jacobs, Jacqueline J L (2015) MAD2L2 controls DNA repair at telomeres and DNA breaks by inhibiting 5' end resection. *Nature* **521:** 537–540

Bonizec M, Hérissant L, Pokrzywa W, Geng F, Wenzel S, Howard GC, Rodriguez P, Krause S, Tansey WP, Hoppe T & Dargemont C (2014) The ubiquitin-selective chaperone Cdc48/p97 associates with Ubx3 to modulate monoubiquitylation of histone H2B. *Nucleic Acids Research* **42:** 10975–10986

Brinkman EK, Chen T, Amendola M & van Steensel B (2014) Easy quantitative assessment of genome editing by sequence trace decomposition. *Nucleic Acids Research* **42:** e168

Britton S, Coates J & Jackson SP (2013) A new method for high-resolution imaging of Ku foci to decipher mechanisms of DNA double-strand break repair. *The Journal of Cell Biology* **202:** 579–595

Brown JS, Lukashchuk N, Sczaniecka-Clift M, Britton S, Le Sage C, Calsou P, Beli P, Galanty Y & Jackson SP (2015) Neddylation Promotes Ubiquitylation and Release of Ku from DNA-Damage Sites. *Cell reports* **11:** 704–714

Burma S, Chen BP, Murphy M, Kurimasa A & Chen DJ (2001) ATM phosphorylates histone H2AX in response to DNA double-strand breaks. *J. Biol. Chem.* **276:** 42462–42467

Caldecott KW (2008) Single-strand break repair and genetic disease. *Nature Reviews Genetics* **9:** 619

Cao K, Nakajima R, Meyer HH & Zheng Y (2003) The AAA-ATPase Cdc48/p97 regulates spindle disassembly at the end of mitosis. *Cell* **115:** 355–367

Caron NS, Wright GEB & Hayden MR. Caron NS, Wright GEB & Hayden MR (2018) *Huntington Disease.* University of Washington, Seattle

Carpenter AE, Jones TR, Lamprecht MR, Clarke C, Kang IH, Friman O, Guertin DA, Chang JH, Lindquist RA, Moffat J, Golland P & Sabatini DM (2006) CellProfiler: image analysis software for identifying and quantifying cell phenotypes. *Genome Biol.* **7:** R100

Cavanagh BL, Walker T, Norazit A & Meedeniya ACB (2011) Thymidine analogues for tracking DNA synthesis. *Molecules (Basel, Switzerland)* **16:** 7980–7993

Ceccaldi R, Sarangi P & D'Andrea AD (2016) The Fanconi anaemia pathway: New players and new functions. *Nature Reviews Molecular Cell Biology* **17:** 337

Certo MT, Ryu BY, Annis JE, Garibov M, Jarjour J, Rawlings DJ & Scharenberg AM (2011) Tracking genome engineering outcome at individual DNA breakpoints. *Nature methods* **8:** 671–676

Chanut P, Britton S, Coates J, Jackson SP & Calsou P (2016) Coordinated nuclease activities counteract Ku at single-ended DNA double-strand breaks. *Nature communications* **7:** 12889

Chapman JR, Barral P, Vannier J-B, Borel V, Steger M, Tomas-Loba A, Sartori AA, Adams IR, Batista FD & Boulton SJ (2013) RIF1 is essential for 53BP1-dependent nonhomologous end joining and suppression of DNA double-strand break resection. *Molecular Cell* **49:** 858–871

Cheng Y-L & Chen R-H (2010) The AAA-ATPase Cdc48 and cofactor Shp1 promote chromosome bi-orientation by balancing Aurora B activity. *J. Cell. Sci.* **123:** 2025–2034

Chu K, Niu X & Williams LT (1995) A Fas-associated protein factor, FAF1, potentiates Fas-mediated apoptosis. *Proceedings of the National Academy of Sciences of the United States of America* **92:** 11894–11898

Ciccia A & Elledge SJ (2010) The DNA damage response: Making it safe to play with knives. *Molecular Cell* **40:** 179–204

Cooper MP, Machwe A, Orren DK, Brosh RM, Ramsden D & Bohr VA (2000) Ku complex interacts with and stimulates the Werner protein. *Genes Dev.* **14:** 907–912

Cortés-Ledesma F & Aguilera A (2006) Double-strand breaks arising by replication through a nick are repaired by cohesin-dependent sister-chromatid exchange. *EMBO Rep.* **7:** 919–926

Cortés-Ledesma F, El Khamisy SF, Zuma MC, Osborn K & Caldecott KW (2009) A human 5'-tyrosyl DNA phosphodiesterase that repairs topoisomerase-mediated DNA damage. *Nature* **461:** 674–678

Davis EJ, Lachaud C, Appleton P, Macartney TJ, Näthke I & Rouse J (2012) DVC1 (C1orf124) recruits the p97 protein segregase to sites of DNA damage. *Nat. Struct. Mol. Biol.* **19:** 1093–1100

DeHoratius C & Silver PA (1996) Nuclear transport defects and nuclear envelope alterations are associated with mutation of the Saccharomyces cerevisiae NPL4 gene. *Mol. Biol. Cell* **7:** 1835–1855

Deshaies RJ (2014) Proteotoxic crisis, the ubiquitin-proteasome system, and cancer therapy. *BMC biology* **12:** 94

Dewar JM, Low E, Mann M, Räschle M & Walter JC (2017) CRL2(Lrr1) promotes unloading of the vertebrate replisome from chromatin during replication termination. *Genes Dev.* **31:** 275–290

Dewar JM & Walter JC (2017) Mechanisms of DNA replication termination. *Nature Reviews Molecular Cell Biology* **18:** 507

Digweed M & Sperling K (2004) Nijmegen breakage syndrome: Clinical manifestation of defective response to DNA double-strand breaks. *Recent Developments in Non-Homologous End Joining* **3:** 1207–1217

Dobrynin G, Popp O, Romer T, Bremer S, Schmitz MHA, Gerlich DW & Meyer H (2011) Cdc48/p97-Ufd1-Npl4 antagonizes Aurora B during chromosome segregation in HeLa cells. *J. Cell. Sci.* **124:** 1571–1580

Doench JG, Fusi N, Sullender M, Hegde M, Vaimberg EW, Donovan KF, Smith I, Tothova Z, Wilen C, Orchard R, Virgin HW, Listgarten J & Root DE (2016) Optimized sgRNA design to maximize activity and minimize off-target effects of CRISPR-Cas9. *Nature Biotechnology* **34:** 184

Doil C, Mailand N, Bekker-Jensen S, Menard P, Larsen DH, Pepperkok R, Ellenberg J, Panier S, Durocher D, Bartek J, Lukas J & Lukas C (2009) RNF168 binds and amplifies ubiquitin conjugates on damaged chromosomes to allow accumulation of repair proteins. *Cell* **136:** 435–446

Doudna JA & Charpentier E (2014) Genome editing. The new frontier of genome engineering with CRISPR-Cas9. *Science* **346:** 1258096

Dueva R & Iliakis G (2013) Alternative pathways of non-homologous end joining (NHEJ) in genomic instability and cancer. *Translational Cancer Research* **2:** 163–177

Elia AEH, Wang DC, Willis NA, Boardman AP, Hajdu I, Adeyemi RO, Lowry E, Gygi SP, Scully R & Elledge SJ (2015) RFWD3-Dependent Ubiquitination of RPA Regulates Repair at Stalled Replication Forks. *Molecular Cell* **60:** 280–293

Emadi A, Jones RJ & Brodsky RA (2009) Cyclophosphamide and cancer: Golden anniversary. *Nature Reviews Clinical Oncology* **6:** 638

Enokido Y, Tamura T, Ito H, Arumughan A, Komuro A, Shiwaku H, Sone M, Foulle R, Sawada H, Ishiguro H, Ono T, Murata M, Kanazawa I, Tomilin N, Tagawa K, Wanker EE & Okazawa H (2010) Mutant huntingtin impairs Ku70-mediated DNA repair. *The Journal of Cell Biology* **189:** 425–443

Escribano-Díaz C, Orthwein A, Fradet-Turcotte A, Xing M, Young, Jordan T F, Tkáč J, Cook MA, Rosebrock AP, Munro M, Canny MD, Xu D & Durocher D (2013) A cell cycle-dependent regulatory circuit composed of 53BP1-RIF1 and BRCA1-CtIP controls DNA repair pathway choice. *Molecular Cell* **49:** 872–883

Ewens CA, Panico S, Kloppsteck P, McKeown C, Ebong I-O, Robinson C, Zhang X & Freemont PS (2014) The p97-FAF1 protein complex reveals a common mode of p97 adaptor binding. *The Journal of biological chemistry* **289:** 12077–12084

Falck J, Coates J & Jackson SP (2005) Conserved modes of recruitment of ATM, ATR and DNA-PKcs to sites of DNA damage. *Nature* **434:** 605–611

Feeney L, Muñoz IM, Lachaud C, Toth R, Appleton PL, Schindler D & Rouse J (2017) RPA-Mediated Recruitment of the E3 Ligase RFWD3 Is Vital for Interstrand Crosslink Repair and Human Health. *Molecular Cell* **66:** 610-621.e4

Feng L & Chen J (2012) The E3 ligase RNF8 regulates KU80 removal and NHEJ repair. *Nat. Struct. Mol. Biol.* **19:** 201–206

Fragkos M, Ganier O, Coulombe P & Méchali M (2015) DNA replication origin activation in space and time. *Nature Reviews Molecular Cell Biology* **16:** 360

Franken NAP, Rodermond HM, Stap J, Haveman J & van Bree C (2006) Clonogenic assay of cells in vitro. *Nat Protoc* **1:** 2315–2319

Franz A, Orth M, Pirson PA, Sonneville R, Blow JJ, Gartner A, Stemmann O & Hoppe T (2011) CDC-48/p97 coordinates CDT-1 degradation with GINS chromatin dissociation to ensure faithful DNA replication. *Molecular Cell* **44:** 85–96

Franz A, Pirson PA, Pilger D, Halder S, Achuthankutty D, Kashkar H, Ramadan K & Hoppe T (2016) Chromatin-associated degradation is defined by UBXN-3/FAF1 to safeguard DNA replication fork progression. *Nature communications* **7:** 10612

Fullbright G, Rycenga HB, Gruber JD & Long DT (2016) p97 Promotes a Conserved Mechanism of Helicase Unloading during DNA Cross-Link Repair. *Mol. Cell. Biol.* **36:** 2983–2994

Gaillard H, García-Muse T & Aguilera A (2015) Replication stress and cancer. *Nature Reviews Cancer* **15:** 276

Gao X, Liu W, Huang L, Zhang T, Mei Z, Wang X, Gong J, Zhao Y, Xie F, Ma J & Qian L (2015) HSP70 inhibits stress-induced cardiomyocyte apoptosis by competitively binding to FAF1. *Cell Stress and Chaperones* **20:** 653–661

Gatti M, Pinato S, Maiolica A, Rocchio F, Prato MG, Aebersold R & Penengo L (2015) RNF168 promotes noncanonical K27 ubiquitination to signal DNA damage. *Cell reports* **10:** 226–238

Ghosal G, Leung JW-C, Nair BC, Fong K-W & Chen J (2012) Proliferating cell nuclear antigen (PCNA)-binding protein C1orf124 is a regulator of translesion synthesis. *J. Biol. Chem.* **287:** 34225–34233

Gibbs-Seymour I, Oka Y, Rajendra E, Weinert BT, Passmore LA, Patel KJ, Olsen JV, Choudhary C, Bekker-Jensen S & Mailand N (2015) Ubiquitin-SUMO Circuitry Controls Activated Fanconi Anemia ID Complex Dosage in Response to DNA Damage. *Molecular Cell* **57:** 150–164

Goldberg M, Stucki M, Falck J, D'Amours D, Rahman D, Pappin D, Bartek J & Jackson SP (2003) MDC1 is required for the intra-S-phase DNA damage checkpoint. *Nature* **421:** 952

Gomez-Cabello D, Jimeno S, FernÃ¡ndez-Ãvila M-aJ, Huertas P & Lichten M (2013) New Tools to Study DNA Double-Strand Break Repair Pathway Choice. *PloS one* **8:** e77206

Goodman MF & Tippin B (2000) Sloppier copier DNA polymerases involved in genome repair. *Current opinion in genetics & development* **10:** 162–168

Grundy GJ, Rulten SL, Arribas-Bosacoma R, Davidson K, Kozik Z, Oliver AW, Pearl LH & Caldecott KW (2016) The Ku-binding motif is a conserved module for recruitment and stimulation of non-homologous end-joining proteins. *Nat Commun* **7:** 11242

Haince J-F, McDonald D, Rodrigue A, Déry U, Masson J-Y, Hendzel MJ & Poirier GG (2008) PARP1-dependent kinetics of recruitment of MRE11 and NBS1 proteins to multiple DNA damage sites. *J. Biol. Chem.* **283:** 1197–1208

Hanahan D & Weinberg RA (2011) Hallmarks of cancer: The next generation. *Cell* **144:** 646–674

Hang LE, Lopez CR, Liu X, Williams JM, Chung I, Wei L, Bertuch AA & Zhao X (2014) Regulation of Ku-DNA association by Yku70 C-terminal tail and SUMO modification. *J. Biol. Chem.* **289:** 10308–10317

Hänzelmann P, Buchberger A & Schindelin H (2011) Hierarchical binding of cofactors to the AAA ATPase p97. *Structure (London, England : 1993)* **19:** 833–843

Hänzelmann P & Schindelin H (2016) Structural Basis of ATP Hydrolysis and Intersubunit Signaling in the AAA+ ATPase p97. *Structure* **24:** 127–139

Hartlerode AJ, Morgan MJ, Wu Y, Buis J & Ferguson DO (2015) Recruitment and activation of the ATM kinase in the absence of DNA-damage sensors. *Nat. Struct. Mol. Biol.* **22:** 736–743

He J, Zhu Q, Wani G, Sharma N, Han C, Qian J, Pentz K, Wang Q-E & Wani AA (2014) Ubiquitin-specific Protease 7 Regulates Nucleotide Excision Repair through Deubiquitinating XPC Protein and Preventing XPC Protein from Undergoing Ultraviolet Light-induced and VCP/p97 Protein-regulated Proteolysis. *J. Biol. Chem.* **289:** 27278–27289

Hendriks IA, Treffers LW, Verlaan-de Vries M, Olsen JV & Vertegaal, Alfred C. O. (2015) SUMO-2 Orchestrates Chromatin Modifiers in Response to DNA Damage. *Cell reports* **10:** 1778–1791

Her J & Bunting SF (2018) How cells ensure correct repair of DNA double-strand breaks. *J. Biol. Chem.* **293:** 10502–10511

Hipp MS, Park S-H & Hartl FU (2014) Proteostasis impairment in protein-misfolding and -aggregation diseases. *Trends in cell biology* **24:** 506–514

Hoeijmakers JH (2001) Genome maintenance mechanisms for preventing cancer. *Nature* **411:** 366–374

Hoeijmakers JHJ (2009) DNA damage, aging, and cancer. *The New England journal of medicine* **361:** 1475–1485

Inano S, Sato K, Katsuki Y, Kobayashi W, Tanaka H, Nakajima K, Nakada S, Miyoshi H, Knies K, Takaori-Kondo A, Schindler D, Ishiai M, Kurumizaka H & Takata M (2017) RFWD3-Mediated Ubiquitination Promotes Timely Removal of Both RPA and RAD51 from DNA Damage Sites to Facilitate Homologous Recombination. *Molecular Cell* **66:** 622-634.e8

Inoue M, Iida A, Hayashi S, Mori-Yoshimura M, Nagaoka A, Yoshimura S, Shiraishi H, Tsujino A, Takahashi Y, Nonaka I, Hayashi YK, Noguchi S & Nishino I (2018) Two novel VCP missense variants identified in Japanese patients with multisystem proteinopathy. *Human Genome Variation* **5:** 9

Ishida N, Nakagawa T, Iemura S-I, Yasui A, Shima H, Katoh Y, Nagasawa Y, Natsume T, Igarashi K & Nakayama K (2017) Ubiquitylation of Ku80 by RNF126 Promotes Completion of Nonhomologous End Joining-Mediated DNA Repair. *Mol. Cell. Biol.* **37**

Ismail IH, Gagné J-P, Genois M-M, Strickfaden H, McDonald D, Xu Z, Poirier GG, Masson J-Y & Hendzel MJ (2015) The RNF138 E3 ligase displaces Ku to promote DNA end resection and regulate DNA repair pathway choice. *Nat Cell Biol* **17:** 1446–1457

Jemal A, Bray F, Center MM, Ferlay J, Ward E & Forman D (2011) Global cancer statistics. *CA: a cancer journal for clinicians* **61:** 69–90

Jiang N, Shen Y, Fei X, Sheng K, Sun P, Qiu Y, Larner J, Cao L, Kong X & Mi J (2013) Valosin-containing protein regulates the proteasome-mediated degradation of DNA-PKcs in glioma cells. *Cell Death Dis* **4:** e647

Jiricny J (2013) Postreplicative mismatch repair. *Cold Spring Harbor perspectives in biology* **5:** a012633

Johnson ES, Ma, P. C. M., Ota IM & Varshavsky A (1995) A Proteolytic Pathway That Recognizes Ubiquitin as a Degradation Signal. *Journal of Biological Chemistry* **270:** 17442–17456

Ju J-S, Fuentealba RA, Miller SE, Jackson E, Piwnica-Worms D, Baloh RH & Weihl CC (2009) Valosin-containing protein (VCP) is required for autophagy and is disrupted in VCP disease. *The Journal of Cell Biology* **187:** 875–888

Keeney S, Giroux CN & Kleckner N (1997) Meiosis-specific DNA double-strand breaks are catalyzed by Spo11, a member of a widely conserved protein family. *Cell* **88:** 375–384

Klein JB, Barati MT, Wu R, Gozal D, Sachleben, Leroy R Jr, Kausar H, Trent JO, Gozal E & Rane MJ (2005) Akt-mediated valosin-containing protein 97 phosphorylation regulates its association with ubiquitinated proteins. *J. Biol. Chem.* **280:** 31870–31881

Kuefner MA, Brand M, Engert C, Schwab SA & Uder M (2015) Radiation Induced DNA Double-Strand Breaks in Radiology. *RoFo : Fortschritte auf dem Gebiete der Rontgenstrahlen und der Nuklearmedizin* **187:** 872–878

Lafranchi L, Boer HR de, Vries EGE de, Ong S-E, Sartori AA & van Vugt MATM (2014) APC/C(Cdh1) controls CtIP stability during the cell cycle and in response to DNA damage. *The EMBO journal* **33:** 2860–2879

Langerak P, Mejia-Ramirez E, Limbo O & Russell P (2011) Release of Ku and MRN from DNA ends by Mre11 nuclease activity and Ctp1 is required for homologous recombination repair of double-strand breaks. *PLoS Genet.* **7:** e1002271

Lavin MF, Gueven N, Bottle S & Gatti RA (2007) Current and potential therapeutic strategies for the treatment of ataxia-telangiectasia. *Br Med Bull* **81-82:** 129–147

Lawrence KS, Chau T & Engebrecht J (2015) DNA Damage Response and Spindle Assembly Checkpoint Function throughout the Cell Cycle to Ensure Genomic Integrity. *PLoS Genet.* **11:** e1005150

Lee DH & Goldberg AL (1998) Proteasome inhibitors: Valuable new tools for cell biologists. *Trends in cell biology* **8:** 397–403

Lee J-J, Kim YM, Jeong J, Bae DS & Lee K-J (2012) Ubiquitin-associated (UBA) domain in human Fas associated factor 1 inhibits tumor formation by promoting Hsp70 degradation. *PloS one* **7:** e40361

Lee J-J, Park JK, Jeong J, Jeon H, Yoon J-B, Kim EE & Lee K-J (2013) Complex of Fas-associated factor 1 (FAF1) with valosin-containing protein (VCP)-Npl4-Ufd1 and polyubiquitinated proteins promotes endoplasmic reticulum-associated degradation (ERAD). *The Journal of biological chemistry* **288:** 6998–7011

Lee K-J, Saha J, Sun J, Fattah KR, Wang S-C, Jakob B, Chi L, Wang S-Y, Taucher-Scholz G, Davis AJ & Chen DJ (2016) Phosphorylation of Ku dictates DNA double-strand break (DSB) repair pathway choice in S phase. *Nucleic Acids Res* **44:** 1732–1745

Lemaître C, Grabarz A, Tsouroula K, Andronov L, Furst A, Pankotai T, Heyer V, Rogier M, Attwood KM, Kessler P, Dellaire G, Klaholz B, Reina-San-Martin B & Soutoglou E (2014) Nuclear position dictates DNA repair pathway choice. *Genes Dev.* **28:** 2450–2463

Li B & Comai L (2001) Requirements for the nucleolytic processing of DNA ends by the Werner syndrome protein-Ku70/80 complex. *J. Biol. Chem.* **276:** 9896–9902

Li G, Zhao G, Schindelin H & Lennarz WJ (2008) Tyrosine phosphorylation of ATPase p97 regulates its activity during ERAD. *Biochemical and Biophysical Research Communications* **375:** 247–251

Li J-M, Wu H, Zhang W, Blackburn MR & Jin J (2014) The p97-UFD1L-NPL4 protein complex mediates cytokine-induced IκBα proteolysis. *Molecular and cellular biology* **34:** 335–347

Lindahl T (1993) Instability and decay of the primary structure of DNA. *Nature* **362:** 709–715

Liu H, Zhang H, Wang X, Tian Q, Hu Z, Peng C, Jiang P, Wang T, Guo W, Chen Y, Li X, Zhang P & Pei H (2015) The Deubiquitylating Enzyme USP4 Cooperates with CtIP in DNA Double-Strand Break End Resection. *Cell reports* **13:** 93–107

Liu S, Opiyo SO, Manthey K, Glanzer JG, Ashley AK, Amerin C, Troksa K, Shrivastav M, Nickoloff JA & Oakley GG (2012) Distinct roles for DNA-PK, ATM and ATR in RPA

phosphorylation and checkpoint activation in response to replication stress. *Nucleic Acids Res* **40:** 10780–10794

Liu Y & Ye Y (2012) Roles of p97-Associated Deubiquitinases in Protein Quality Control at the Endoplasmic Reticulum. *CPPS* **13:** 436–446

Livingstone M, Ruan H, Weiner J, Clauser KR, Strack P, Jin S, Williams A, Greulich H, Gardner J, Venere M, Mochan TA, DiTullio RA, Moravcevic K, Gorgoulis VG, Burkhardt A & Halazonetis TD (2005) Valosin-containing protein phosphorylation at Ser784 in response to DNA damage. *Cancer Res.* **65:** 7533–7540

Lou Z, Minter-Dykhouse K, Wu X & Chen J (2003) MDC1 is coupled to activated CHK2 in mammalian DNA damage response pathways. *Nature* **421:** 957

Lu C-S, Truong LN, Aslanian A, Shi LZ, Li Y, Hwang PY-H, Koh KH, Hunter T, Yates JR, Berns MW & Wu X (2012) The RING finger protein RNF8 ubiquitinates Nbs1 to promote DNA double-strand break repair by homologous recombination. *J. Biol. Chem.* **287:** 43984–43994

Lukas C, Melander F, Stucki M, Falck J, Bekker-Jensen S, Goldberg M, Lerenthal Y, Jackson SP, Bartek J & Lukas J (2004) Mdc1 couples DNA double-strand break recognition by Nbs1 with its H2AX-dependent chromatin retention. *EMBO J* **23:** 2674–2683

Ma Q, Li P, Xu M, Yin J, Su Z, Li W & Zhang J (2012) Ku80 is highly expressed in lung adenocarcinoma and promotes cisplatin resistance. *Journal of experimental & clinical cancer research : CR* **31:** 99

Ma Y, Lu H, Tippin B, Goodman MF, Shimazaki N, Koiwai O, Hsieh C-L, Schwarz K & Lieber MR (2004) A biochemically defined system for mammalian nonhomologous DNA end joining. *Molecular Cell* **16:** 701–713

Ma Y, Schwarz K & Lieber MR (2005) The Artemis:DNA-PKcs endonuclease cleaves DNA loops, flaps, and gaps. *DNA Repair* **4:** 845–851

Madeo F, Schlauer J, Zischka H, Mecke D & Frohlich K-U (1998) Tyrosine Phosphorylation Regulates Cell Cycle-dependent Nuclear Localization of Cdc48p. *Mol. Biol. Cell* **9:** 131–141

Magnaghi P, D'Alessio R, Valsasina B, Avanzi N, Rizzi S, Asa D, Gasparri F, Cozzi L, Cucchi U, Orrenius C, Polucci P, Ballinari D, Perrera C, Leone A, Cervi G, Casale E, Xiao Y, Wong C, Anderson DJ & Galvani A et al (2013) Covalent and allosteric inhibitors of the ATPase VCP/p97 induce cancer cell death. *Nature chemical biology* **9:** 548–556

Mahaney BL, Hammel M, Meek K, Tainer JA & Lees-Miller SP (2013) XRCC4 and XLF form long helical protein filaments suitable for DNA end protection and alignment to facilitate DNA double strand break repair. *Biochemistry and cell biology = Biochimie et biologie cellulaire* **91:** 31–41

Mailand N, Bekker-Jensen S, Faustrup H, Melander F, Bartek J, Lukas C & Lukas J (2007) RNF8 Ubiquitylates Histones at DNA Double-Strand Breaks and Promotes Assembly of Repair Proteins. *Cell* **131:** 887–900

Maréchal A, Li J-M, Ji XY, Wu C-S, Yazinski SA, Nguyen HD, Liu S, Jiménez AE, Jin J & Zou L (2014) PRP19 transforms into a sensor of RPA-ssDNA after DNA damage and drives ATR activation via a ubiquitin-mediated circuitry. *Molecular Cell* **53:** 235–246

Mari P-O, Florea BI, Persengiev SP, Verkaik NS, Brüggenwirth HT, Modesti M, Giglia-Mari G, Bezstarosti K, Demmers JAA, Luider TM, Houtsmuller AB & van Gent DC (2006) Dynamic assembly of end-joining complexes requires interaction between Ku70/80 and XRCC4. *Proc. Natl. Acad. Sci. U.S.A.* **103:** 18597–18602

Maric M, Maculins T, Piccoli G de & Labib K (2014) Cdc48 and a ubiquitin ligase drive disassembly of the CMG helicase at the end of DNA replication. *Science* **346:** 1253596

Maric M, Mukherjee P, Tatham MH, Hay R & Labib K (2017) Ufd1-Npl4 Recruit Cdc48 for Disassembly of Ubiquitylated CMG Helicase at the End of Chromosome Replication. *Cell reports* **18:** 3033–3042

Marteijn JA, Lans H, Vermeulen W & Hoeijmakers JHJ (2014) Understanding nucleotide excision repair and its roles in cancer and ageing. *Nat. Rev. Mol. Cell Biol.* **15:** 465–481

Matsuoka S, Ballif BA, Smogorzewska A, McDonald ER, Hurov KE, Luo J, Bakalarski CE, Zhao Z, Solimini N, Lerenthal Y, Shiloh Y, Gygi SP & Elledge SJ (2007) ATM and ATR substrate analysis reveals extensive protein networks responsive to DNA damage. *Science (New York, N.Y.)* **316:** 1160–1166

McBlane JF, van Gent DC, Ramsden DA, Romeo C, Cuomo CA, Gellert M & Oettinger MA (1995) Cleavage at a V(D)J recombination signal requires only RAG1 and RAG2 proteins and occurs in two steps. *Cell* **83:** 387–395

Meerang M, Ritz D, Paliwal S, Garajova Z, Bosshard M, Mailand N, Janscak P, Hübscher U, Meyer H & Ramadan K (2011) The ubiquitin-selective segregase VCP/p97 orchestrates the response to DNA double-strand breaks. *Nat Cell Biol* **13:** 1376–1382

Mehta A & Haber JE (2014) Sources of DNA double-strand breaks and models of recombinational DNA repair. *Cold Spring Harbor perspectives in biology* **6:** a016428

Mehta PA & Tolar J. Mehta PA & Tolar J (2018) *Fanconi Anemia.* University of Washington, Seattle

Menges CW, Altomare DA & Testa JR (2009) FAS-associated factor 1 (FAF1): diverse functions and implications for oncogenesis. *Cell cycle (Georgetown, Tex.)* **8:** 2528–2534

Meyer H & Weihl CC (2014) The VCP/p97 system at a glance: Connecting cellular function to disease pathogenesis. *J. Cell. Sci.* **127:** 3877–3883

Meyer HH, Shorter JG, Seemann J, Pappin D & Warren G (2000) A complex of mammalian Ufd1 and Npl4 links the AAA-ATPase, p97, to ubiquitin and nuclear transport pathways. *EMBO J* **19:** 2181–2192

Meyer HH, Wang Y & Warren G (2002) Direct binding of ubiquitin conjugates by the mammalian p97 adaptor complexes, p47 and Ufd1-Npl4. *EMBO J* **21:** 5645–5652

Moreno SP, Bailey R, Campion N, Herron S & Gambus A (2014) Polyubiquitylation drives replisome disassembly at the termination of DNA replication. *Science* **346:** 477–481

Mori-Konya C, Kato N, Maeda R, Yasuda K, Higashimae N, Noguchi M, Koike M, Kimura Y, Ohizumi H, Hori S & Kakizuka A (2009) p97/valosin-containing protein (VCP) is highly modulated by phosphorylation and acetylation. *Genes to Cells* **14:** 483–497

Mosbech A, Gibbs-Seymour I, Kagias K, Thorslund T, Beli P, Povlsen L, Nielsen SV, Smedegaard S, Sedgwick G, Lukas C, Hartmann-Petersen R, Lukas J, Choudhary C, Pocock R, Bekker-Jensen S & Mailand N (2012) DVC1 (C1orf124) is a DNA damage-targeting p97 adaptor that promotes ubiquitin-dependent responses to replication blocks. *Nat. Struct. Mol. Biol.* **19:** 1084–1092

Mouysset J, Deichsel A, Moser S, Hoege C, Hyman AA, Gartner A & Hoppe T (2008) Cell cycle progression requires the CDC-48UFD-1/NPL-4 complex for efficient DNA replication. *Proc. Natl. Acad. Sci. U.S.A.* **105:** 12879–12884

Munshi A, Hobbs M & Meyn RE (2005) Clonogenic cell survival assay. *Methods in molecular medicine* **110:** 21–28

Myler LR, Gallardo IF, Soniat MM, Deshpande RA, Gonzalez XB, Kim Y, Paull TT & Finkelstein IJ (2017) Single-Molecule Imaging Reveals How Mre11-Rad50-Nbs1 Initiates DNA Break Repair. *Molecular Cell* **67:** 891-898.e4

Neal JA, Sugiman-Marangos S, VanderVere-Carozza P, Wagner M, Turchi J, Lees-Miller SP, Junop MS & Meek K (2014) Unraveling the complexities of DNA-dependent protein kinase autophosphorylation. *Mol. Cell. Biol.* **34:** 2162–2175

Nick McElhinny SA, Havener JM, Garcia-Diaz M, Juárez R, Bebenek K, Kee BL, Blanco L, Kunkel TA & Ramsden DA (2005) A gradient of template dependence defines distinct biological roles for family X polymerases in nonhomologous end joining. *Molecular Cell* **19:** 357–366

Nick McElhinny SA, Snowden CM, McCarville J & Ramsden DA (2000) Ku recruits the XRCC4-ligase IV complex to DNA ends. *Mol. Cell. Biol.* **20:** 2996–3003

Nishi R, Wijnhoven P, Le Sage C, Tjeertes J, Galanty Y, Forment JV, Clague MJ, Urbé S & Jackson SP (2014) Systematic characterization of deubiquitylating enzymes for roles in maintaining genome integrity. *Nature cell biology* **16:** 1016-26, 1-8

Niwa H, Ewens CA, Tsang C, Yeung HO, Zhang X & Freemont PS (2012) The role of the N-domain in the ATPase activity of the mammalian AAA ATPase p97/VCP. *J. Biol. Chem.* **287:** 8561–8570

Ochi T, Blackford AN, Coates J, Jhujh S, Mehmood S, Tamura N, Travers J, Wu Q, Draviam VM, Robinson CV, Blundell TL & Jackson SP (2015) DNA repair. PAXX, a paralog of XRCC4 and XLF, interacts with Ku to promote DNA double-strand break repair. *Science (New York, N.Y.)* **347:** 185–188

O'Connor MJ (2015) Targeting the DNA Damage Response in Cancer. *Molecular Cell* **60:** 547–560

Ohta T, Sato K & Wu W (2011) The BRCA1 ubiquitin ligase and homologous recombination repair. *Ubiquitin Family Proteins in DNA Damage Response* **585:** 2836–2844

Orthwein A, Noordermeer SM, Wilson MD, Landry S, Enchev RI, Sherker A, Munro M, Pinder J, Salsman J, Dellaire G, Xia B, Peter M & Durocher D (2015) A mechanism for the suppression of homologous recombination in G1 cells. *Nature* **528:** 422

Panier S & Boulton SJ (2014) Double-strand break repair: 53BP1 comes into focus. *Nat. Rev. Mol. Cell Biol.* **15:** 7–18

Pannunzio NR, Watanabe G & Lieber MR (2018) Nonhomologous DNA end-joining for repair of DNA double-strand breaks. *J. Biol. Chem.* **293:** 10512–10523

Papadopoulos C, Kirchner P, Bug M, Grum D, Koerver L, Schulze N, Poehler R, Dressler A, Fengler S, Arhzaouy K, Lux V, Ehrmann M, Weihl CC & Meyer H (2017) VCP/p97 cooperates with YOD1, UBXD1 and PLAA to drive clearance of ruptured lysosomes by autophagy. *The EMBO journal* **36:** 135–150

Partridge JJ, Lopreiato JO, Latterich M & Indig FE (2003) DNA damage modulates nucleolar interaction of the Werner protein with the AAA ATPase p97/VCP. *Mol. Biol. Cell* **14:** 4221–4229

Peterson SE, Stellwagen AE, Diede SJ, Singer MS, Haimberger ZW, Johnson CO, Tzoneva M & Gottschling DE (2001) The function of a stem-loop in telomerase RNA is linked to the DNA repair protein Ku. *Nature genetics* **27:** 64

Pierce AJ, Johnson RD, Thompson LH & Jasin M (1999) XRCC3 promotes homology-directed repair of DNA damage in mammalian cells. *Genes Dev.* **13:** 2633–2638

Pommier Y, Sun Y, Huang S-yN & Nitiss JL (2016) Roles of eukaryotic topoisomerases in transcription, replication and genomic stability. *Nature Reviews Molecular Cell Biology* **17:** 703

Postow L & Funabiki H (2013) An SCF complex containing Fbxl12 mediates DNA damage-induced Ku80 ubiquitylation. *Cell Cycle* **12:** 587–595

Postow L, Ghenoiu C, Woo EM, Krutchinsky AN, Chait BT & Funabiki H (2008) Ku80 removal from DNA through double strand break-induced ubiquitylation. *The Journal of Cell Biology* **182:** 467–479

Presolski SI, Hong VP & Finn MG (2011) Copper-Catalyzed Azide-Alkyne Click Chemistry for Bioconjugation. *Current protocols in chemical biology* **3:** 153–162

Price BD & D'Andrea AD (2013) Chromatin remodeling at DNA double-strand breaks. *Cell* **152:** 1344–1354

Puumalainen M-R, Lessel D, Rüthemann P, Kaczmarek N, Bachmann K, Ramadan K & Naegeli H (2014) Chromatin retention of DNA damage sensors DDB2 and XPC through loss of p97 segregase causes genotoxicity. *Nat Commun* **5:** 3695

Pye VE, Beuron F, Keetch CA, McKeown C, Robinson CV, Meyer HH, Zhang X & Freemont PS (2007) Structural insights into the p97-Ufd1-Npl4 complex. *Proc. Natl. Acad. Sci. U.S.A.* **104:** 467–472

Ramadan K, Bruderer R, Spiga FM, Popp O, Baur T, Gotta M & Meyer HH (2007) Cdc48/p97 promotes reformation of the nucleus by extracting the kinase Aurora B from chromatin. *Nature* **450:** 1258–1262

Raman M, Havens CG, Walter JC & Harper, J. Wade (2011) A Genome-wide Screen Identifies p97 as an Essential Regulator of DNA Damage-Dependent CDT1 Destruction. *Molecular Cell* **44:** 72–84

Ran FA, Hsu PD, Wright J, Agarwala V, Scott DA & Zhang F (2013) Genome engineering using the CRISPR-Cas9 system. *Nature Protocols* **8:** 2281

Regairaz M, Zhang Y-W, Fu H, Agama KK, Tata N, Agrawal S, Aladjem MI & Pommier Y (2011) Mus81-mediated DNA cleavage resolves replication forks stalled by topoisomerase I-DNA complexes. *The Journal of Cell Biology* **195:** 739–749

Reynolds P, Botchway SW, Parker AW & O'Neill P (2013) Spatiotemporal dynamics of DNA repair proteins following laser microbeam induced DNA damage - when is a DSB not a DSB? *Mutation research* **756:** 14–20

Richa, Sinha RP & Häder D-P (2015) Physiological Aspects of UV-Excitation of DNA. In *DNA fragments and phenomenological aspects,* Barbatti M, Borin AC, Ullrich S (eds) pp. 203–248. Cham: Springer

Rogakou EP, Boon C, Redon C & Bonner WM (1999) Megabase Chromatin Domains Involved in DNA Double-Strand Breaks in Vivo. *The Journal of Cell Biology* **146:** 905–916

Rogakou EP, Pilch DR, Orr AH, Ivanova VS & Bonner WM (1998) DNA Double-stranded Breaks Induce Histone H2AX Phosphorylation on Serine 139. *J. Biol. Chem.* **273:** 5858–5868

Rousseau A & Bertolotti A (2018) Regulation of proteasome assembly and activity in health and disease. *Nature reviews. Molecular cell biology:* 1

Rueden CT, Schindelin J, Hiner MC, DeZonia BE, Walter AE, Arena ET & Eliceiri KW (2017) ImageJ2: ImageJ for the next generation of scientific image data. *BMC bioinformatics* **18:** 529

Rybak P, Hoang A, Bujnowicz L, Bernas T, Berniak K, Zarębski M, Darzynkiewicz Z & Dobrucki J (2016) Low level phosphorylation of histone H2AX on serine 139 (γH2AX) is not associated with DNA double-strand breaks. *Oncotarget* **7:** 49574–49587

Ryu S-W, Lee S-J, Park M-Y, Jun J-I, Jung Y-K & Kim E (2003) Fas-associated factor 1, FAF1, is a member of Fas death-inducing signaling complex. *The Journal of biological chemistry* **278:** 24003–24010

Sakasai R & Iwabuchi K (2016) The distinctive cellular responses to DNA strand breaks caused by a DNA topoisomerase I poison in conjunction with DNA replication and RNA transcription. *Genes & genetic systems* **90:** 187–194

Sakasai R, Teraoka H & Tibbetts RS (2010) Proteasome inhibition suppresses DNA-dependent protein kinase activation caused by camptothecin. *DNA Repair* **9:** 76–82

Sallmyr A & Tomkinson AE (2018) Repair of DNA double-strand breaks by mammalian alternative end-joining pathways. *J. Biol. Chem.* **293:** 10536–10546

Schindelin J, Arganda-Carreras I, Frise E, Kaynig V, Longair M, Pietzsch T, Preibisch S, Rueden C, Saalfeld S, Schmid B, Tinevez J-Y, White DJ, Hartenstein V, Eliceiri K, Tomancak P & Cardona A (2012) Fiji: An open-source platform for biological-image analysis. *Nature methods* **9:** 676–682

Schipler A & Iliakis G (2013) DNA double-strand–break complexity levels and their possible contributions to the probability for error-prone processing and repair pathway choice. *Nucleic Acids Research* **41:** 7589–7605

Schmidt CK, Galanty Y, Sczaniecka-Clift M, Coates J, Jhujh S, Demir M, Cornwell M, Beli P & Jackson SP (2015) Systematic E2 screening reveals a UBE2D-RNF138-CtIP axis promoting DNA repair. *Nat Cell Biol* **17:** 1458–1470

Schwertman P, Bekker-Jensen S & Mailand N (2016) Regulation of DNA double-strand break repair by ubiquitin and ubiquitin-like modifiers. *Nature reviews. Molecular cell biology* **17:** 379–394

Scully R & Xie A (2013) Double strand break repair functions of histone H2AX. *Mutation research* **750:** 5–14

Shamanna RA, Lu H, Freitas JK de, Tian J, Croteau DL & Bohr VA (2016) WRN regulates pathway choice between classical and alternative non-homologous end joining. *Nature communications* **7:** 13785

Shibata A (2017) Regulation of repair pathway choice at two-ended DNA double-strand breaks. *Mutation research* **803-805:** 51–55

Sibanda BL, Chirgadze DY, Ascher DB & Blundell TL (2017) DNA-PKcs structure suggests an allosteric mechanism modulating DNA double-strand break repair. *Science (New York, N.Y.)* **355:** 520–524

Song C, Wang Q & Li C-CH (2003) ATPase activity of p97-valosin-containing protein (VCP). D2 mediates the major enzyme activity, and D1 contributes to the heat-induced activity. *J. Biol. Chem.* **278:** 3648–3655

Sonneville R, Moreno SP, Knebel A, Johnson C, Hastie CJ, Gartner A, Gambus A & Labib K (2017) CUL-2LRR-1 and UBXN-3 drive replisome disassembly during DNA replication termination and mitosis. *Nat Cell Biol* **19:** 468–479

St Charles JA, Liberti SE, Williams JS, Lujan SA & Kunkel TA (2015) Quantifying the contributions of base selectivity, proofreading and mismatch repair to nuclear DNA replication in Saccharomyces cerevisiae. *DNA Repair* **31:** 41–51

Stach L & Freemont PS (2017) The AAA+ ATPase p97, a cellular multitool. *Biochem. J.* **474:** 2953–2976

Staker BL, Feese MD, Cushman M, Pommier Y, Zembower D, Stewart L & Burgin AB (2005) Structures of three classes of anticancer agents bound to the human topoisomerase I-DNA covalent complex. *Journal of medicinal chemistry* **48:** 2336–2345

Stewart GS, Panier S, Townsend K, Al-Hakim AK, Kolas NK, Miller ES, Nakada S, Ylanko J, Olivarius S, Mendez M, Oldreive C, Wildenhain J, Tagliaferro A, Pelletier L, Taubenheim N, Durandy A, Byrd PJ, Stankovic T, Taylor AMR & Durocher D (2009) The RIDDLE syndrome protein mediates a ubiquitin-dependent signaling cascade at sites of DNA damage. *Cell* **136:** 420–434

Stewart GS, Wang B, Bignell CR, Taylor AMR & Elledge SJ (2003) MDC1 is a mediator of the mammalian DNA damage checkpoint. *Nature* **421:** 961

Stiff T, O'Driscoll M, Rief N, Iwabuchi K, Löbrich M & Jeggo PA (2004) ATM and DNA-PK Function Redundantly to Phosphorylate H2AX after Exposure to Ionizing Radiation. *Cancer Res.* **64:** 2390–2396

Stingele J, Bellelli R, Alte F, Hewitt G, Sarek G, Maslen SL, Tsutakawa SE, Borg A, Kjær S, Tainer JA, Skehel JM, Groll M & Boulton SJ (2016) Mechanism and Regulation of DNA-Protein Crosslink Repair by the DNA-Dependent Metalloprotease SPRTN. *Molecular Cell* **64:** 688–703

Stingele J & Jentsch S (2015) DNA–protein crosslink repair. *Nature Reviews Molecular Cell Biology* **16:** 455

Stolz A, Hilt W, Buchberger A & Wolf DH (2011) Cdc48: a power machine in protein degradation. *Trends in Biochemical Sciences* **36:** 515–523

Stucki M, Clapperton JA, Mohammad D, Yaffe MB, Smerdon SJ & Jackson SP (2005) MDC1 directly binds phosphorylated histone H2AX to regulate cellular responses to DNA double-strand breaks. *Cell* **123:** 1213–1226

Sul J-W, Park M-Y, Shin J, Kim Y-R, Yoo S-E, Kong Y-Y, Kwon K-S, Lee YH & Kim E (2013) Accumulation of the parkin substrate, FAF1, plays a key role in the dopaminergic neurodegeneration. *Human molecular genetics* **22:** 1558–1573

Sun J, Lee K-J, Davis AJ & Chen DJ (2012) Human Ku70/80 protein blocks exonuclease 1-mediated DNA resection in the presence of human Mre11 or Mre11/Rad50 protein complex. *J. Biol. Chem.* **287:** 4936–4945

Swatek KN & Komander D (2016) Ubiquitin modifications. *Cell research* **26:** 399

Tanaka A, Cleland MM, Xu S, Narendra DP, Suen D-F, Karbowski M & Youle RJ (2010) Proteasome and p97 mediate mitophagy and degradation of mitofusins induced by Parkin. *The Journal of Cell Biology* **191:** 1367–1380

Tang WK & Di Xia (2016) Role of the D1-D2 Linker of Human VCP/p97 in the Asymmetry and ATPase Activity of the D1-domain. *Scientific reports* **6:** 20037

Taylor JP (2015) Multisystem proteinopathy: Intersecting genetics in muscle, bone, and brain degeneration. *Neurology* **85:** 658–660

Thorslund T, Ripplinger A, Hoffmann S, Wild T, Uckelmann M, Villumsen B, Narita T, Sixma TK, Choudhary C, Bekker-Jensen S & Mailand N (2015) Histone H1 couples initiation and amplification of ubiquitin signalling after DNA damage. *Nature* **527:** 389–393

Tsujimoto Y, Tomita Y, Hoshida Y, Kono T, Oka T, Yamamoto S, Nonomura N, Okuyama A & Aozasa K (2004) Elevated expression of valosin-containing protein (p97) is associated with poor prognosis of prostate cancer. *Clinical cancer research : an official journal of the American Association for Cancer Research* **10:** 3007–3012

Valentin J (2007) *The 2007 recommendations of the International Commission on Radiological Protection (supersedes ICRP 60).* Published for the International Commission on Radiological Protection by Elsevier, Oxford

van den Boom J & Meyer H (2018) VCP/p97-Mediated Unfolding as a Principle in Protein Homeostasis and Signaling. *Molecular Cell* **69:** 182–194

van den Boom J, Wolf M, Weimann L, Schulze N, Li F, Kaschani F, Riemer A, Zierhut C, Kaiser M, Iliakis G, Funabiki H & Meyer H (2016) VCP/p97 Extracts Sterically Trapped Ku70/80 Rings from DNA in Double-Strand Break Repair. *Molecular Cell* **64:** 189–198

Vaz B, Halder S & Ramadan K (2013) Role of p97/VCP (Cdc48) in genome stability. *Front Genet* **4:** 60

Vaz B, Popovic M, Newman JA, Fielden J, Aitkenhead H, Halder S, Singh AN, Vendrell I, Fischer R, Torrecilla I, Drobnitzky N, Freire R, Amor DJ, Lockhart PJ, Kessler BM, McKenna GW, Gileadi O & Ramadan K (2016) Metalloprotease SPRTN/DVC1 Orchestrates Replication-Coupled DNA-Protein Crosslink Repair. *Molecular Cell* **64:** 704–719

Verma R, Oania R, Fang R, Smith GT & Deshaies RJ (2011) Cdc48/p97 mediates UV-dependent turnover of RNA Pol II. *Molecular Cell* **41:** 82–92

Walker JR, Corpina RA & Goldberg J (2001) Structure of the Ku heterodimer bound to DNA and its implications for double-strand break repair. *Nature* **412:** 607–614

Wallace SS, Murphy DL & Sweasy JB (2012) Base excision repair and cancer. *Cancer letters* **327:** 73–89

Wang M, Wu W, Wu W, Rosidi B, Zhang L, Wang H & Iliakis G (2006) PARP-1 and Ku compete for repair of DNA double strand breaks by distinct NHEJ pathways. *Nucleic Acids Res* **34:** 6170–6182

Wang T, Birsoy K, Hughes NW, Krupczak KM, Post Y, Wei JJ, Lander ES & Sabatini DM (2015) Identification and characterization of essential genes in the human genome. *Science (New York, N.Y.)* **350:** 1096–1101

Wang Y, Ghosh G & Hendrickson EA (2009) Ku86 represses lethal telomere deletion events in human somatic cells. *Proc. Natl. Acad. Sci. U.S.A.* **106:** 12430–12435

Ward IM & Chen J (2001) Histone H2AX is phosphorylated in an ATR-dependent manner in response to replicational stress. *J. Biol. Chem.* **276:** 47759–47762

Watts, Giles D J, Wymer J, Kovach MJ, Mehta SG, Mumm S, Darvish D, Pestronk A, Whyte MP & Kimonis VE (2004) Inclusion body myopathy associated with Paget disease of bone and frontotemporal dementia is caused by mutant valosin-containing protein. *Nature genetics* **36:** 377–381

Weber GF (2015) Molecular Analysis of a Recurrent Sarcoma Identifies a Mutation in FAF1. *Sarcoma* **2015:** 839182

Wijnhoven P, Konietzny R, Blackford AN, Travers J, Kessler BM, Nishi R & Jackson SP (2015) USP4 Auto-Deubiquitylation Promotes Homologous Recombination. *Molecular Cell* **60:** 362–373

Wójcik C, Yano M & DeMartino GN (2004) RNA interference of valosin-containing protein (VCP/p97) reveals multiple cellular roles linked to ubiquitin/proteasome-dependent proteolysis. *J. Cell. Sci.* **117:** 281–292

Wright WD, Shah SS & Heyer W-D (2018) Homologous recombination and the repair of DNA double-strand breaks. *J. Biol. Chem.* **293:** 10524–10535

Wu J, Zhang X, Zhang L, Wu C-Y, Rezaeian AH, Chan C-H, Li J-M, Wang J, Gao Y, Han F, Jeong YS, Yuan X, Khanna KK, Jin J, Zeng Y-X & Lin H-K (2012) Skp2 E3 ligase integrates ATM activation and homologous recombination repair by ubiquitinating NBS1. *Molecular Cell* **46:** 351–361

Xu G, Chapman JR, Brandsma I, Yuan J, Mistrik M, Bouwman P, Bartkova J, Gogola E, Warmerdam D, Barazas M, Jaspers JE, Watanabe K, Pieterse M, Kersbergen A, Sol W, Celie, Patrick H N, Schouten PC, van den Broek, Bram, Salman A & Nieuwland M et al (2015) REV7 counteracts DNA double-strand break resection and affects PARP inhibition. *Nature* **521:** 541–544

Xue L, Blythe EE, Freiberger EC, Mamrosh JL, Hebert AS, Reitsma JM, Hess S, Coon JJ & Deshaies RJ (2016) Valosin-containing protein (VCP)-Adaptor Interactions are Exceptionally Dynamic and Subject to Differential Modulation by a VCP Inhibitor. *Molecular & cellular proteomics : MCP* **15:** 2970–2986

Yamamoto S, Tomita Y, Hoshida Y, Iizuka N, Kidogami S, Miyata H, Takiguchi S, Fujiwara Y, Yasuda T, Yano M, Nakamori S, Sakon M, Monden M & Aozasa K (2004a) Expression level of valosin-containing protein (p97) is associated with prognosis of esophageal carcinoma. *Clinical cancer research : an official journal of the American Association for Cancer Research* **10:** 5558–5565

Yamamoto S, Tomita Y, Hoshida Y, Iizuka N, Monden M, Yamamoto S, Iuchi K & Aozasa K (2004b) Expression Level of Valosin-Containing Protein (p97) Is Correlated With Progression and Prognosis of Non-Small-Cell Lung Carcinoma. *Annals of Surgical Oncology* **11:** 697–704

Yamamoto S, Tomita Y, Hoshida Y, Sakon M, Kameyama M, Imaoka S, Sekimoto M, Nakamori S, Monden M & Aozasa K (2004c) Expression of Valosin-Containing Protein in Colorectal Carcinomas as a Predictor for Disease Recurrence and Prognosis. *Clinical cancer research : an official journal of the American Association for Cancer Research* **10:** 651–657

Yang G, Liu C, Chen S-H, Kassab MA, Hoff JD, Walter NG & Yu X (2018) Super-resolution imaging identifies PARP1 and the Ku complex acting as DNA double-strand break sensors. *Nucleic Acids Research* **46:** 3446–3457

Yang SW, Burgin AB, Huizenga BN, Robertson CA, Yao KC & Nash HA (1996) A eukaryotic enzyme that can disjoin dead-end covalent complexes between DNA and type I topoisomerases. *Proc. Natl. Acad. Sci. U.S.A.* **93:** 11534–11539

Yano K-i, Morotomi-Yano K, Wang S-Y, Uematsu N, Lee K-J, Asaithamby A, Weterings E & Chen DJ (2008) Ku recruits XLF to DNA double-strand breaks. *EMBO Rep.* **9:** 91–96

Ye Y, Meyer HH & Rapoport TA (2003) Function of the p97-Ufd1-Npl4 complex in retrotranslocation from the ER to the cytosol: dual recognition of nonubiquitinated polypeptide segments and polyubiquitin chains. *The Journal of Cell Biology* **162:** 71–84

Yin Y, Seifert A, Chua JS, Maure J-F, Golebiowski F & Hay RT (2012) SUMO-targeted ubiquitin E3 ligase RNF4 is required for the response of human cells to DNA damage. *Genes Dev.* **26:** 1196–1208

Yoo S & Dynan WS (1998) Characterization of the RNA binding properties of Ku protein. *Biochemistry* **37:** 1336–1343

Yoo S, Kimzey A & Dynan WS (1999) Photocross-linking of an Oriented DNA Repair Complex. *J. Biol. Chem.* **274:** 20034–20039

Yu C, Kim B-S & Kim E (2016) FAF1 mediates regulated necrosis through PARP1 activation upon oxidative stress leading to dopaminergic neurodegeneration. *Cell death and differentiation* **23:** 1873–1885

Yurchenko V, Xue Z & Sadofsky MJ (2006) SUMO modification of human XRCC4 regulates its localization and function in DNA double-strand break repair. *Mol. Cell. Biol.* **26:** 1786–1794

Zeman MK & Cimprich KA (2014) Causes and consequences of replication stress. *Nature cell biology* **16:** 2–9

Zhang H-F, Tomida A, Koshimizu R, Ogiso Y, Lei S & Tsuruo T (2004) Cullin 3 Promotes Proteasomal Degradation of the Topoisomerase I-DNA Covalent Complex. *Cancer Res* **64:** 1114–1121

Zhao G, Zhou X, Wang L, Li G, Schindelin H & Lennarz WJ (2007) Studies on peptide:N-glycanase-p97 interaction suggest that p97 phosphorylation modulates endoplasmic reticulum-associated degradation. *Proc. Natl. Acad. Sci. U.S.A.* **104:** 8785–8790

Zhou H-L, Geng C, Luo G & Lou H (2013) The p97-UBXD8 complex destabilizes mRNA by promoting release of ubiquitinated HuR from mRNP. *Genes Dev.* **27:** 1046–1058

Abbreviations

53BP1	p53-binding protein 1
6-4 PP	6-4 photoproducts
A	adenine
AAA	ATPases associated with diverse cellular activities
ADP	adenosine diphosphate
alt-EJ	alternative end-joining
ANOVA	analysis of variance
ATM	ataxia-telangiectasia mutated
ATP	adenosine triphosphate
ATR	ataxia telangiectasia and Rad3-related
ATRIP	ATR-interacting protein
BARD1	BRCA1-associated RING domain protein 1
BER	base excision repair
BIR	break-induced replication
BLM	Bloom syndrome helicase
BrdU	5-bromo-2'-deoxyuridine
BRCA1	breast cancer type 1 susceptibility protein
BRCA2	breast cancer type 2 susceptibility protein
C	cytosine
CAD	chromatin-associated degradation
Cdc	cell-division cycle
CDK	cyclin dependent kinase
CMG	Cdc45-Mcm-GINS complex
CPC	cyclobutane pyrimidine dimer
CPT	camptothecin
CRISPR	clustered regularly interspaced short palindromic repeats
cs	catalytic subunit
CSK	cytoskeleton buffer
CtIP	C-terminal-binding protein 1-interacting protein
CYREN	cell cycle regulator of NHEJ
DAPI	4′,6-Diamidin-2-phenylindol
DDR	DNA damage response
de	double-ended
D-loop	displacement loop
DMSO	dimethyl sulfoxide
DNA	deoxyribonucleic acid
DNA2	DNA replication helicase/nuclease 2
DNA-PK	DNA-dependent protein kinase
DPC	DNA protein crosslink
DSB	double strand break
DUB	deubiquitinating enzyme

EDTA	ethylenediaminetetraacetic acid
EdU	5-ethynyl-2'-desoxyuridine
EJ	end-joining
ERAD	endoplasmic reticulum-associated degradation
ERCC1	excision repair cross-complementing group 1 protein
EXO1	exonuclease 1
FA	Fanconi anemia
FEN1	flap structure-specific endonuclease 1
G	guanine
$G_{1/2}$ phase	gap phase
GFP	green fluorescent protein
HRR	homologous recombination repair
ID complex	FANCI and FANCD2 complex
IRIF	irradiation-induced foci
K	lysine
KD	knockdown
KO	knockout
LET	linear energy transfer
LFQ-MS	label-free quantitative mass spectrometry
MAD	mitochondria-associated degradation
Mcm	minichromosome maintenance complex
MMR	mismatch repair
MMEJ	microhomology-mediated end-joining
M phase	mitotic phase
MRE11	meiotic recombination 11
Nbs1	Nijmegen breakage syndrome protein 1
NER	nucleotide excision repair
NHEJ	non-homologous end-joining
NOS	reactive nitrogen species
Npl4	nuclear protein localization
NZF	Npl4 zinc finger
PALB2	partner and localizer of BRCA2
PALF	polynucleotide kinase and aprataxin-like forkhead-associated protein
PAXX	paralog of XRCC4 and XLF
PCNA	proliferating cell nuclear antigen
PCR	polymerase chain reaction
PDB	protein data bank
PFGE	pulsed-field gel electrophoresis
PIKK	phosphatidylinositol 3-kinase (PI3K)-related kinase
Pol μ	DNA polymerase mu
Pol λ	DNA polymerase lambda
Rad50	radiation sensitive 50
Rad51	radiation sensitive 51

RBE	relative biological effectiveness
RC	replication complex
RING	really interesting new gene
RNA	ribonucleic acid
RNF	RING finger protein
ROS	reactive oxygen species
RPA	replication protein A
RYBP	RING1-YY1-binding protein
SDSA	synthesis dependent strand annealing
se	single-ended
SIM	structured illumination microscopy
SIM	SUMO-interacting motif
S phase	synthesis phase
SSA	single-strand annealing
SSB	single strand break
STUbL	SUMO-targeted ubiquitin ligase
SUMO	small ubiquitin-like modifier
T	thymidine
TDP1	tyrosyl-DNA phosphodiesterase 1
TdT	terminal deoxynucleotidyl transferase
TLS	translesion synthesis
Top1	topoisomerase I
Top1cc	topoisomerase I cleavage complex
Ufd1	ubiquitin fusion degradation 1
UPS	ubiquitin-proteasome system
VCP	valosin-containing protein
WRN	Werner syndrome helicase
XLF	XRCC4-like factor
XPF	Xeroderma pigmentosum group F-complementing protein
XRCC1	X-ray cross-complementing group 1
XRCC4	X-ray cross-complementing group 4

Acknowledgements

I am thankful to Hemmo Meyer for the chance to stay in his group after my Master's thesis, the opportunity to work on this interesting project, and to let me join the GRK1739. I appreciate your valuable advices and your trust in my skills. Further, I enjoyed the freedom to develop my own ideas and that you were around to keep them on the right course.

Special thanks to Johannes van den Boom for his continuous support and advice that are very helpful. It is always exciting to discuss ideas and results. Thank you for critical reading of this thesis.

Many thanks to all current and past colleagues of the Meyer lab that made and make it a fun time. You create a wonderful working atmosphere and are always around to help. I also enjoy the times with you outside the lab.

I would like to thank the colleagues that supported my experiments: Nina Schulze from the ICCE for teaching me a lot about microscopy and her support in imaging and image analysis. Further Anthony Squire from the IMCES for his help with SIM and Marc Schuster for his help with flow cytometry.

I thank Sabine Effenberger, Miriam Schmidt, and Christina Kamp-Meltzer for the technical and organizational support that keep the lab running.

During my thesis, I joined the DFG GRK1739 and want to thank for funding and the interesting time in graduate school that expanded my knowledge to new topics.

Finally, I want to thank my family, especially Katharina Wolf, for their love, patience and support.

Curriculum vitae

Der Lebenslauf ist in der Online-Version aus Gründen des Datenschutzes nicht enthalten.

The CV is not included in the online version for privacy reasons.

Affidavits / Erklärungen

Erklärung:

Hiermit erkläre ich, gem. § 7 Abs. (2) d) + f) der Promotionsordnung der Fakultät für Biologie zur Erlangung des Dr. rer. nat., dass ich die vorliegende Dissertation selbständig verfasst und mich keiner anderen als der angegebenen Hilfsmittel bedient, bei der Abfassung der Dissertation nur die angegeben Hilfsmittel benutzt und alle wörtlich oder inhaltlich übernommenen Stellen als solche gekennzeichnet habe.

Essen, den _____

_____

Unterschrift des/r Doktoranden/in

Erklärung:

Hiermit erkläre ich, gem. § 7 Abs. (2) e) + g) der Promotionsordnung der Fakultät für Biologie zur Erlangung des Dr. rer. nat., dass ich keine anderen Promotionen bzw. Promotionsversuche in der Vergangenheit durchgeführt habe und dass diese Arbeit von keiner anderen Fakultät/Fachbereich abgelehnt worden ist.

Essen, den _____

_____

Unterschrift des Doktoranden

Erklärung:

Hiermit erkläre ich, gem. § 6 Abs. (2) g) der Promotionsordnung der Fakultät für Biologie zur Erlangung der Dr. rer. nat., dass ich das Arbeitsgebiet, dem das Thema „Analysis of p97-mediated Ku80 extraction in DNA double-strand break repair in cells“ zuzuordnen ist, in Forschung und Lehre vertrete und den Antrag von Markus Andreas Wolf befürworte und die Betreuung auch im Falle eines Weggangs, wenn nicht wichtige Gründe dem entgegenstehen, weiterführen werde.

Essen, den _____

_____

Unterschrift eines Mitglieds der Universität Duisburg-Essen